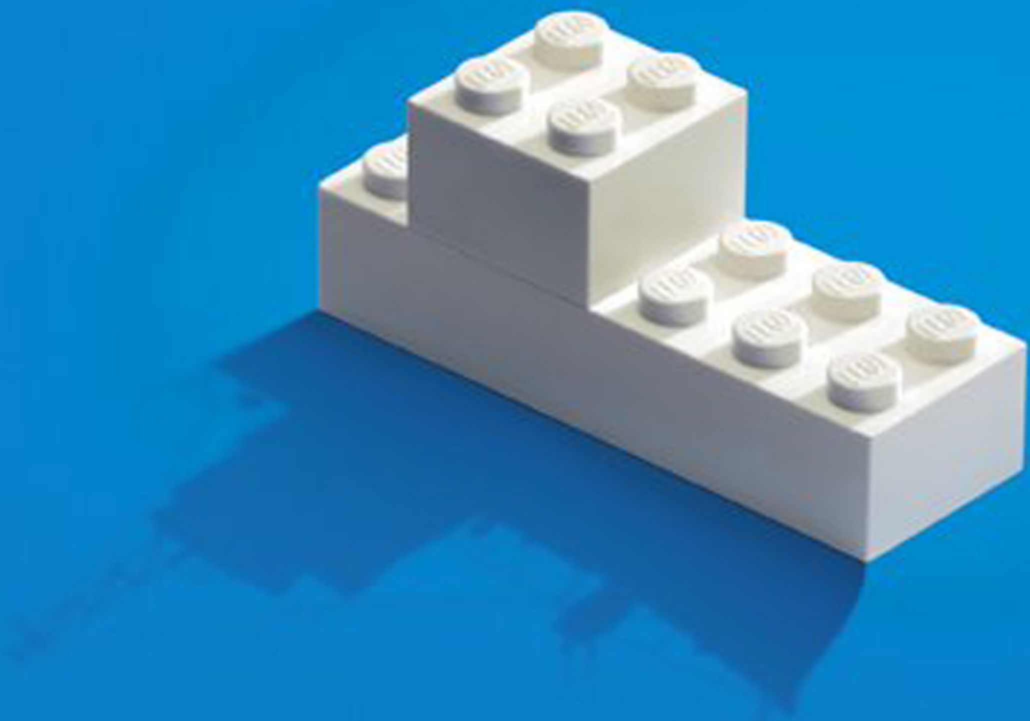

LINE OF SIGHT GUIDANCE & FAULT DIAGNOSIS OF A SURFACE VESSEL

MASTER THESIS JUNE 2015

AALBORG UNIVERSITET

I would like to dedicate my dissertation work to my father,
Flemming Ole Knudsen (✝11.12.2013)

Aalborg University
The Faculty of Engineering and Science
School of Information and
Communication Technology
Frederik Bajers Vej 7
9220 Aalborg Ø
Tlf.: 9940 9730
Telefax: 9940 9725
http://www.es.aau.dk

AALBORG UNIVERSITY
STUDENT REPORT

Subject: Control and Automation
Title: Line of Sight Guidance & Fault Diagnosis of a Surface Vessel
Project period: September 1^{th} 2014 – June 3^{th} 2015
Semester: 10^{th} Semester (P10)
Project group: 1031

Author:

Kevin Lyn-Knudsen

Supervisor: Jan Dimon Bendtsen
Secondary Supervisor: Jesper Abildgaard Larsen

Number of copies: 3
Pages: 134
Appendices: 5 Appendices
Attachments: 1 CD

Abstract:

The aim of the present thesis is to investigate active fault diagnosis as a solution to improve the reliability of a surface vessel.

The Port of Aalborg have asked the University of Aalborg to investigate the possibility of automating some of the tasks they conduct. Based on this inquire a prototype vessel, AAUSHIP, has been designed. Based on the designed prototype a dynamical model is derived.
Based on the model derived an EKF and an UKF is designed. It is wanted to compared them, and based on the comparison, choose one of them for future work.
To make the vessel sail autonomously a path-following cascade controller is designed and implemented based on a LOS guidance law.
A fault analysis is conducted to identify the possible component faults, and their frequency of occurrence and the severity of their end-effects. A fault diagnosis scheme is then designed to accommodate one of the faults determined.
An active fault diagnosis method is implemented based on the theory of auxiliary signal design. The fault diagnosis is to detect the faults determined by the fault analysis.
It is verified that the path-following controller together with the chosen extended Kalman filter complies with the requirements presented in the thesis. It was not possible to determine if active fault diagnosis can improve the reliability of AAUSHIP during operations, because of a failed acceptance test.

Preface

This thesis is handed in as a partial fulfilment of the requirements for a Master of Science(M.Sc) degree within Engineering, specialising in Control and Automation at Aalborg University, Department of Control and Automation. The thesis is a long termination thesis which have been written in the period between 1st of September 2014 to the 3rd of June 2015. The oral defence of the thesis will take place on the 8th of June.

The subject of the thesis is the design of a path-following control system and active fault diagnosis.

The developed code is located on the attached CD together with some of the documentation used through the present thesis.

The thesis supervisors have been Associate Professor, PhD Jan Dimon Bendtsen and Lektor, PhD Jesper Abildgaard Larsen.

I would like to extend a thank to my supervisors for helping me in the aim of getting an article published and the extra hours this implied.

Acknowledgements

I would like to extend his gratitude towards the following persons: Assistant Professor, PhD Christoffer Ege Sloth for the time he has taken to discuss the design of an auxiliary signal, i would also like to thank M.Sc Jeppe Dam and M.Sc Nick Østergaard for taking the time to execute the tests used in the present thesis, and fellow students Kasper Hemme and Michael Nauheimer for taking part in technical discussions. I will also like to extend a thank to PhD Mark Lyksborg from DTU Compute for taking the time to help structuring the thesis.

Lastly I will very much like to give a special thank to my girlfriend, *Tina*, for all of her love and support which have been a blessing.

Kevin Lyn-Knudsen
June 2015, Aalborg, Denmark

Nomenclature

Abbreviations

BODY Body-Fixed Reference Frame

CG Center of Gravity

CO Center of Origin

CoM Center of Mass

DOF Degrees of Freedom

ECEF Earth-centered Earth-fixed Reference Frame

ECI Earth-Centered Inertial Reference Frame

FMEA Failure Mode and Effect Analysis

GPS Global Positioning System

GRV Gaussian Random Variable

HLI High Level Interface

IMU Inertial Measurement Unit

LLI Low Level Interface

LOS Line of Sight

NED North-East-Down Reference Frame

PF Path-fixed Reference Frame

TPBVP Two Point Boundary Value Problem

Terminology

Barre Is a different name for a sandbank

Bathymetry Is the study of underwater depths

Buoyancy Is the force that keeps the vessel floating

Course Angle Is the angle between x_n and the relative velocity vector

Greenwich Meridian Is the Meridian which passes through Greenwich

Heading Is the angle between x_n and x_b determining the direction of travel

Heave The up- and downwards translational motion of the body

Hydrodynamics Is the force acting on the vessel's hull while travelling through water

Hydrofoil Is a lifting surface or foil which is used to stabilise the vessel

Hydrographic Surveying Is the applied science of measuring and describing features such as sea depth and seabed configuration

Hydrostatics Is the force that returns the vessel to its steady state when pulled away

Limfjorden Is a fjord separating the Northern part of Jutland from the rest of Jutland

Pitch The rotational motion around the y-axis

Port side The side of the ship to left looking from aft to fore

Roll The rotational motion around the x-axis

Starboard The side of the ship to right looking from aft to fore

Surge The translational motion along the body

Sway Is translational motion in direction of the Y-axis of the body-fixed reference frame

Yaw The rotational motion around the z-axis

The next section will give a short introduction to the notation used in the present thesis.

Vector and Matrix Notation

The notation used through out this thesis is defined in this section. Matrices will be denoted as a bold upper case letters, vectors will be denoted as a bold italic lower case letters, these notation can be seen in equation 1.

$$\dot{\mathbf{x}} = \mathbf{A}\mathbf{x} + \mathbf{B}\mathbf{u} \tag{1}$$

The identity and zero matrices are denoted with a bold **I** and a bold **0** , respectively, with a subscript stating their dimensions.

$$\mathbf{I}_{3\times3} \quad \mathbf{0}_{3\times3} \tag{2}$$

The reference frame axes are represented as it is seen in Table 1

The sub/superscript is used to represent vectors in different reference frames like

Reference frame	Axes	sub/superscript
ECEF	$x_e\,, y_e\,, z_e$	e
ECI	$x_i\,, y_i\,, z_i$	i
NED	$x_n\,, y_n\,, z_n$	n
BODY	$x_b\,, y_b\,, z_b$	b
PF	$x_p\,, y_p\,, z_p$	p

Table 1: The table presents the reference frames and their respective axes

$$ {}^{\mathrm{b}}\mathbf{v}, \quad {}^{\mathrm{n}}\mathbf{v}, \quad {}^{\mathrm{e}}\mathbf{v}, \quad {}^{\mathrm{i}}\mathbf{v}, \quad {}^{\mathrm{b}}\mathbf{v} \tag{3} $$

The equation shows the velocity vector represented in different reference frames. This is what the superscript denotes. The sub script is used in rotation, to describe to which frame from which frame, e.g a rotation from NED to BODY.

Rotations

The rotation between frames are done using rotation matrices. The left hand side superscript indicates the frame which the variable is expressed. The left hand side subscript indicates the frame which is to be rotated into the superscripted frame, this can be seen in equation 4

$$ {}^{\mathrm{n}}\mathbf{p}(t) = {}^{\mathrm{n}}_{\mathrm{b}}\mathbf{R}\,{}^{\mathrm{b}}\mathbf{p}(t) \tag{4} $$

The rotation matrix is used to transform equations of motion, represented in a inertial reference frame(NED), to equations of motion in a rotating frame(BODY) without any loss of generality. There is also used another rotation but it is described in a later section. The rotation matrix can be used to reverse the rotation, this is done by inverting the rotation matrix.

$$ {}^{\mathrm{b}}\mathbf{p}(t) = {}^{\mathrm{n}}_{\mathrm{b}}\mathbf{R}^{-1}\,{}^{\mathrm{n}}\mathbf{p}(t) = {}^{\mathrm{b}}_{\mathrm{n}}\mathbf{R}\,{}^{\mathrm{n}}\mathbf{p}(t) \Rightarrow {}^{\mathrm{b}}_{\mathrm{n}}\mathbf{R} = {}^{\mathrm{n}}_{\mathrm{b}}\mathbf{R}^{-1} \tag{5} $$

These previous sections has explained some of the background theory behind the modelling of a marine vessel. The notation used through out this thesis was also presented. The next section will present the non-linear model of a marine vessel.

This is a short introduction to the notation used in the present thesis.

Contents

List of Figures

List of Tables

Chapter 1

Introduction

The aim of this chapter is to give an overview of the problems considered in the present thesis. The first section presents the motivation for the present thesis. This leads to a description of the surface vessel prototype developed to solve the problem stated in the motivation. Then a section will the describe some further problems which is not mentioned in the motivation. The sections mentioned leads to a project scope which will outline the focus of the present thesis. The is finished of with outline of the thesis, which will provide an overview of the forthcoming chapters.

1.1 Motivation and The AAUSHIP Project

The Port of Aalborg has directed an inquire to Aalborg University, to investigate the use of autonomous surface vessels to assist in the conducting of their tasks [Dam 14]. One of the major tasks for the Port of Aalborg is to update *Limfjorden*'s bathymetric data, so vessels can navigate through the channel without running aground. It is wanted to perform this task using one or a multiple of autonomous vessels, the use of autonomous vessels will give them the possibility to update their maps more frequently [Dam 14]. The current main surveying vessel used to perform hydrographic surveying, is a manned tugboat named Alba, shown in figure 1.1. This figure also demonstrates the concept of hydrographic surveying where a single beam sonar is used to probe the sea floor to construct a depth map. The current surveying vessel is equipped with a multi-beam sonar which uses a multiple of beams to measure a larger area at the same time, a comparison of single beam and multi-beam sonar are shown in Figure 1.3.

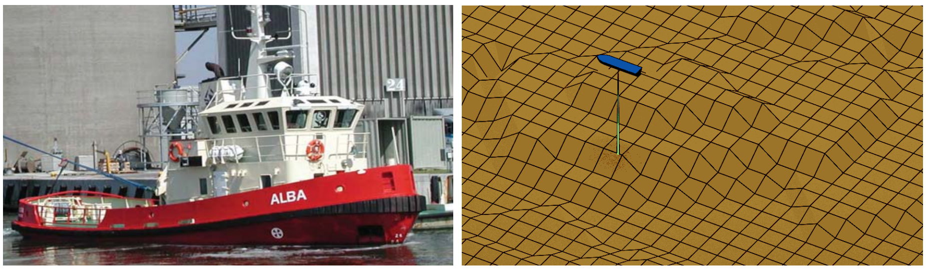

Figure 1.1: The first figure shows the present surveying vessel Alba. The second figure shows how hydrographic surveying is performed using a single beam sonar. [Dam 14]

The current surveying vessel is relatively large with a length of 22m and a draught of 3.8m [Traffic 15]. The size of the vessel makes it difficult for it to survey shallow areas and areas close

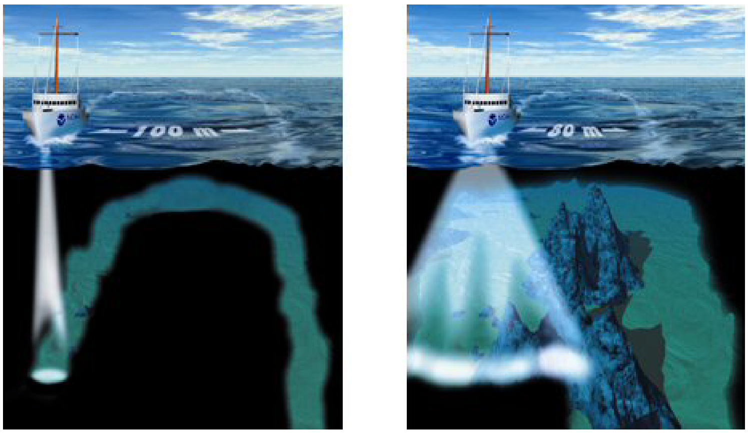

Single Beam Sonar Surveying

Multibeam Sonar Surveying

Figure 1.2: The figure shows the difference between the use of a single beam sonar and a multi-beam sonar when surveying [Monster 15].

to the shore/quay. They have smaller vessel which is a bit smaller, 12m, to perform surveying smaller areas, such as in harbour areas [Dam 14].

The manned vessels covers a stretch, around Aalborg, of approximately 70 km[Havn 15]. The surveying of this stretch is currently performed every third year, but around the sandbank Hals Barre there is a need for more frequent surveying, this area is surveyed every third month. The sandbank stretches around 4 km into the sea with a depth of 2-3 m, so a channel has been dug so the ship traffic can pass through [Bencke 15]. The channel has to be maintained so ships can pass through it, every year 40000 m^3 of sand has to be moved to maintain the channel. If the Port of Aalborg had an autonomous surveying vessel at their disposal it would permit a higher update frequency of the nautical maps compared to the present update frequency.

Figure 1.3: The first figure shows the placement of the Port of Aalborg compared to the city of Aalborg and Hals Barre. The second figure shows the actual sandbank and the channel which is dug through it make a passage [Google].

The Port of Aalborg also have other tasks to perform such as piloting. Piloting is done to safely guide large ships or ships which are not familiar with the channel to their docking positions or just through the channel. Piloting is currently performed by a pilot operating a pilot boat, which intercepts the vessel and escorts it safely in to the dock. It is also wanted to perform this manoeuvre using an autonomous surface vessel, the vessel is to intercept the vessel and to some extend take over the control and guide the vessel to the dock [Dam 14].

For the purpose of accommodating the proposed objectives of the Port of Aalborg, a prototype vessel has been made, AAUSHIP. The objective of the AAUSHIP project is mainly to create a usable solution for the Port of Aalborg. The versatility of the AAUSHIP platform, permit it to be used to many other projects/experiments revolving around water, such measuring of the saline content or oxygen levels which is a big problem in *Limfjorden* during hot summers.

The previous section described the motivation based on the inquire done by the Port of Aalborg. The next section will give a detailed description of the composition of AAUSHIP.

1.2 AAUSHIP - *a Marine Surveying Prototype*

The hull of AAUSHIP is 1m in length and 30cm in width, inside the hull there are two dedicated payload bays which can be used for experiments. The prototype is propelled by two main thrusters located at the aft of the vessel. The thrusters are powered by two Graupner Brushless Inline 750 14.8V which can deliver 1200W of power [University 15]. Attached to thrusters are two contra rotating propellers used to propel the vessel, see Figure 1.4. By controlling the propellers separately it is possible to turn the vessel in a given direction. A hydrofoil is mounted at the back of the vessel to stabilise the vessel when stationary and to keep the planing at low revolutions. The vessel is also equipped with two additional thrusters which is to be used when docking or if one of the main thrusters fail. The additional thrusters have propellers located inside the hull and their delivered force results in a sideways or a turning motion.

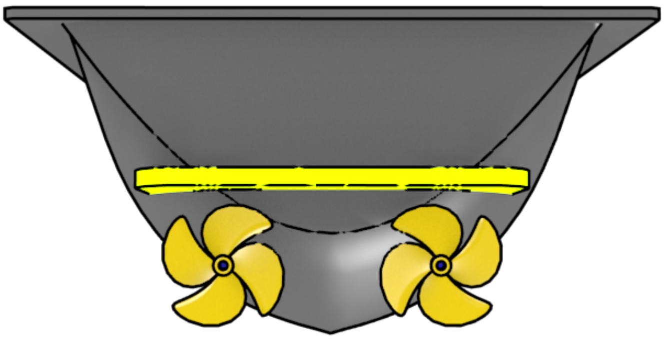

Figure 1.4: A aft view of AAUSHIP, where the two contra propellers can be seen together with the aft hydrofoil above them.[University 15]

One of the main objective is for the boat to travel autonomously. To accommodate this requirement the vessel is equipped with sensors to help it navigate. AAUSHIP is equipped with GPS which is used to determine its position. To track the velocity and the orientation of the vessel an ADIS16405 tri-axis high precision inertial measurement unit(IMU) is used. The IMU contains three tri-axis sensors, an accelerometer, a gyroscope, and a magnetometer. The accelerometer is used to monitor the actual travelling speed of the vessel during missions. The magnetometer is used to determine the actual orientation/attitude of the vessel, this information is used to monitor the travelling direction of the vessel. The gyroscope is at the moment not used for navigation but it can be used to do dead reckoning if the magnetometer fails or to verify that the magnetometer is working. To perform the surveying it is planned to equip the vessel with a sonar, this has not been done yet. Instead there have been a focus on developing the navigation and control system for the vessel. The sonar considered for implementation is one similar to the one equipped on Alba. The placement of the sensors can be seen in Figure 1.5.

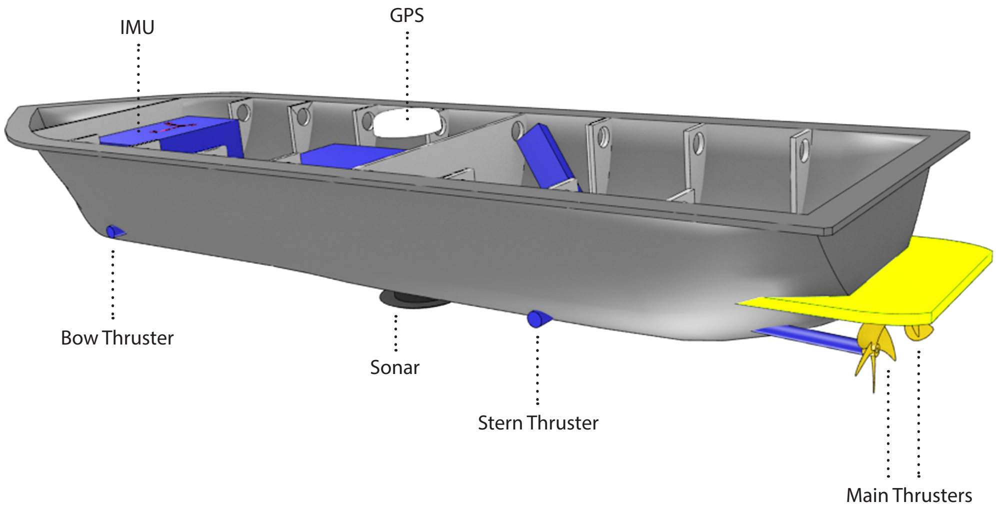

Figure 1.5: A rendered image of the boat describing where the different parts are located

The actuators and the sensors are connected to a low level interface(LLI) that handles the specific details concerning commutation of the brushless DC-motor and sampling of the sensors. The LLI is then connected to a high level interface(HLI) which controls the LLI by e.g setting the propeller velocity. The HLI computes the control inputs, calculated based on the sensor measurements, which should be relayed to the LLI. Besides these tasks the HLI also handles the communication to the operator and the relay of sonar measurements.

For more specific details about the motor or sensors, see Appendix E. In this section an overview of the AAUSHIP design has been given to explain the specific platform used in the present thesis. The next section will give a more detailed description of the mission AAUSHIP is to complete.

1.3 Safety Concerns

The concept of using an autonomous vessel to perform hydrographic surveying has been investigated in previous projects, such as [Dam 14, Christensen 13], therefore this will not be the only focus of the present thesis. The main focus of the present thesis will be on how to ensure the safety of the vessel and other vessels travelling in *Limfjorden*.

AAUSHIP will sail autonomously, therefore it is of great importance to guarantee the safety of other vessels in the same area. If the fjord was free of other trafficking vessels, it would not present any major safety issues. The problem arises when there are trafficking ships in the same area as where the surveying is conducted. The ships entering the surveying area do not have any information of the travelling trajectory of the autonomous vessel. This entails a hazard to the autonomous vessel which might collide with other ships, however it does not entail a direct hazard to the ship because of the relative size of the ship compared to AAUSHIP. As a result of this hazard it is wanted to make the autonomous vessel more robust if it becomes faulty after such collision, so there is no need to fetch the vessel using a manned vessel.

Considering the second assignment for the AAUSHIP to accomplish, which is piloting, there are other safety critical consequences. Piloting of a marine vessel through shallow water is a very safety critical manoeuvre which requires a clear communication between the pilot boat and the ship which needs piloting. If the ship is not guided through the shallow waters correctly there is a high risk of running aground. The outcome of this does not only affect the ship, as an materialistic object, but also the health and safety of the passengers/personnel aboard the ship.

Both of the above mentioned risks can become a reality if the autonomous vessel becomes faulty during operations. The first risk means that the vessel needs to be fetched by a manned vessel. The other risk is to bring harm to other ships due to a faulty vessel. The present thesis will try to eliminate these risks by using fault diagnosis. The fault diagnosis shall be used to determine if the autonomous vessel has become faulty and therefore non-operational. The fault diagnosis itself does not return the vessel to a non-faulty state but it is meant as the groundwork on the way to implement fault tolerant control, which might be able to recover the vessel to a non-faulty state or reduced performance state. On AAUSHIP there are, at the present time, not implemented any automatic way to determine if a fault has occurred.

This section has explained some of the safety hazards a autonomous surface vessel might be subject to. It has been stated that the present thesis will investigate the use of fault diagnosis as a solution to the safety hazards presented. The next section will describe the main scope of the present thesis.

1.4 Project Scope

The scope of the present project is to ensure safe operation of AAUSHIP, even in the presence of faults in the system. The project will lay the groundwork for a possible implementation of a fault tolerant control system to accommodate the faults. The previous sections have given some insight in the hazards revolving autonomous marine vessels in trafficked areas. Based on these hazards a fault diagnosis system will be designed and tested to investigate if it is possible to improve the reliability of AAUSHIP.

The main focus of the present thesis is the following: It is wanted to design a control law for a surface vessel which makes the vessel sail autonomously. While the vessel is sailing it shall be able to perform fault diagnosis to improve the reliability of the vessel.

AAUSHIP is used as a hardware platform, and the present project will try to design systems based on this hardware structure. The systems designed in the present project will be based on this platform. below the systems to be designed are explained.

Position and Attitude Estimation

To diminish the influence of noise affecting the sensor, a position and attitude determination algorithm will be designed. The determination algorithm will be based on the Kalman filter algorithm. Different Kalman filter methods will be used to determine the best suited solution for the mission explained earlier in this chapter. A sensor analysis shall be done to determine the magnitude of the sensor noise. This is done to make the simulation results more like the expected results seen during implementation.

Path-following Navigation

As is described earlier in this chapter it is wanted to create an autonomous surveying vessel. Because the vessel has to be autonomous there is a need to develop a way of steering the vessel autonomously. For the purpose of steering the vessel a control law shall be designed. The control law shall be able to steer the vessel along a mission specified path.

Fault Diagnosis

To improve the reliability of the vessel a fault diagnosis system will be implemented and tested. It is wanted to implement an active fault diagnosis scheme, this is chosen by the author to gain experience within the field of active fault diagnosis. The fault diagnosis shall be able to detect faults which is determined by a fault analysis.

The next section will give a short overview of thesis to come, and explain the content of the different chapters to come.

1.5 Thesis Outline

The content of the thesis is arranged as follows:

Chapter 2 introduces the model of the surface vessel which consists of the rigid body kinetics, hydrostatic forces and hydrodynamic forces. The notation and reference frames used to represent the derived model are also explained.

Chapter 3 presents the system requirements set up for the present project. The are given arguments for the different system requirements determined together with a test to verify each of the subsystem.

Chapter 4 presents the design of two estimation methods which can handle the non-linear characteristics of the model. The two methods presented is the extended Kalman filter and the unscented Kalman filter. Besides the design of the Kalman filters, a short description of complications during the implementation of the methods is presented.

Chapter 5 contains the design of a path-following controller, utilising a guidance law. The guidance law is based on a Line of Sight guidance law which is used to determine the desired heading of the vessel based on a predetermined path. Based on the guidance law are cascaded controller is designed to steer the vessel towards the desired path. Together with the way-point tracking, a way-point switching algorithm have been made to support multiple way-points.

Chapter 6 describes the fault analysis performed to select the faults to be detected by the fault diagnosis. The fault analysis is based on a failure mode and effect analysis combined with a severity and occurrence analysis. The failure mode and effect analysis are used to determine the propagation of faults through the system and to determine which faults are the most critical to detect, the severity and occurrence analysis is used.

Chapter 7 presents the design of a active fault diagnosis method based on the design of an auxiliary signal. The design of the auxiliary signal is explained together with some of the numerical issues arising from the design method.

Chapter 8 contains a description of the acceptance test to be performed together with the results obtained during the accept test. The chapter contains a section describing some of the possible causes of error when implementing an auxiliary signal.

Chapter 9 Will conclude on the results obtained through the present thesis. The chapter also contains a description of possible improvements and ideas for future work.

The present chapter has sought to clarify some of the issues when performing hydrographic surveying autonomously. The chapter has narrowed down the field of study which has led to a project scope as described in the previous section. At the end of the chapter a thesis outline is presented to give an overview of the forthcoming chapters. The next chapter will present a non-linear model of AAUSHIP based on the work done by [Dam 14]. The model shall be used to the design the systems specified in the project scope.

Chapter 2

Modelling of a Surface Vessel

The following chapter will present a non-linear model of AAUSHIP. The chapter first part of the chapter is used to present some background theory of the kinematics used to model a surface vessel. The subsequent section will introduce the notation used to describe the motion of a surface vessel. After the notation is presented, a short explanations of the rotation matrix is presented. After the background theory has been presented, the rigid body model of a surface vessel is derived. The subsequent sections will describe the retarding forces affecting the vessel. The last section will combine the rigid body kinetics with the retarding forces into a state space model. The following section are based on the work of [Fossen 11].

2.1 Kinematics

In the following section the different reference frames used for modelling of a marine craft is introduced, together with the connection between them. There are five different reference frames introduced, two Earth-centered and three geographic.

ECI - Earth-Centered Inertial Reference Frame

The Earth-Centered Inertial Reference Frame (ECI) reference frame has its origin in the Center of Mass (CoM) of the Earth. The z-axis of the reference frame is perpendicular to the equatorial plane and passes through the North Pole. The x-axis of the ECI reference frame lies in the equatorial plane, at vernal equinox the Greenwich Meridian aligns with the x-axis. The y-axis is a cross product of the x- and z-axis. The ECI reference frame is stationary at all times i.e inertial. Inertial reference frames is used to represent classical Newtonian mechanics without the addition of fictitious force. The representation of the ECI frame compared to the Earth can be seen in Figure 2.1.

ECEF - Earth-Centered Earth-Fixed Reference Frame

The Earth-centered Earth-fixed Reference Frame (ECEF) reference frame has its origin in the CoM of the Earth, i.e it shares its origin and z-axis with the ECI reference frame. At vernal equinox the ECEF reference frame and ECI reference frame is aligned, at the time between every vernal equinox they are different. The ECEF is rotating with a angular velocity, ω_e, of 7.2921e-5 rad/s relative to ECI. The ECEF reference frame is used to determine the geographical position of an element of the surface of the Earth.

NED - North-East-Down Reference Frame

The North-East-Down Reference Frame (NED) reference frame has its origin on the surface of the Earth, also called Earth's reference ellipsoid. The NED reference frame is defined as a tangential plane upon the surface of the Earth moving with the ECEF reference frame, see Figure 2.1. The x-axis is pointing towards true North at all time. The y-axis points towards East, the z-axis is perpendicular to the plane spanned by x and y i.e in a downwards direction. This reference frame is used when navigating a vessel in local areas, which means the Earth rotation can be neglected.

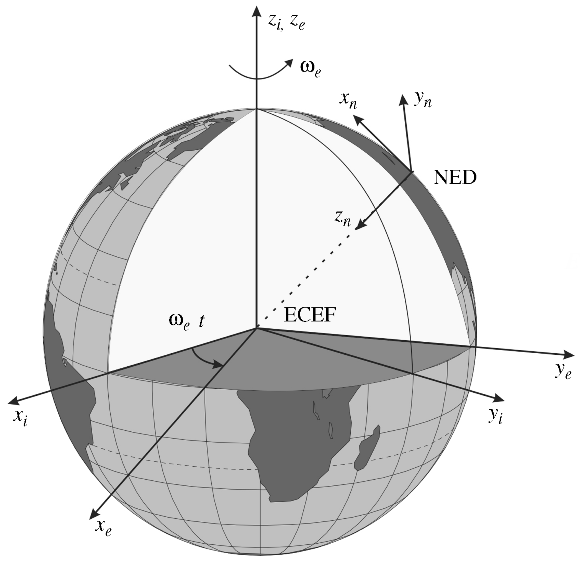

Figure 2.1: The figure shows the ECI frame located within the Earth, the axes pertaining to the ECI frame is x_i, y_i, z_i. The ECEF reference frame is also shown as a part of the figure, the axes pertaining to the ECEF reference frame is x_e, y_e, z_e. The NED reference frame is presented as a tangential plane on the surface of the Earth, the axes pertaining to the NED reference frame is, x_n, y_n, z_n [Fossen 11].

BODY - Body-Fixed Reference Frame

The Body-Fixed Reference Frame (BODY) reference frame has its origin in the CoM of a body. The x-axis describes the longitudinal axis(directed from aft to fore) of the body. The y-axis describes the transversal axis(directed to Starboard) of a body. The z-axis describes the normal axis (directed from top to bottom) of a body. The location of the BODY reference frame can be seen in Figure 2.2. The BODY reference frame is a moving reference frame relative to the inertial reference frame (ECI or NED). The BODY reference frame is used to describe the attitude and translational motion of a body relative to a inertial reference frame.

Path-Fixed Reference Frame

The path-fixed reference frame(PF) is a geographic reference frame which is used when considering Line of Sight guidance. It is mainly used to describe the distance between a vessel and a path, based on this knowledge it is possible to control the vessel towards the path by changing the heading of the vessel. The path-fixed frame is obtained by positive rotation around the z-axis of NED according using right hand convention, and translational movement of NED so the x-axis of NED aligns with the x-axis of PF.

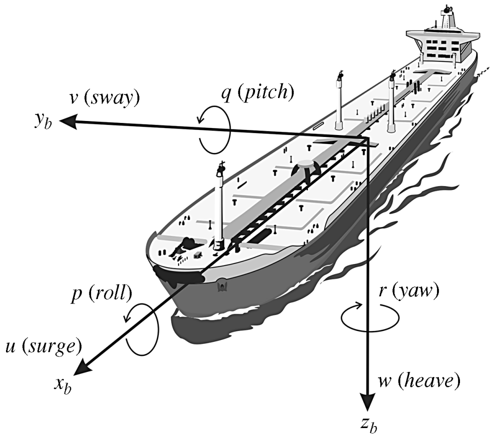

Figure 2.2: The figure shows the placement of the body frame within a vessel. The notation of the axes will be defined later in the present chapter [Fossen 11].

2.2 Notation

The NED reference frame can be considered to be an inertial frame, when flat Earth navigation is used. By using flat Earth navigation it is assumed that the vessel is operating in local waters and not over transatlantic distances. When considering the NED reference frame as a inertial reference frame the Coriolis and centripetal forces caused by the Earth's rotation can be neglected.

The notation used to describe a rigid body is based on the notation seen in Table 2.1.

Movement	Forces and Torques	Linear and Angular Velocities	Position and Euler Angles
Motion in direction of x_b	X	u	x
Motion in direction of y_b	Y	v	y
Motion in direction of z_b	Z	w	z
Rotation around x_b	K	p	ϕ
Rotation around y_b	M	q	θ
Rotation around z_b	N	r	ψ

Table 2.1: The table presents the notation used when modelling a marine vessel [Fossen 11].

The positions and angles of the vessel is represented in the NED reference frame because the NED reference frame is assumed to be the inertial reference frame. The velocities are represented in the BODY frame. The following sections will explain the concepts of terms used when considering a marine vessel.

Heading Angle

The angle ψ, is the angle from the x-axis of NED to the x-axis of BODY see Figure 2.3. Using right hand convention this is done by positive rotation about the z-axis. ψ will further be referred to as the heading angle of the vessel and it is controlled by the main thrusters or the bow thrusters.

Sideslip Angle

The angle β_s, is the angle between the x-axis of BODY and the velocity vector U of the vessel, see Figure 2.3. The rotation is done using right hand convention by positive rotation of the z-axis of BODY. The angle is defined as: $\beta_s \triangleq \arcsin\left(\frac{v}{|U|}\right)$. The sideslip angle is not really considered because it is assumed that the vessel travels in calm waters. But it is present in the formulas in preparation for future work.

Course Angle

The angle χ_c, is the angle from x-axis of NED to the velocity vector U of the vessel. Using right hand convention yields a positive rotation around the z-axis of NED. The course angle is a sum of the heading angle and the sideslip angle: $\chi_\mathrm{c} = \psi + \beta_\mathrm{s}$. AAUSHIP use only the main thrusters to propel it self, the course angle will therefore always align with the x-axis of the BODY frame.

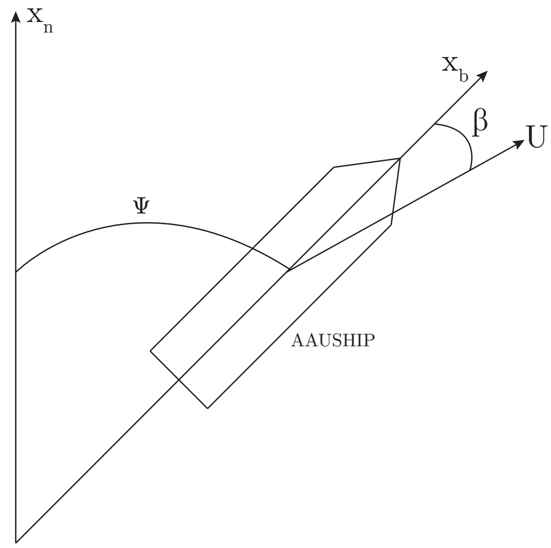

Figure 2.3: Shows how the sideslip angle β relates to the heading angle ψ. The course angle χ_c is a sum of the two angles. U is the resulting velocity vector.

2.3 Rigid Body Kinetics Matrix Representation

The previous section presented the notation used together with the reference frames considered in the present project. The next section will present the non-linear model of a marine vessel. The first section introduces the rigid body kinetics of a marine vessel. The subsequent sections will present the retarding forces which affects a surface vessel. Then the rigid body kinetics and the retarding forces are combined into a state space representation.

The rigid body kinetics for a surface vessel are described by two forces, translational force and rotational force. A surface vessel's translational motion can be described as

$$ {}^{\mathrm{b}}\mathbf{F} = m\,{}^{\mathrm{b}}\dot{\mathbf{v}} + m\,{}^{\mathrm{b}}\boldsymbol{\omega} \times {}^{\mathrm{b}}\mathbf{v} \quad , \tag{2.1} $$

where
${}^{b}\mathbf{F}$ is the force vector of the surface vessel represented in the BODY reference frame
m is the mass of the surface vessel
${}^{b}\dot{\mathbf{v}}$ is the acceleration of the surface vessel represented in the BODY frame
${}^{b}\boldsymbol{\omega}$ is the angular velocity vector described in the BODY reference frame
${}^{b}\mathbf{v}$ is the translational velocity of the surface vessel represented in the BODY reference frame.

For a surface vessel with the center of gravity(CG) coinciding with the center of origin(CO), the total force is described as mass times acceleration For a vessel with differing CG and CO, a rotation around CG will cause a translational movement of CO, this is what the last term in Equation 2.1 describes. The rotational motion of a surface vessel can be described as

$$ {}^{b}\boldsymbol{\tau}(t) = \mathbf{J}{}^{b}\dot{\boldsymbol{\omega}}(t) + {}^{b}\boldsymbol{\omega}(t) \times \mathbf{J}{}^{b}\boldsymbol{\omega}(t) \quad , \tag{2.2} $$

where
${}^{b}\boldsymbol{\tau}(t)$ is the torque vector of the surface vessel represented in the BODY frame
$\mathbf{J}$ is the inertia of the surface vessel represented in the BODY reference frame
${}^{b}\dot{\boldsymbol{\omega}}(t)$ is the angular acceleration of the surface vessel described in the BODY reference frame
${}^{b}\boldsymbol{\omega}(t)$ is the angular velocity of the surface vessel represented in the BODY reference frame.

The inertia of the vessel has been determined by [Dam 14], and the same inertia matrix will be used in the present project. The translational and rotational force equations can be put together in matrix form

$$ \underbrace{\begin{bmatrix} m\mathbf{I}_{3\times3} & 0_{3\times3} \\ 0_{3\times3} & \mathbf{J} \end{bmatrix}}_{\mathbf{M}_{\mathrm{RB}}} \begin{bmatrix} {}^{b}\dot{\mathbf{v}} \\ {}^{b}\dot{\boldsymbol{\omega}} \end{bmatrix} + \underbrace{\begin{bmatrix} \mathrm{m}\,\mathbf{S}({}^{b}\boldsymbol{\omega}) & 0_{3\times3} \\ 0_{3\times3} & -\mathbf{S}(\mathrm{I}{}^{b}\boldsymbol{\omega}) \end{bmatrix}}_{\mathbf{C}_{\mathrm{RB}}} \begin{bmatrix} {}^{b}\mathbf{v} \\ {}^{b}\boldsymbol{\omega} \end{bmatrix} = \begin{bmatrix} {}^{b}\mathbf{F} \\ {}^{b}\boldsymbol{\tau} \end{bmatrix} \quad , \tag{2.3} $$

where
$\mathrm{S}({}^{b}\boldsymbol{\omega}){}^{b}\mathbf{v}$ is ${}^{b}\boldsymbol{\omega} \times {}^{b}\mathbf{v}$ represented as a skew-symmetric matrix.
$\mathbf{M}_{\mathrm{RB}}$ is a combined mass and inertia matrix
$\mathbf{C}_{\mathrm{RB}}$ is the rigid body Coriolis and centripetal force matrix
${}^{b}\boldsymbol{\tau}$ is the torque vector seen in the BODY frame.

The matrix $\mathbf{C}_{\mathrm{RB}}$ represents the force introduced due to the misalignment of the center of gravity and the origin of the body frame. It is not to be confused with the Coriolis and centripetal force caused by the Earth's rotation. Equation 2.3 is made much simpler by removing the Coriolis matrix, since the vessel is of smaller scale and the operational speed of the vessel is small, $||u|| < 2$ [Wondergem 05, Fossen 11].

The origin of the body is a fixed geometrical point within the body, whilst the center of gravity changes depending on the weight distribution of the vessel. In the case of AAUSHIP they both coincide because the weight distribution is constant so it is possible to position the origin of the BODY frame within the center of gravity. The described assumptions makes it possible to neglect the Coriolis and centripetal force matrix, $\mathbf{C}_{\mathrm{RB}}$. Besides neglecting the Coriolis and centripetal force, these assumptions also makes the mass and inertia matrix a diagonal matrix.

The inertia matrix determined by [Dam 14] is shown in Equation 2.4. It is seen from the equation that the inertia of the vessel is mainly distributed around its principal axes. When considering a control problem it is important to control in the principal axes, otherwise it is hard to avoid inducing a torque around other axes than the one controlled. To represent the inertia as a simpler model, an eigenanalysis of the matrix is performed, see Appendix C.2. Based on the analysis it is decided to use an approximated inertia matrix

$$ \mathbf{J} = \begin{bmatrix} 0.06541 & -0.01260 & -0.05359 \\ -0.01260 & 1.08921 & -0.00108 \\ -0.05359 & -0.00108 & 1.10675 \end{bmatrix} \approx \begin{bmatrix} 0.06541 & 0 & 0 \\ 0 & 1.08921 & 0 \\ 0 & 0 & 1.10675 \end{bmatrix} \quad , \tag{2.4} $$

The assumptions mentioned above is used to simplify the model to

$$\begin{bmatrix} m\mathbf{I}_{3\times3} & 0_{3\times3} \\ 0_{3\times3} & \mathbf{J} \end{bmatrix} \begin{bmatrix} {}^{\mathrm{b}}\dot{\mathbf{v}} \\ {}^{\mathrm{b}}\dot{\boldsymbol{\omega}} \end{bmatrix} = \begin{bmatrix} {}^{\mathrm{b}}\mathbf{F} \\ {}^{\mathrm{b}}\boldsymbol{\tau} \end{bmatrix} \quad . \tag{2.5}$$

This equation will be used through the rest of the present thesis to describe the motion of the surface vessel. The rigid body kinetics has been modelled and it is now needed to consider the retarding forces which affects the vessel. The retarding forces is modelled to make the model of the rigid more accurate. The retarding forces considered are hydrostatic forces and hydrodynamic forces, and they will be explained in the forthcoming sections.

2.4 Hydrostatics

The hydrostatics of a marine vessel are the buoyancy forces and gravitational forces also called restoring forces. The buoyancy forces can be interpreted as the spring forces for a mass-spring damper system in fluid. There exist two types of restoring forces, underwater restoring forces and surface restoring forces. The AAUSHIP is a floating vessel so therefore the derivations of the restoring forces are done based on surface restoring forces. For a surface vessel the restoring forces are determined by the volume of the fluid displaced, the placement of the center of buoyancy, the area of the water plane and its moments.

$$\boldsymbol{\tau}(t) = \mathbf{M}_{\mathrm{RB}}\mathbf{v}(t) + g(\boldsymbol{\eta}(t)) \tag{2.6}$$

where

$g(\boldsymbol{\eta})$	is the restoring forces dependent on the position and angles of the rigid body
$\mathbf{v}$	is the velocity vector for the rigid body
$\boldsymbol{\eta}$	is the position and angle vector of the rigid body
$\boldsymbol{\tau}$	is the force and torque vector of the rigid body

For a floating vessel at rest, buoyancy and weight is in balance. The restoring force can be understood as the force which resist inclinations of the boat away from its steady state position when it has been pulled away, see Figure 2.4. An example of this is if the vessel is rotated around the roll axis 10 degrees towards the starboard side, then the restoring force is the force which will pull it towards its initial position.

According to [Fossen 11, pp. 64] the restoring forces for a surface vessel can be expressed as seen in Equation 2.7.

$$\mathrm{g}(\eta) = \begin{bmatrix} -\rho g \int_0^z \mathrm{A}_{wp}(\zeta)d\zeta \ \sin\theta \\ \rho g \int_0^z \mathrm{A}_{wp}(\zeta)d\zeta \ \cos\theta\sin\phi \\ \rho g \int_0^z \mathrm{A}_{wp}(\zeta)d\zeta \ \cos\theta\cos\phi \\ \rho g\nabla\overline{GM}_{\mathrm{T}} \ \sin\phi\cos\theta\cos\phi \\ \rho g\nabla\overline{GM}_{\mathrm{L}} \ \sin\theta\cos\theta\cos\phi \\ \rho g\nabla\left(-\overline{GM}_{\mathrm{L}}\cos\theta + \overline{GM}_{\mathrm{T}}\right)\sin\phi\sin\theta \end{bmatrix} \tag{2.7}$$

where

g	is the gravitational force
∇	is the nominal displaced water volume
ρ	is the water density
A_{wp}	is the water plane area
$\overline{GM}_{\mathrm{L}}$	is the lateral metacentric height
$\overline{GM}_{\mathrm{T}}$	is the transverse metacentric height
ϕ	is the pitch angle
θ	is the roll angle

The nominal displaced water volume is the water moved by the hull when the vessel is e.g pushed down in the heave direction. The gravitational force and water density is approximately constant.

The lateral metacentric height is the distance from the center of gravity to the lateral metacentre, and the same for the transverse metacentric height, only it is the distance to the transverse metacentre. The metacentre are determined by the volume of the vessel and how well the waterline width of the vessel resists overturning. Wide and shallow or narrow and deep hulls have very high metacentres which means that it has a very quick roll and is very hard to overturn. The transverse and lateral metacentric height can be interpreted as stiffness parameter of a boat.

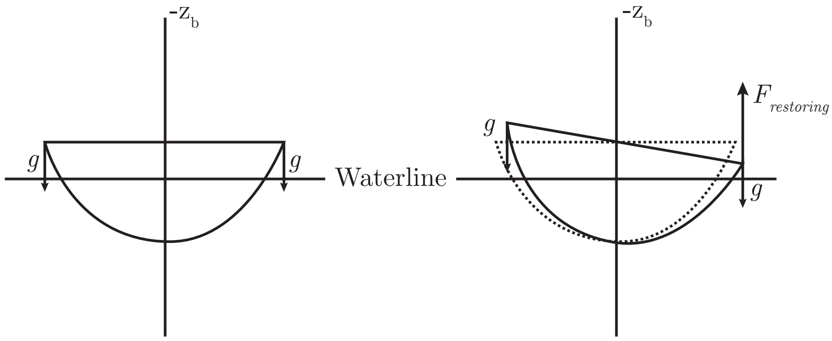

Figure 2.4: The first figure shows the vessel in steady state and the second figure shows a vessel pulled away from its steady state. The second figure shall be seen as the force applied at starboard side has just been removed and therefore a force towards the port side is applied to the vessel.

To simplify and linearise the restoring force expression, a linear small angle theory for boxed shaped vessels can be used. According to [Fossen 11, pp. 64] it is convenient to consider a linear approximation of the restoring forces as

$$g(\boldsymbol{\eta}) \approx \mathbf{G}\boldsymbol{\eta} \tag{2.8}$$

where
$\boldsymbol{\eta}$ is the position and angle vector combined
$\mathbf{G}$ is the restoring force matrix.

The linear approximation is valid due to three assumptions. The first assumption states that the angle ϕ, θ and the position z is small. The second assumption made is that the integral of the water plane area can be approximated to the water plane area at $\zeta = 0$ times the heave position,

$$\int_0^z \mathrm{A}_{wp}(\zeta)d\zeta \approx \mathrm{A}_{wp}(0)z\,. \tag{2.9}$$

The last assumption made is an assumption about the sine and cosine for small angles as

$$\begin{aligned} \sin(\theta) \approx \theta, &\quad \cos(\theta) \approx 1 \\ \sin(\phi) \approx \phi, &\quad \cos(\phi) \approx 1\,. \end{aligned} \tag{2.10}$$

The restoring force matrix has been determined by [Dam 14], and based on the assumptions the restoring force matrix can be approximated to

$$\mathbf{G} = \texttt{diag}\begin{bmatrix} -\rho g \mathrm{A}_{wp}(0)z\ \theta \\ \rho g \mathrm{A}_{wp}(0)z\ \ \phi \\ \rho g \mathrm{A}_{wp}(0)z \\ \rho g \nabla \overline{GM}_{\mathrm{T}}\ \phi \\ \rho g \nabla \overline{GM}_{\mathrm{L}}\ \theta \\ \rho g \nabla\left(-\overline{GM}_{\mathrm{L}} + \overline{GM}_{\mathrm{T}}\right)\phi\,\theta \end{bmatrix} \approx \texttt{diag}\begin{bmatrix} 0 \\ 0 \\ 0 \\ 6.9736 \\ 131.8316 \\ 0 \end{bmatrix}\,. \tag{2.11}$$

The are missing some parameters in the restoring force model, they have not been determined because there are no facilities available at the moment. So if future work with AAUSHIP is considered it might be advantageous to determine all of the parameters again. This section has determined the restoring forces affecting AAUSHIP. The next section will determine the hydrodynamic forces affecting AAUSHIP.

2.5 Hydrodynamics

The hydrodynamic forces can be modelled according to two formalisms, seakeeping theory and manoeuvring theory. Seakeeping theory refers to the motional study of a marine vessel with constant course and constant speed, when there is wave excitation. Manoeuvring theory considers the motion of a vessel not affected by wave excitation i.e calm waters. The seakeeping theory is a linear theory and is therefore limited because of the need for approximating the fluid memory effect using transfer function or impulse responses. It is assumed that AAUSHIP has to travel in waters that are calm due to the relatively small size and weight of the vessel. It is also wanted to model the non-linear hydrodynamic forces, therefore the hydrodynamic forces to be considered in the forthcoming section will be based on manoeuvring theory.

The hydrodynamics are included in the model of the marine vessel, see Equation 2.12, this is done by adding a matrix $\mathbf{D}(\boldsymbol{\nu})$ which is dependent on the velocity of the vessel

$$\boldsymbol{\tau}(t) = \mathbf{M}_{\mathrm{RB}}\mathbf{v}(t + \mathbf{G}\boldsymbol{\eta}(t) + \mathbf{D}(\boldsymbol{\nu}(t))\boldsymbol{\nu}(t) \quad . \tag{2.12}$$

where

$\boldsymbol{\nu}(t)$	is the translational and rotational velocities combined into one vector
$\mathbf{D}(\boldsymbol{\nu}(t))$	is the hydrodynamic force dependent on the combined velocity vector.

When considering the damping of a marine vessel there are three effects that are very important. The first on is called added mass which is a force caused by the inertia of the surrounding fluid. The second effect is viscous damping which is caused by skin friction, wave drift damping, vortex shedding and lift/drag. The last effect are radiation-induced potential damping, due to the energy carried away by generated surface waves. All of the effects described above is collected into one matrix called the hydrodynamic damping matrix. The total hydrodynamic damping matrix $\mathbf{D}(\boldsymbol{\nu}(t)$ is the sum of both the linear damping, $\mathbf{D}$, and the non-linear damping,$\mathbf{D}_n(\boldsymbol{\nu}(t))$. According to [Fossen 11, pp. 130] the non-linear damping matrix can be expressed as seen in Equation 2.13 and the linear damping matrix can be seen in Equation 2.14.

$$\mathrm{D}_n(\nu) = -\begin{bmatrix} X_{|u|u}\,|u| & 0 & 0 & 0 & 0 & 0 \\ 0 & Y_{|v|v}\,|v| + Y_{|r|v}\,|r| & 0 & 0 & 0 & Y_{|v|r}\,|v| + Y_{|r|r}\,|r| \\ 0 & 0 & Z_{|w|w}\,|w| & 0 & 0 & 0 \\ 0 & 0 & 0 & K_{|p|p}\,|p| & 0 & 0 \\ 0 & 0 & 0 & 0 & M_{|q|q}\,|q| & 0 \\ 0 & N_{|v|v}\,|v| + N_{|r|v}\,|r| & 0 & 0 & 0 & N_{|v|r}\,|v| + N_{|r|r}\,|r| \end{bmatrix} \tag{2.13}$$

The parameters shown in Equation 2.13 shall be seen as damping forces and torques affecting the velocity of the vessel in different ways.

$$\mathbf{D} = -\begin{bmatrix} X_u & 0 & 0 & 0 & 0 & 0 \\ 0 & Y_v & 0 & Y_p & 0 & Y_r \\ 0 & 0 & Z_w & 0 & Z_q & 0 \\ 0 & K_v & 0 & K_p & 0 & K_r \\ 0 & 0 & M_w & 0 & M_q & 0 \\ 0 & N_v & 0 & N_p & 0 & N_r \end{bmatrix} \tag{2.14}$$

The total damping of a marine vessel is the sum of these two damping matrices 2.15

$$\mathbf{D}(\boldsymbol{\nu}(t)) = \mathbf{D} + \mathbf{D}_n(\boldsymbol{\nu}(t))\,. \tag{2.15}$$

The total damping matrix can be determined by the use of different commercial programs, these programs are not available during the present project. The damping matrix has therefore been determined experimentally by [Dam 14]. The damping matrix determined is the total damping matrix, the matrix is lacking some of the damping parameters due to unavailability of proper facilities. In Equation 2.16 the experimentally determined parameters can be seen, these will be the ones used in the model

$$\mathbf{D}(\boldsymbol{\nu}) \approx -\begin{bmatrix} 2.86\,|u| & 0 & 0 & 0 & 0 & 0 \\ 0 & 32\,|v| & 0 & 0 & 0 & 0 \\ 0 & 0 & 0 & 0 & 0 & 0 \\ 0 & 0 & 0 & 0.1094\,|p| & 0 & 0 \\ 0 & 0 & 0 & 0 & 2.2030\,|q| & 0 \\ 0 & 0 & 0 & 0 & 0 & 0.26285\,|r| \end{bmatrix} \tag{2.16}$$

The previous subsections has presented the rigid body kinetics together with the retarding forces. The rigid body kinetics is based on the derivations explained in Appendix C and in [Fossen 11]. The retarding forces modelled are based on the experimental work done by [Dam 14]. In the following section a state space representation of the model presented in Equation 2.12 will be presented.

2.6 State-Space Representation of Surface Vessel Model

The complete model determined in the previous section will in this section be represented in state space form. Two different state space models will be represented, one describing 6 degrees of freedom(DOF) and one describing 3 DOF. The models presented will have different uses which will be explained in the respective section.

2.6.1 6 DOF State Space Model

In control and estimation theory the standard representation of a system model is state-space representation. The state space form of the surface vessel can be seen in Equation 2.17. The model contains; the system matrix which holds the dynamics of the system, the input matrix which determines the distribution of the input signal and which state it should influence, The disturbance distribution matrix which is used to determine which states the wind and waves are affecting. All of the matrices have a vector connected to them; the state vector determines which states the system has for a marine vessel it is the 6 DOF, the input vector is determined by the propulsion system, the disturbance vector is determined by the weather conditions or model uncertainties.

$$\dot{\mathbf{x}}(t) = \mathbf{A}\mathbf{x}(t) + \mathbf{B}\mathbf{u}(t) + \mathbf{E}\mathbf{d}(t) \tag{2.17}$$

where

$\mathbf{A}$	is the system matrix which contains the system dynamics
$\mathbf{B}$	is the input matrix containing the distribution of the input signal
$\mathbf{E}$	is the disturbance distribution matrix
$\mathbf{x}(t)$	is the state vector containing positions, angles and velocities, $\mathbf{x}(t) = \begin{bmatrix}\boldsymbol{\eta}(t) & \boldsymbol{\nu}(t)\end{bmatrix}^{\mathrm{T}}$
$\mathbf{u}(t)$	is the input vector containing external torques form the propulsion system.
$\mathbf{d}(t)$	is the disturbance vector due to wind and waves

According to [Fossen 11, pp. 175] the model represented in the earlier sections can be transformed into a state space representation in the following way:

$$\mathbf{A} = \begin{bmatrix} \mathbf{0}_{6x6} & \mathbf{I}_{6x6} \\ -\mathbf{M}_{\mathrm{RB}}^{-1}\mathbf{G} & -\mathbf{M}_{\mathrm{RB}}^{-1}\mathbf{D} \end{bmatrix}, \quad \mathbf{B} = \begin{bmatrix} \mathbf{0}_{6x6} \\ \mathbf{M}_{\mathrm{RB}}^{-1} \end{bmatrix}, \quad \mathbf{E} = \begin{bmatrix} \mathbf{0}_{6x6} \\ \mathbf{M}_{\mathrm{RB}}^{-1} \end{bmatrix} \tag{2.18}$$

The measurement model is based on the sensors implemented on AAUSHIP. The measurements from the sensors are not necessarily the measured state,there might be a need to convert some of the measurements to retrieve the states. This conversion will not be handle in the present thesis. The sensors is therefore chosen to be equal to the state they should measure with added noise. This means e.g the magnetometer is modelled as the angles and the angular velocities with added noise. The sensors will from this point on be referred to as the actual sensor or just the state name e.g heading sensor instead of magnetometer. The output equation can be seen below

$$\mathbf{y} = \mathbf{C}\mathbf{x}(t) + \mathbf{w}(t) \tag{2.19}$$

where
$\mathbf{y}$ is the output vector of the system
$\mathbf{w}$ is the noise vector
$\mathbf{C}$ is the output matrix

It is assumed that the states are measured directly so, the matrix $\mathbf{C}$ is chosen as a identity matrix. It can be seen from the equation that the sensor measurements are affected by noise. To determine the magnitude of the noise vector a sensor noise analysis have been performed by making a static test of the sensors, see Appendix B.

2.6.2 3 DOF State Space Model

Further in the present thesis fault diagnosis and a control law is designed. When considering the surface vessel as a control problem or a fault diagnosis problem it is not needed to include states that are not relevant for the motion of the surface vessel. The model is therefore reduced to a 3 DOF model

$$\dot{\begin{bmatrix} x \\ y \\ \psi \end{bmatrix}} = \mathbf{A}_{3\times3} \begin{bmatrix} x \\ y \\ \psi \end{bmatrix} + \mathbf{B}_{3\times3} \begin{bmatrix} X \\ Y \\ N \end{bmatrix} + \mathbf{E}\mathbf{d} \tag{2.20}$$

This model will be used when considering the control problem and the design of auxiliary signal. The three states included in the 3 DOF model is x, y, and ψ. These are also the only states affected by the generalised input vector. The next section will describe the thrust allocation, which will represent the generalised input vector as a combination of the thrust applied to each of the vessel's thrusters.

2.7 Thrust Allocation

The state space model derived uses a generalised input vector, this input vector needs to be changed into a input vector matching the propulsion system of the AAUSHIP. The vessel has four thrusters which is not yet included in the model, this will be done in this section.

It is normal practice to use a dynamic model to represent the thrusters, in the case of the present thrusters it is not needed, due to their very high time constants. This means that the thrusters can be modelled just by allocating their influence on the total force. The allocation can be done for both the translational force and rotational force separately. The allocation of thrust can be set up mathematically as

$$\mathbf{F}_{\mathrm{ext}} = \mathbf{B}'_{\mathbf{F}}\mathbf{u}_{\mathrm{m}} \tag{2.21}$$

where

$\mathbf{B}'_\mathrm{F}$	is a motor thrust allocation matrix
$\mathbf{u}$	is the motor input to each of the four motors
$\mathbf{F}_\mathrm{ext}$	is the total force applied in the direction of the three axes.

The matrix $\mathbf{B}'_\mathrm{f}$ is designed based on the location of the motors within the AAUSHIP body, as shown in Chapter 1. The vector $\mathbf{u}_\mathrm{m}$ is the force input to each of the four thrusters, which combined will result in the generalized force vector acting on the system. The allocation of the torques are done as

$$\boldsymbol{\tau}_\mathrm{ext} = \mathbf{B}'_\tau \mathbf{u}_\mathrm{m} \tag{2.22}$$

where

$\mathbf{B}'_\tau$	is a motor torque allocation matrix
$\boldsymbol{\tau}_\mathrm{ext}$	is the total torque applied around the three axes.

As for the force allocation the matrix $\mathbf{B}'_\tau$ is designed based on the location of the thrusters within the vessel body. The vector $\mathbf{u}_\mathrm{m}$ is as for the force allocation the force input of each of the thrusters, which combined results in the generalised torque vector.

AAUSHIP is equipped with four thrusters which pairwise when given the right input will give a thrust in one direction. The vessel will e.g travel in the surge direction if a correct input is given to the main thrusters, the same for the starboard and port side thrusters. The port side and starboard thrusters are not used in the present project, but they are included to show that there is other ways of controlling the vessel even if a thruster fails. The yaw motion allocation, caused by the thrusters displacements, seen in the last row of the matrix is calculated as

$$\boldsymbol{\tau}_{1-4} = \mathbf{d}_{1-4} \times \mathbf{F}_{1-4} \tag{2.23}$$

This displacement causes a torque around the z-axis of the BODY frame if there is a difference between the input applied to each of the main thrusters. The displacement of the thrusters can be seen in figure 2.5.

By calculating the torque caused by the displacement of the thrusters, a joined allocation matrix can be designed as

$$\mathbf{B}' = \begin{bmatrix} 1 & 1 & 0 & 0 \\ 0 & 0 & 1 & 1 \\ 0 & 0 & 0 & 0 \\ 0 & 0 & 0 & 0 \\ 0 & 0 & 0 & 0 \\ 0.05 & -0.05 & 0.2 & -0.42 \end{bmatrix} \tag{2.24}$$

It can be seen from the matrix that the port side and starboard thrusters are not displaced equally from the center of mass. A consequence of this is that the input vector has to weigh one of the thrusters to compensate for this. The port side and starboard thrusters are not used in the present project so no further work will be done to resolve this problem, but it is important to consider this problem if they are to be used. The thrust allocation matrix is combined with the 6 DOF state space model describe in the previous section

$$\dot{\mathbf{x}}(t) = \mathbf{A}\mathbf{x}(t) + \mathbf{B}\mathbf{B}'\mathbf{u}(t) + \mathbf{E}\mathbf{d}(t) \tag{2.25}$$

The implementation of the thrust allocation makes it possible to simulate a fault occurring on one of the vessel's thrusters. Besides this it is also important to implement the thrust allocation

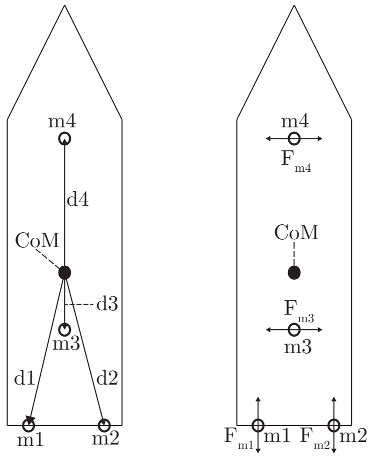

Figure 2.5: The picture shows two sketches of the vessel. The first vessel shows the displacement vector from CoM to the four motors, each of the displacement vectors are used to determine the yaw torque exerted by the four motors. The second vessel shows in what direction each of the four motors is able to apply a translational force.

matrix to make the model and the real vessel more alike. The next section will describe the how the model verification is done. This is important to check if the model exhibits the expected behaviour.

2.8 Model Verification

The model is verified by applying a input sequence to the model and seeing if the model exhibits the expected behaviour, the input sequence used can be seen in Figure 2.7.

Based on the thrust allocation described previously the model should sail in a straight line when the input to both main thrusters are equivalent and turn when they are different from each other. The input sequence is designed so the vessel sails straight at the beginning of the trajectory and starts to turn after about 3 seconds into the simulation. The exhibited behaviour of the model can be seen in Figure 2.6, it can be seen from the figure that the model exhibits the behaviour which was expected using the designed input sequence.

By using the designed input sequence the vessel sails with a velocity evolution over the simulated time interval which can be seen in Figure 2.8. The input sequence is designed to have nine changes, in the velocity(counting the initial input as the first change) which is consistent with the changes seen on the velocity evolution.

The vessel's acceleration during the travelled trajectory can be seen in Figure 2.8. The figure shows that the acceleration changes nine times as would be expected using the designed input sequence. The magnitude of the acceleration also lies within the expected area considering the force applied to the vessel. By comparing the velocity and the acceleration plot it can also be seen that they are consistent with each other as would have been expected if the model was correct.

Subconclusion

Based on the verification of the model it is determined that the model exhibits the expected behaviour. The trajectory which the vessel sailed is consistent with the trajectory expected considering the designed input sequence. The velocity and acceleration during the test also matched the expected result based on the designed input sequence.

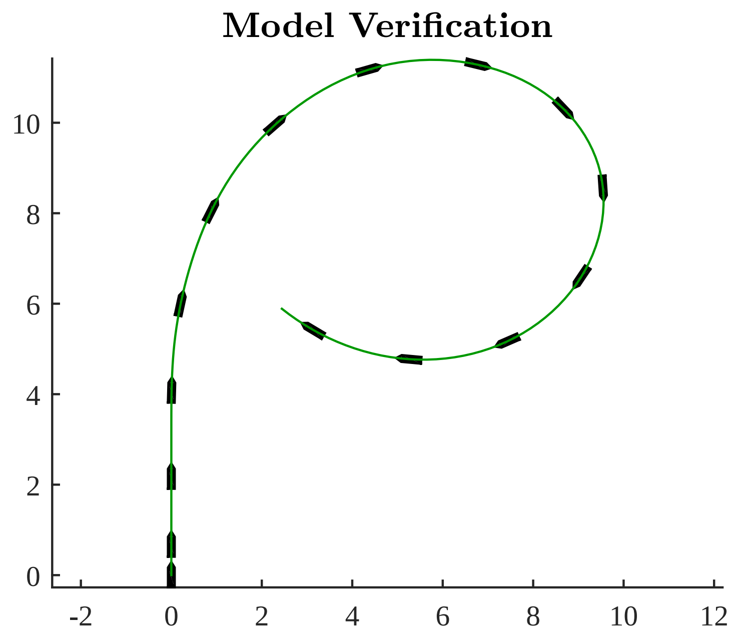

Figure 2.6: The picture shows the simulated model of the vessel, implemented in MATLAB. The green line indicates the trajectory of the vessel. The black masses represents the vessel and its heading at a given position. The input vector is a designed sequence which makes the vessel sail straight and then turn.

In future work some improvements can be done to improve the accuracy of the model such as determining some of the undetermined parameters in the damping force and the restoring force. Besides improving the retarding force models it is also possible to improve the measuring model so it contains the GPS clock drift and the noise colour of the sensors as described in Appendix B.

This chapter derived a model for the marine vessel AAUSHIP based on its rigid body kinetics, hydrostatics and the hydrodynamics of the vessel. The derived model has then been transformed into a state space model which will be used further on in the present thesis. The model has been verified and it exhibits the desired behaviour.

The forthcoming chapters will revolve around the design of different subsystems based on the derived model. The systems to be designed, based on the overall project scope and the model of the vessel, can be seen in Figure 2.9.

The aim of the present thesis is to design a a path/following control system together with an active fault diagnosis scheme. The next chapter will set up some requirements for the systems to be designed. The requirements are based on the information gained in Chapter 1.

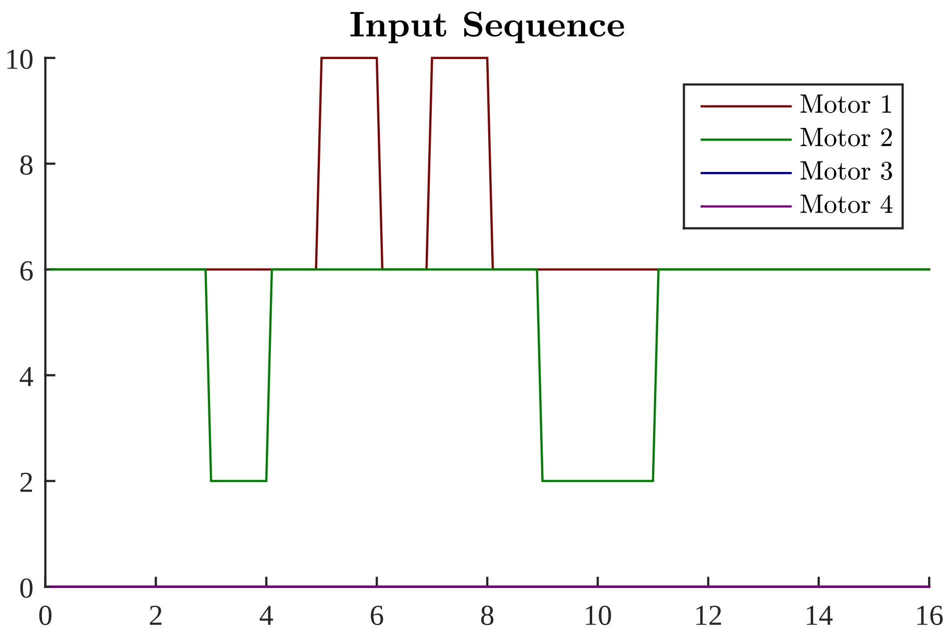

Figure 2.7: The figure shows the input sequence used to verify the model, it shall be noted that the vessel starts the verification at a input level of 6.

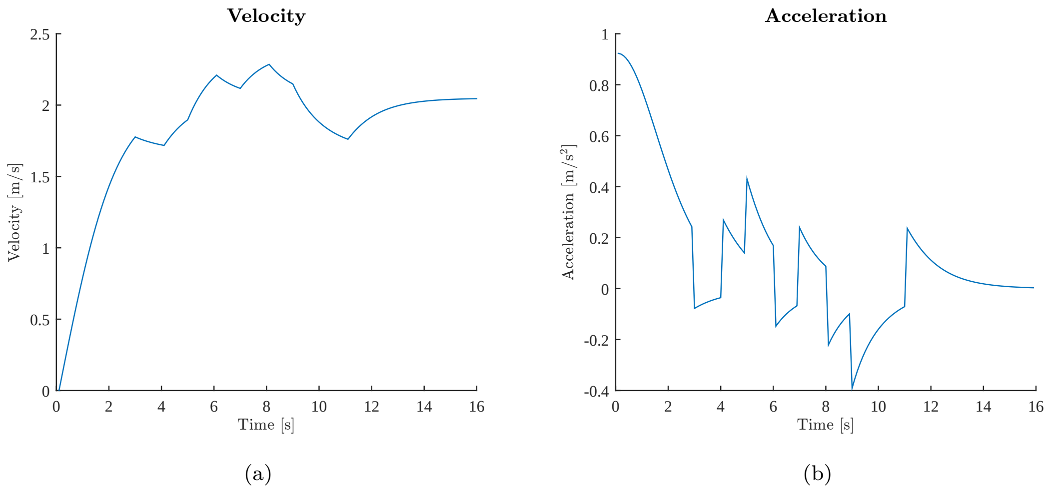

Figure 2.8: The figure presents the evolution of the velocity and the acceleration. It can be seen in the figure that the velocity and the acceleration plots is consistent with each other.

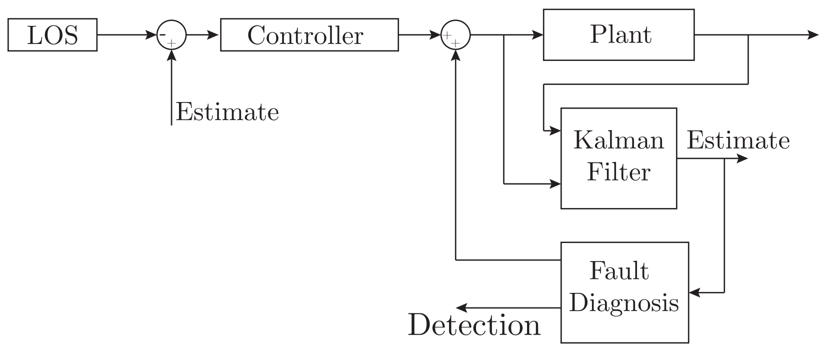

Figure 2.9: The figure presents the overall design strategy for the present thesis. The figure is just a sketch to show the functionality of the system designed.

Chapter 3

AAUSHIP Requirements Specification

To verify the systems designed in the present thesis a set of requirements are presented. The overall system shall comply with a set of requirements which will be used to determine the success of the system. Besides the overall system requirements, will each subsystem have a set of requirements to which they shall comply.

3.1 Overall System Requirements

The overall system requirements are based on the performance of the fault diagnosis designed. When considering requirements for a fault diagnosis system it is important to avoid false detections and missed detections, the most important of the two is the missed detection. The amount of false detections describes the number of faults which are detected without being present. A missed detection describes the opposite situation where a fault has occurred without being detected. The mission for AAUSHIP is to survey and pilot. During these tasks there are some very safety critical manoeuvres. So to avoid any dangerous situations it is desired to have no missed detections. The false detections are not as critical as the missed detections, but they can become an annoyance for the user/operator of the vessel. Besides becoming an annoyance, to many false detections will also deem the fault diagnosis unreliable and it therefore losses its function. Therefore it is chosen to allow one false detection per 100 missions.

Identifier	Requirement	Value	Unit
M1.R1	False Detections	1%	[·]
M1.R2	False Detection Duration	1	[s]
M1.R3	Missed Detections	0	[·]
M1.R4	Maximum Path Deviation	3	[m]

To assist the operator in determining whether a fault has occurred, the false detections may only be present in a maximum duration of 1s. It is desired to have a vessel which does not deviate form the path, this is an ideal requirement which can not be obtained. It is therefore chosen to have a requirement stating that the vessel may not deviate a significant distance from the path. For the present thesis it is deemed sufficient to have a path deviation below 3m. This requirement can be changed if there is a needed of increased accuracy.

Verification of Requirements

The requirements stated here will be verified by an accept-test. The vessel will be carrying out a surveying mission, and during the mission a fault will enter the system in a specified time. The fault diagnosis designed shall then register that a fault has occurred. The test will be performed a 100 times to determine if there will be any false detections or missed detections.

3.2 Subsystem Requirements

The mission of AAUSHIP is to perform hydrographic surveying autonomously. This means that it shall be possible for a operator to generate a path which the vessel shall follow. For the purpose of this a path-following controller will be designed together with a position and attitude determination scheme. The verification of these two subsystems will be done based on the requirements presented in the forthcoming section.

3.2.1 Path-Following Control

The AAUSHIP is assumed to be equipped with a multi-beam echo-sounder which is the same type which is used on the existing surveying vessel. For AAUSHIP to be successful it has to perform as good as or better than the existing surveying vessel. A commercial multi-beam echo-sounder, as the M3 sonar system from Kongsberg Maritime, is used as a guideline for the requirements because of its shallow water surveying capabilities [Maritime 15]. The maximum speed at which the echo-sounder has been operated is 9.5 kts, which is equivalent to 4.88 m/s. It is not wanted to operate the sonar at its limit so the speed requirement is set to 2 m/s.

Identifier	Requirement	Value	Unit
SS1.R1	Max Path Deviation	2.5	[m]
SS1.R2	Turning Radius	180	[°]
SS1.R3	Mean Velocity	2	[m/s]

Table 3.1: The table shows the requirements for the path-following control, the results obtained at the end of the present thesis will determine if the results are accomplished.

The operator has the possibility to generate different paths for the purpose accomplishing different objectives such as surveying and piloting. To accommodate the majority of paths, a requirement is set up for the turning radius of the vessel. For the purpose of surveying the most realistic path would be a lawn mower pattern, which will cover a square in a minimal amount of turns and no areas will be covered twice, the pattern will be shown later on. Many other paths can be generated but for the present thesis this path is assumed to be the best fit for the task. The path used for piloting can not be determined beforehand because it is problem dependent path. This means that the operator has to change the path dependent on the piloting task. When piloting there might be a need to turn the vessel around to intercept the ship, which needs piloting. Based on these needs the vessel shall be able to make a turn of minimum 180 °. This is possible to do for a majority of vessels if there are no restrictions on the path deviation. To ensure the safety of AAUSHIP and other vessels in the vicinity of AAUSHIP, it is desired to restrict the path deviation. This leads to the next requirement which is; the vessel's path deviation may not be more than 3m when the vessel is on the path. A minimum turn radius of 180° is a requirement specified for the piloting operation of the vessel, and not so much for the surveying, but it is wanted to have a vessel which is versatile and can do both assignments without doing adjustments. This is desired because the operators background is not known so it is not certain that the operator has a engineering background which gives him the competences to change the software on the vessel.

Verification of Requirements

The path-following control will be tested using two different paths. The first path which is a straight line will be used to test requirement SS1.R2. The vessel shall follow a straight line segment until it reaches a way-point and has to return to its start position. This test will reveal if the vessel is able to turn 180° without exceeding requirement SS1.R1. The second path shall be used to verify compliance with requirement SS1.R1 and SS1.R3. The path will be a surveying path, which the vessel shall follow. During this test the vessel may not deviate from the path by more than 3m as specified by requirement SS1.R1. The vessel shall also be sailing with a mean constant speed of at least 2m/s as specified by requirement SS1.R3.

3.2.2 Position and Attitude Determination

The requirements for the position and attitude determination is based on the requirements stated in the previous section. The maximum path deviation for the path-following controller is determined to be 2.5m, this leaves 0.5m of deviation for the position and attitude determination. The requirement for the accuracy of the position estimate is chosen to be 0.5m. The surge velocity estimate will be used to help verify the performance of the position and attitude determination. If a surge velocity controller is to be designed it would be necessary to have a good estimate, so the vessel do not overshoot the path. Therefore it is chosen to have surge velocity requirement of 0.1 m/s.

Identifier	Requirement	Value	Unit
SS2.R1	Position Estimate Accuracy	0.5	[m]
SS2.R2	Velocity Estimate Accuracy	0.1	[m/s]
SS2.R3	Heading Estimate Accuracy	3.6	[°]

The last requirement set up for the position and attitude determination is for the heading estimate. Because there is a requirement for the position estimate it is also needed to set up a requirement for the heading estimate to make sure that the vessel do not travel in the wrong direction which will lead to a increase in the cross track error because the vessel will stray from the path. The heading estimate requirement is set to 3.6 ° because this will result in a increase in the cross-track error of 2.5cm considering a vessel travelling with a speed of 4 m/s and a sample rate of 10 Hz.

Verification of Requirements

The position and attitude determination is tested using a designed input sequence which turns in different directions. The estimation performed during this trajectory will then be analysed to determine how accurate the estimate is. The obtained results will then be compared with the system requirements stated above. Three things will be investigated, the position estimation error, the heading estimation error and the velocity estimation error.

The test requirements for the systems to be designed have now been presented. The success and failure of a system will be determine based their compliance with the listed requirements. The next section will present the designed position and attitude determinations. The chapter will compare two methods to find the best suited for implementation on the vessel.

Chapter 4

Position and Attitude Determination

Based on the sensor analysis performed in Appendix B, two position and attitude determination methods was designed. The two estimation filters considered in the present thesis is, an extended Kalman filter and an unscented Kalman filter. The performance of the two filters were investigated to determine which one of them performed the best. It is chosen to investigate these two filters, because they are known to handle non-linearities in dynamic models. The non-linearities of the model is caused by the damping forces, and has the characteristics of a second order polynomial. The results obtained in the forthcoming sections will determine which of the filters should be implemented on AAUSHIP.

4.1 Kalman Filter

The Kalman filter can in general be divided into two parts, a prediction step and a update step, see Figure 4.1. The prediction step is used guess the present value of the state, based on the model, the inputs, the process covariance and the posteriori error covariance. The estimate can be computed based on the prediction, the measurement and the sensor model. The estimate is then weighted by the Kalman gain which is is used to correct the estimate based on the error covariance. This is the fundamental steps in both filters, but there are differences in the way they are computed. The chapter is based on the sources [Grewal 08, Kim 11][Thr06] located on the CD.

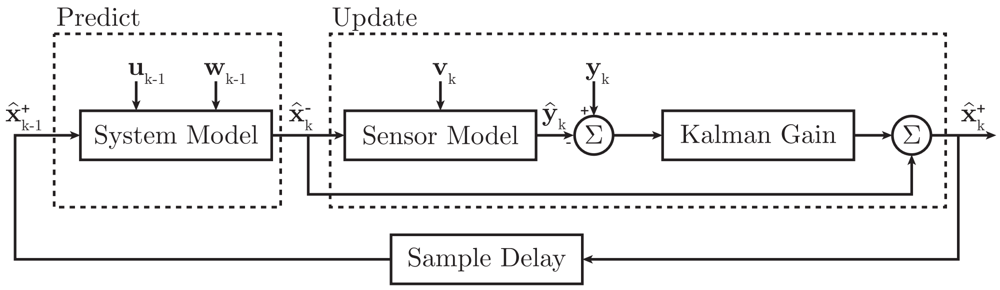

Figure 4.1: The block diagram illustrates the two steps used in the Kalman filter. The predict step contains the propagation of the model and the update step contains the sensor model and the Kalman gain.

A main characteristic of the extended Kalman filter is that it uses a linearisation of the model utilising the previous estimate as an operational point. So at every time step the operational point changes and the model is linearised in the new operational point. This is the biggest difference between the linear Kalman filter and the extended Kalman filter. The unscented Kalman filter differs a bit from the previous mentioned filters. The state distribution of the uncented Kalman filter is still represented as a Gaussian random variable(GRV), but it is now specified by a minimal set of carefully chosen sample points. These sample points are to catch the true mean and covariance of the GRV, and when propagated through the non-linear model, also catch the posterior mean and covariance up to a 3$^{\text{rd}}$ order Taylor approximation.

This section explained some of the differences between an extended Kalman filter and an unscented Kalman filter. The differences described here will also help determine which filter is to be implemented. The calculations used to implement the Kalman filter can be seen in Appendix A. The next section will describe the implementation and results of the two filters and at the end of the section a conclusion on both filters will be made. Based on the conclusion one of the filters are chosen for further work.

4.2 Kalman Filter Implementation

An important part of tuning a Kalman filter is to determine the right relationship between the process covariance matrix, $\mathbf{Q}$, and the measurement covariance matrix, $\mathbf{R}$. The measurement covariance matrix is determined using the variances obtained from the sensor analysis, see Appendix B. The $\mathbf{R}$ is designed to be a diagonal matrix containing the variances shown in Table 4.1.

Sensor	Noise Magnitude	Unit
Magnetometer	10^{-6}	[G]
Accelerometer	10^{-4}	[g]
Gyroscope	10^{-1}	[$\circ$/s]
GPS Longitude	10^{-6}	[m]
GPS Latitude	10^{-5}	[m]

Table 4.1: The table shows the magnitude of the noise expected on the output from each sensors based on the sensor noise analyses described in Appendix B

With the $\mathbf{R}$ matrix determined it is possible to use the $\mathbf{Q}$ matrix as a tuning matrix to determine whether to trust the model or the sensors of the system. The initial states are assumed to be zero and the matrix $\mathbf{P}_0$ is designed to contain values which is found realistic considering the range of the different states. This means that all values in $\mathbf{P}_0$ is not set to the same value because this results in unrealistic behaviour, e.g if $\mathbf{P}_0$ is a diagonal matrix containing only the value 10, this means that the translational speed error is 10m/s and the position error is off by 10m. So the matrix $\mathbf{P}_0$ is set to have values corresponding to its expected behaviour. The values used in both filters can be seen below:

$$\mathbf{Q} = \texttt{diag}\begin{bmatrix}1 & 1 & 1 & 1 & 1 & 1 & 1 & 1 & 1 & 1 & 1 & 1\end{bmatrix} \tag{4.1}$$

$$\mathbf{R} = \texttt{diag}\begin{bmatrix}1 & 10 & 0.001 & 1 & 1 & 1 & 100 & 100 & 100 & 1 & 1 & 1\end{bmatrix} 10^{-6} \tag{4.2}$$

$$\mathbf{P} = \texttt{diag}\begin{bmatrix}0.1 & 0.1 & 0.1 & 0.1 & 0.1 & 0.1 & 0.2 & 0.2 & 0.2 & 0.05 & 0.05 & 0.05\end{bmatrix} \tag{4.3}$$

The values shown above are temporary values which can be changed in the individual implementation of the filters when tuned. When determining the values in the matrix $\mathbf{Q}$, one shall bear in mind that small values in $\mathbf{Q}$ is the same as putting more "trust" in the model. The values chosen has to be consistent with the system noise to obtain realistic performance. Due to the uncertainties in the model of AAUSHIP, due to unmodelled disturbances, the values are set very conservatively but with overhead to tune with.

Implementation of EKF

The exteneded Kalman filter is implemented using the equation described in Appendix A. The linearisation performed by the extended Kalman filter is based on the computation of a Jacobian. The Jacobian for the model is determined by taking the derivative of the system matrix described in Chapter 2. The structure of the Jacobian can be seen in Equation 4.4.

$$\boldsymbol{\Phi} = \begin{bmatrix} 0 & 0 & 0 & 0 & 0 & 0 & 1 & 0 & 0 & 0 & 0 & 0 \\ 0 & 0 & 0 & 0 & 0 & 0 & 0 & 1 & 0 & 0 & 0 & 0 \\ 0 & 0 & 0 & 0 & 0 & 0 & 0 & 0 & 1 & 0 & 0 & 0 \\ 0 & 0 & 0 & 0 & 0 & 0 & 0 & 0 & 0 & 1 & 0 & 0 \\ 0 & 0 & 0 & 0 & 0 & 0 & 0 & 0 & 0 & 0 & 1 & 0 \\ 0 & 0 & 0 & 0 & 0 & 0 & 0 & 0 & 0 & 0 & 0 & 1 \\ 0 & 0 & 0 & 0 & 0 & 0 & -0.4400 & 0 & 0 & 0 & 0 & 0 \\ 0 & 0 & 0 & 0 & 0 & 0 & 0 & -4.9231 & 0 & 0 & 0 & 0 \\ 0 & 0 & 0 & 0 & 0 & 0 & 0 & 0 & 0 & 0 & 0 & 0 \\ 0 & 0 & 0 & -106.6137 & 0 & 0 & 0 & 0 & 0 & -3.3451 & 0 & 0 \\ 0 & 0 & 0 & 0 & -121.0341 & 0 & 0 & 0 & 0 & 0 & -4.0451 & 0 \\ 0 & 0 & 0 & 0 & 0 & 0 & 0 & 0 & 0 & 0 & 0 & -0.4750 \end{bmatrix} \tag{4.4}$$

The filter performance shall be tuned to trust both the model and the sensor measurements. This shall be done to smooth out the noise affecting the sensors, but without trusting only the model. During the implementation some problems occurred when trying to tune the matrices, $\mathbf{Q}$ and $\mathbf{R}$. After investigating the matrices and trying to alter their relationship. it was found that by increasing the $\mathbf{R}$ matrix by 10^5 it was possible to remove the problem. The matrix $\mathbf{Q}$ was also multiplied with 10^5 to maintain the relationship between the two matrices. It is assumed that the problems are caused by numerical inaccuracies in MATLAB. This has to be kept in mind when considering implementation of the estimation algorithm on to the prototype.

Implementation of UKF

The unscented Kalman filter is implemented utilising the equations described in Appendix A. There are three scaling parameters to determine for the implementation of the unscented Kalman filter, α, β, and κ. The values for these three parameters are set to 10^{-3}, 0, and 2, respectively. This gives weights in the unscented Kalman filter which sums to $\frac{1}{2}$. The scaling parameters are tuning parameters chosen based on the filter performance.

To determine the sigma points the matrix square root is used, an efficient way to implement the matrix square root is by the use of a Cholesky decomposition as described in [Crassidis 03] and [Vinther 10]. During implementation there have been problems with the $\mathbf{P}$ containing imaginary numbers if the MATLAB function `sqrtm` was used. The variable L is equal to the number of states, this results in 25 sigma point, because the mean value is also include in the sigma points.

When implementing the unscented Kalman filter it is important to include the Q and R matrices in the calculations, some sources exclude these matrices in the calculation of the apriori error covariance and the measurement covariance, see CD material [Thr06]. The Q and R matrices are not tuned any further than described in Equation 4.1 and Equation 4.2, this is because the estimation performance was as desired without tuning the matrices.

4.3 Position and Attitude Determination Verification

A simulation environment is set up in MATLAB to test the two filters performance against each other. The simulation is set up to run with a input sequence creating the trajectory seen in Figure 4.2. The input sequence is just an arbitrary input sequence to test the estimation when the vessel turns in both directions with different turn rates.

The two estimation algorithms compared to each other can be seen in Figure 4.3. It can be seen from the figure that they follow each other very close. The filters have been tuned to estimate

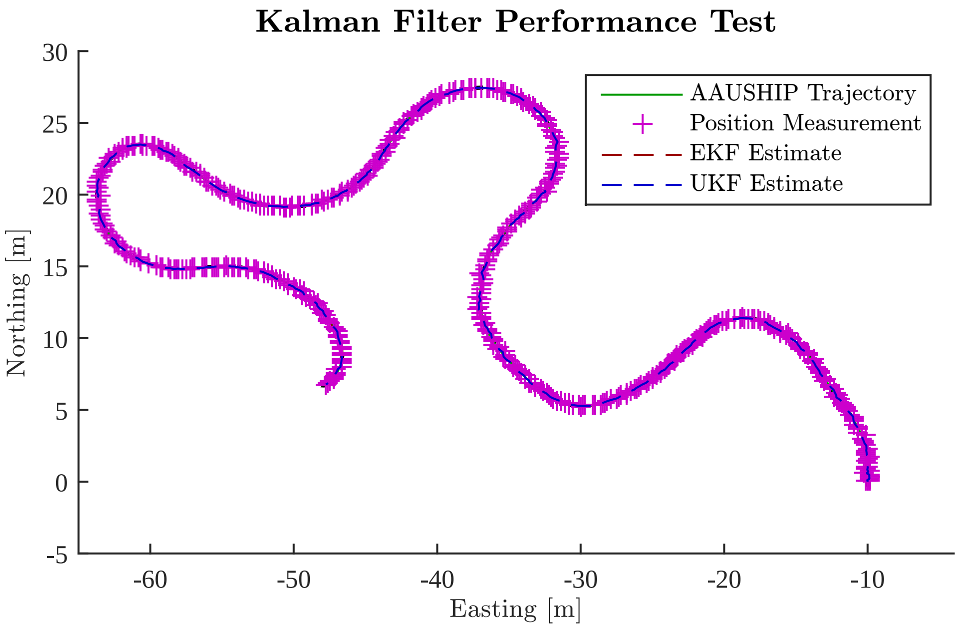

Figure 4.2: The figure shows a plot of the vessel's trajectory during the Kalman filter performance test. The trajectory is created using a input sequence with a duration of 53 seconds.

between the measurements and the model, this has been done to make sure that the vessel will sail as close to the wanted trajectory as possible but without just trusting either the model or the measurements.

The trajectory shown in Figure 4.2 is for 53s of sailing with a speed of approximately 2m/s. The position estimation error for the EKF during the sailing of this trajectory can be seen in Figure 4.4. The estimation error is found by calculating the square root of the squared difference between the actual position and the estimated position, see Equation 4.5.

$$e_{xy} = \sqrt{(x - \hat{x})^2 + (y - \hat{y})^2} \tag{4.5}$$

where
e_{xy} is the absolute x,y position error.

The maximum position estimation error for the extended Kalman filter during the sailing of this trajectory is 0.2146 m. The mean position estimation error is 0.0528m. Comparing these results to the requirement of a error of 0.5m stated in Chapter 3, it can be seen that the extended Kalman filter complies with this requirement by far. The results obtained are actually based on a measurement model with a noise level 10^4 times higher than the noise level determined in the sensor-analysis seen in Appendix B, this is only done to the position measurements. This is done to compensate for some of the unmodelled drift of the GPS which is seen in the sensor-analysis and to test the Kalman filter above the designed specifications.

The position estimation error for the unscented Kalman filter during the same trajectory as for the extended Kalman filter can be seen in Figure 4.5. The maximum position error for the unscented Kalman filter during the sailed trajectory is 0.1854m with a mean position estimation error is 0.0528m. Comparing these results with the requirements specified in Chapter 3, it can be seen that the unscented Kalman filter also complies with the requirement of being a maximum of 0.5m

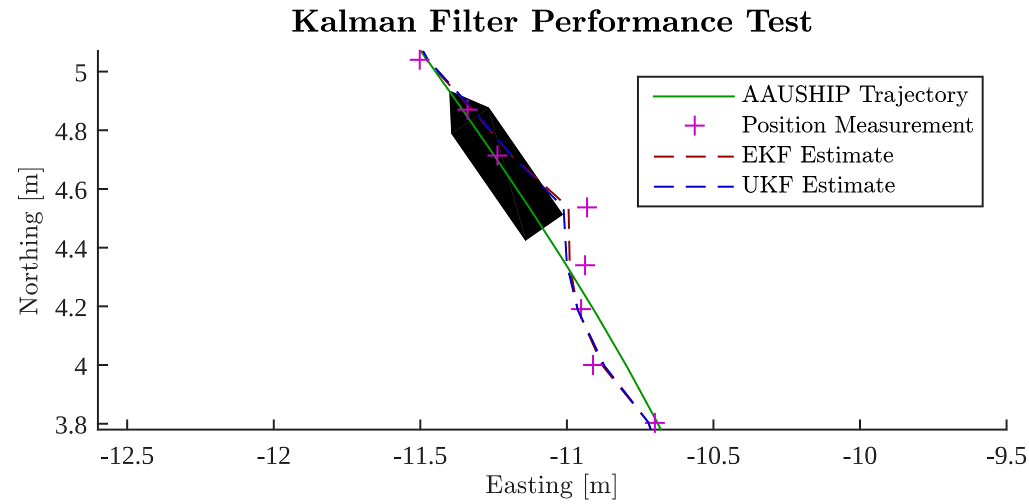

Figure 4.3: The figure shows the difference in estimates and how they follow both the measurements and the model.

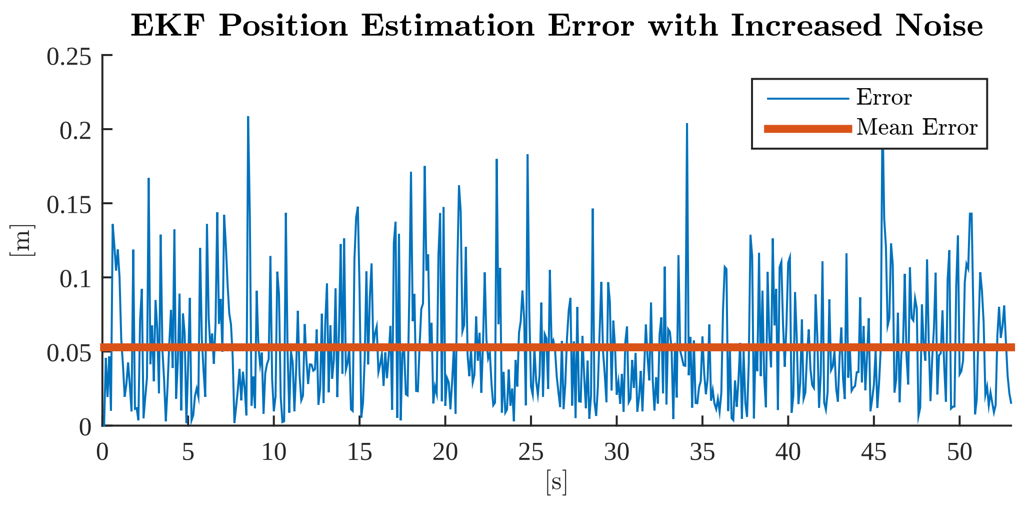

Figure 4.4: The figure shows the position estimation error for the EKF with a increased noise level of 10^4. The red line indicates the mean estimation error calculated to 0.0528m.

away, even with a increased noise level.

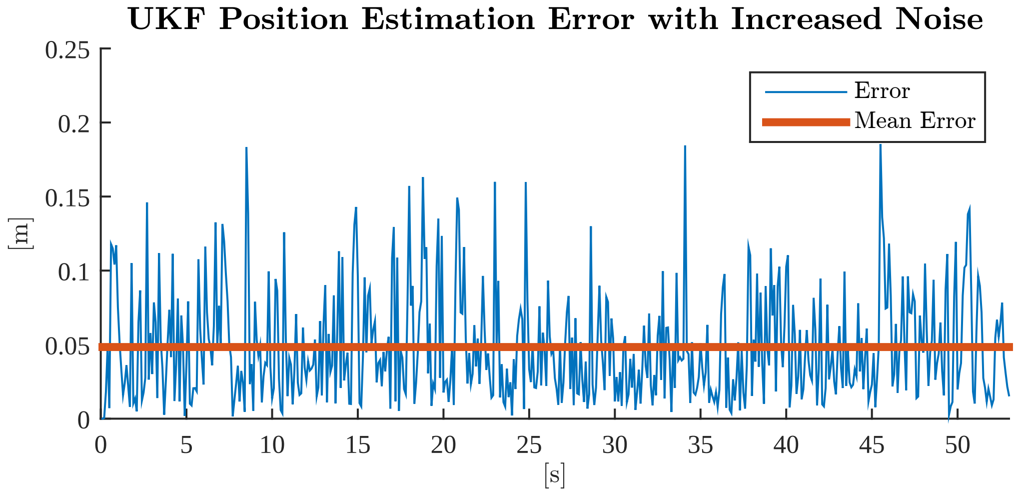

Figure 4.5: The figure shows the position estimation error for the UKF with a increased noise level of 10^4. The red line indicates the mean estimation error which is calculate to 0.0528m.

As mentioned in Chapter 3 there is a requirement regarding the surge velocity of the vessel during operations. This requirement is set to a maximum error 0.1 m/s for the surge velocity. The extended Kalman filter has a mean surge velocity error of 0.0013m/s during the travelled trajectory and a maximum velocity error of 0.0052m/s. This result is well below the requirement of a maximum error of 0.1m/s, as stated in the system requirements. The noise level utilised in the measurement model to test the surge velocity estimate is the noise level determined by the sensor noise analysis.

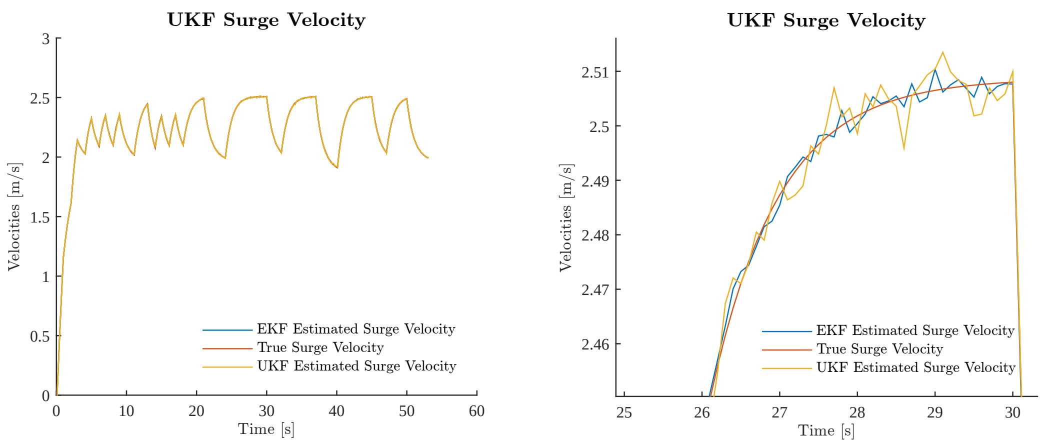

(a)

(b)

Figure 4.6: The figure shows the surge velocity evolution during the travelled trajectory. It can be seen from the plot that both filters estimates the velocity rather well with a slight advantage to the EKF.

The mean and maximum surge velocity errors experience during the travelled path was 0.0027 m/s and 0.0161 m/s, respectively. The results obtained from the unscented Kalman filter is well below the stated requirement, but the error is a bit larger than for the extended Kalman filter.

The last requirement stated for the Kalman filters is to have a heading error below 3.6°. Looking at figure 4.7 it can be seen that the estimation lies very close to the true heading. The extended Kalman filter has a mean heading error of $4.3161{\cdot}10^{-5}$ ° and a maximum heading error 2.2224 $\cdot 10^{-4}$ °. This is a very small deviation but it is very realistic considering the noise levels determined by the sensor noise analysis.

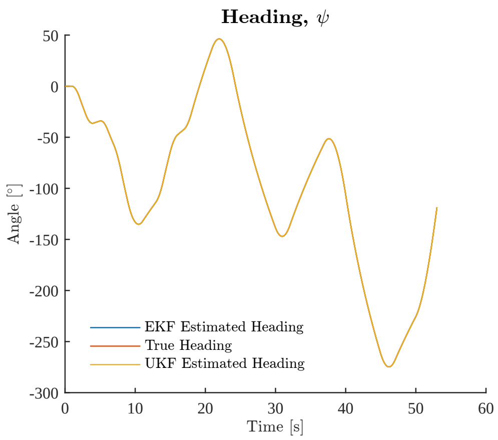

(a)

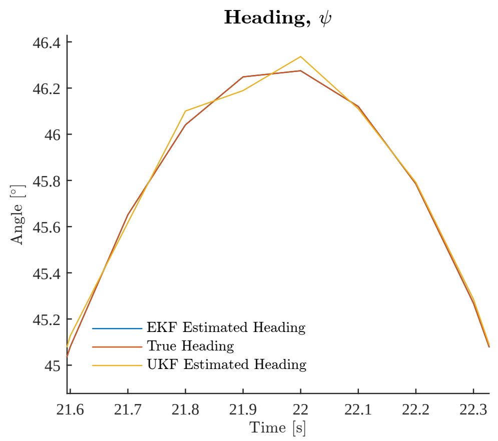

(b)

Figure 4.7: The figure shows the heading evolution during the travelled path. The second figure shows a close up of the first plot. The extended Kalman filter estimation can not be seen on the figure because the estimation error is so small.

The mean and maximum heading error for the unscented Kalman filter during the test is calculated to be 0.0306° and 0.1614°, respectively. This a bit larger error than for the extended Kalman filter, but it still complies with the requirement stated in the system requirements.

The results obtained in this section shows that both Kalman filters complies with the requirements stated in chapter 3. The Kalman filters will in the next section be compared to determine which of the filters shall used further on in this thesis.

Subconclusion

Both filters designed complies with the requirements presented in the system requirements. A selection will be made based on the results obtained through the verification. By comparing the position estimation error of both filters it can be seen that the UKF estimates better than the EKF but only with a mean difference between the two of 0.0476m. It can be seen from the two other plots that the EKF actually is better at estimating the heading and the surge velocity. Both Kalman filters performed rather well during the verification. The EKF is selected to be implemented because it estimated the surge velocity and heading better than the UKF.

This section has explained the implementation and verification of the EKF and UKF. The problems observed during the implementation have been described and solutions has been found. Both filters complied with the system requirements. The EKF is chosen for implementation based on the results obtained during the verification. The next section will describe the design of a path-following guidance law and controller. The controller will use the state estimation from the EKF to calculate a heading reference.

Chapter 5

Way-point Tracking Control

5.1 Way-point Tracking Control

This section will give a description of different methods to perform path-following using way-points as a reference. The method chosen for implementation shall be integrated with the position and attitude determination from the previous chapter. The section will present the definition of way-point when considering a surface vessel. The subsequent section will explain a guidance method called Line of Sight Guidance. Within this method there are two types of implementation, both of these will be presented. One of the implementation are chosen and verified.

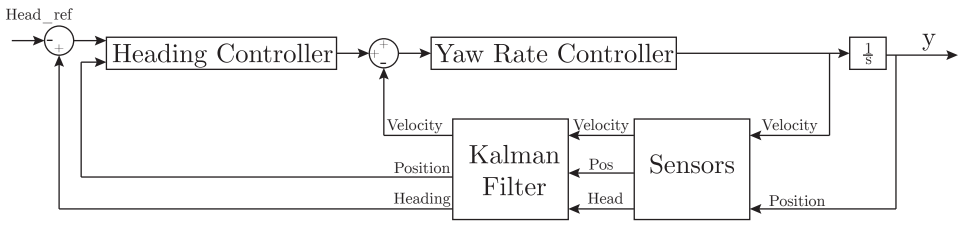

Figure 5.1: The figure shows a sketch of the designed controller as block diagram.

The controller designed has been designed as a cascade controller as can be seen in the figure above. The reason for this design chose is described in the forthcoming sections.

5.1.1 Way-points

The mission for AAUSHIP is to sail autonomously and survey the seabed, for this purpose it is wanted to create a path to be followed by the vessel. The path can be made using way-points, which is set by the operator of the vessel, and can be changed when the mission changes. A way-point is a point which can be described in all of $\mathbb{R}^3$ given as, $\mathbf{p}_\mathrm{k} = \begin{bmatrix} x_\mathrm{k} & y_\mathrm{k} & z_\mathrm{k} \end{bmatrix}^\mathrm{T}$. For a surface vessel as AAUSHIP, it is not needed to take into account the heave position of the way-point because it is only travelling in a plane described in $\{x, y\}$. For AAUSHIP the way-point is then given as $\mathbf{p}_\mathrm{k} = \begin{bmatrix} x_\mathrm{k} & y_\mathrm{k} \end{bmatrix}^\mathrm{T}$. A single straight line is given as the line drawn between two way-points $\mathbf{p}_\mathrm{k}$ and $\mathbf{p}_\mathrm{k}$. A path can be generated by the use of several straight line segments. By using only straight lines it is possible for the vessel to diverge from the desired path due to way-point switching, this will be described later on in this chapter. Way-points is the first part of performing path-following, after a path is generated it is needed to set up a guidance law for path-following, this will be described in the next section.

5.2 Line Of Sight Guidance Laws for Path-Following

A well known guidance law used both within marine craft and ballistic missile guidance is the Line of Sight guidance law, see [Fossen 11]. The Line of Sight guidance law is used to computed a desired heading reference relative to a path fixed frame. There are two general ways of implementing a Line of Sight guidance law, a enclosure-based guidance law or a lookahead-based guidance law. The Line of Sight guidance law is a three-point guidance scheme, due to the fact it is based upon three points: A reference way-point $\mathbf{p}_\mathrm{k}$, a target way-point $\mathbf{p}_\mathrm{k} + 1$, and the actual position of the vessel $\mathbf{p}(t)$. The LOS guidance law can also be used to track a moving target, e.g another ship during piloting as mentioned in Chapter 1, for this case the desired position is time-varying $\mathbf{p}_\mathrm{k}(t)$ or the LOS guidance law can be used to track a certain path in which case the desired position is the next way-point($\mathbf{p}_{\mathrm{k}+1}$) on the path, this is relevant when considering hydrographic surveying. The present thesis will only consider the objective of hydrographic surveying, which will lead to the design of a path-following controller.

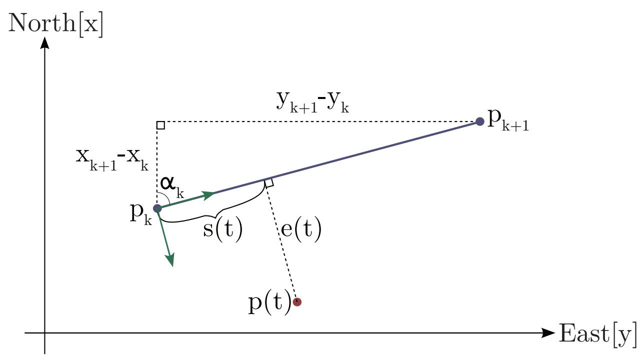

Figure 5.2: The figure shows the how the path-fixed reference frame is related to the NED reference frame. The figure also shows how the cross track error and along track distance is related to the path-fixed reference frame.

When considering the movement of the vessel, it is done in the NED frame, where the x-axis point towards true North and the y-axis points towards East. The path is however represented in a path-fixed reference frame with its origin in $\mathbf{p}_\mathrm{k}$ and its x-axis pointing towards $\mathbf{p}_{\mathrm{k}+1}$. To describe the vessel in the path-fixed reference frame a rotation of the NED frame is needed. This is done by rotating the NED reference frame by α_k degrees about its z-axis and then translating the rotated frame so the origin is aligned with $\mathbf{p}_\mathrm{k}$, see Equation 5.1.

$$\alpha_\mathrm{k} = \arctan\left(\frac{y_{\mathrm{k}+1} - y_\mathrm{k}}{x_{\mathrm{k}+1} - x_\mathrm{k}}\right) \tag{5.1}$$

The transformation from the NED reference frame to the path-fixed reference frame is given as, the rotation between the two frames and the distance between the vessel and the origin of the path-fixed reference frame. The x-axis of the path-fixed reference frame is called the along-track distance, while the y-axis is called the cross-track distance, see Figure 5.2.

$$\boldsymbol{\Gamma}(t) = \begin{bmatrix} s(t) \\ e(t) \end{bmatrix} = \mathbf{R}(\alpha_\mathrm{k})^\mathrm{T}(\mathbf{p}(t) - \mathbf{p}_\mathrm{k}) \tag{5.2}$$

where

$e(t)$	is the cross-track distance
$s(t)$	is the along-track distance
$\mathbf{p}(t)$	is the vessels position
$\mathbf{p}_\mathrm{k}$	is the position of way-point k
$\mathbf{R}(\alpha_\mathrm{k})$	is the rotation matrix between NED and the path-fixed reference frame

and where

$$\mathbf{R}(\alpha_\mathrm{k}) = \begin{bmatrix} \cos(\alpha_\mathrm{k}) & -\sin(\alpha_\mathrm{k}) \\ \sin(\alpha_\mathrm{k}) & \cos(\alpha_\mathrm{k}) \end{bmatrix} \tag{5.3}$$

The objective of the LOS guidance law is to make the vessel converge to the path, this mathematically equals that the cross-track error becomes zero. This gives a control objective given as:

$$\lim_{t \to \infty} \mathrm{c}(t) = 0 \tag{5.4}$$

In the section the two implementations of the Line of Sight guidance will be presented. Ath the end of the section one of the methods are chosen to be implemented.

Enclosure-Based Steering

The enclosure-based guidance law revolves around geometric calculations to calculate a desired heading angle. To calculate the vessel's desired heading angle, a circle with center in $\mathbf{p}(t)$ and radius R has to be computed. The circle's intersection with path is called $\mathbf{p}_\mathrm{los}$ and is needed to calculate the reference heading angle, see Figure 5.3.

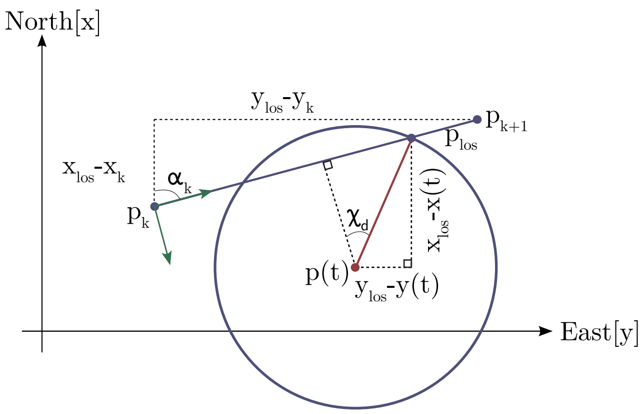

Figure 5.3: The figure shows the concept of a enclosure-based guidance law. The circle intersects the path in the point $\mathbf{p}_\mathrm{los}$ which also can be seen in the figure.

To determine the intersection point $\mathbf{p}_\mathrm{los}$ two geometric equations has to be solved. The first equation to be solved is the equation for the circle, see Equation 5.5 and the second equation states that the slope between two way-points are constant. When these two equation are solved the point $\mathbf{p}_\mathrm{los}$ can be obtained.

$$
\begin{aligned}
\left[x_{\mathrm{los}} - x(t)\right]^2 + \left[y_{\mathrm{los}} - y(t)\right]^2 &= r^2 \\
\tan(\alpha_{\mathrm{k}}) &= \frac{y_{los} - y(t)}{x_{\mathrm{los}} - x(t)}
\end{aligned}
\tag{5.5}
$$

The reference heading angle can then be calculated using the knowledge of the point $\mathbf{p}_{\mathrm{los}}$ and the position of the vessel.

$$
\tan(\chi_{\mathrm{d}}(t)) = \frac{y_{\mathrm{los}} - y(t)}{x_{\mathrm{los}} - x(t)}
\tag{5.6}
$$

Based on the calculated reference heading angle a control law can be designed which will take the cross-track error towards zero.

Lookahead-based Steering

The Lookahead-Based Steering is, of the two Line of Sight guidance methods, the least computationally demanding method. Instead of calculating the intersection $\mathbf{p}_{\mathrm{los}}$, the lookahead-based steering uses a design parameter called Δ which has to be greater than zero to calculate the reference heading angle. In general Δ is called the lookahead distance, it may be a varying function of time, $e(t)$ or other parameters. It is in most cases chosen to be constant, and set to two times the vessel length. The concept of lookahead-based steering can be seen in Figure 5.4

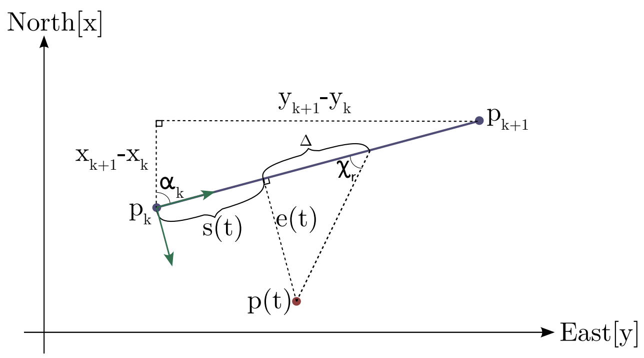

Figure 5.4: The figure shows the concept of a lookahead-based guidance law. The figure also shows how the lookahead distance is related to the path-fixed reference frame.

The reference heading angle is calculated as a sum of the two angles, α_k and χ_r, see Equation 5.7.

$$
\chi_{\mathrm{d}} = \alpha_{\mathrm{k}} + \chi_{\mathrm{r}}
\tag{5.7}
$$

where

χ_{d}	is the reference heading angle
Δ	is the lookahead distance
χ_{r}	is the path relative angle

The angle α is the angle used to rotate the NED reference frame over to the path-fixed reference frame, see equation 5.1. The path relative angle depends on the cross-track error and the lookahead distance, it can be seen from the equation why Δ is to be different from zero

$$\chi_{\mathrm{r}} = \arctan\left(-\frac{e(t)}{\Delta}\right). \tag{5.8}$$

It is chosen to utilise the lookahead-based guidance law because of the advantages it has compared to the enclosure-based guidance law. One of the biggest advantages by using the lookahead-based guidance law is that it is valid for all cross-track error as opposed to the enclosure-based guidance law which is only valid for cross-track errors smaller than or equal to the radius of the circle intersecting the path. The next section will describe how a path-following controller is designed using the reference heading determined by the lookahead-based guidance law.

Path-Following Controllers

The previous sections described the Line of Sight guidance laws, which provides a reference heading angle, χ_{d}, which can be used to design a path-following controller. The calculated reference heading is used to calculate the desired heading angle which makes the cross-track error converge towards zero.

The heading angle of a marine craft is generally affected by the movement of a rudder, but AAUSHIP do not have a rudder so this is done by allocation of the trust input to the two main thrusters. The control signal can be designed using the vessel's actual heading and the calculated reference heading. The vessel's actual heading angle can be obtained from the attitude determination described in Chapter 4. The control signal can then be calculated as the difference between the actual heading and the calculated reference heading , as can be seen in Equation 5.9.

$$\tau_{\mathrm{r}} = \psi - \psi_{\mathrm{d}} + \beta_{\mathrm{s}} \tag{5.9}$$

where
ψ_d is the desired heading angle.

The β_{s} appearing in the control law is the side slip angle as described in Chapter 2. For the present thesis β_{s} is not used because it is assumed that AAUSHIP will operate in calm waters.

Way-Point Switching

The control law is calculated for the way-points, $\mathbf{p}_{\mathrm{k}}$ and $\mathbf{p}_{\mathrm{k+1}}$, When the vessel reaches the way-point $\mathbf{p}_{k+1}$, the index k has to be increased so the way-point aimed for becomes $\mathbf{p}_{k+2}$. This means that the path-fixed frame shall be moved so the origin lies in $\mathbf{p}_{\mathrm{k+1}}$ and the next way-point to be followed is $\mathbf{p}_{\mathrm{k+2}}$. To determine when the switching happens a circle of acceptance around the way-points are calculated, see Figure 5.5. When the vessel approaches the way-point, $\mathbf{p}_{\mathrm{k+1}}$, and enters the circle, the guidance law changes, so the aim of the control law is now to control towards way-point $\mathbf{p}_{\mathrm{k+2}}$.

The mathematical expression for the way-point switching can be seen in Equation 5.10. The circle radius attached to each of the way-points can be set separately so hard turns have a larger radius and small turns have a small radius.

$$(x_{\mathrm{k+1}} - x(\mathrm{t}))^2 + (y_{\mathrm{k+1}} - y(\mathrm{t}))^2 \leq r_{\mathrm{k+1}}^2 \tag{5.10}$$

where
r is the circle radius from the center of p_{k+1}.

Based on the previous sections the way-point tracking control law can now be implemented and tested. The next section will describe some of the parameters tuned in the controller to reach the desired performance of the controller.

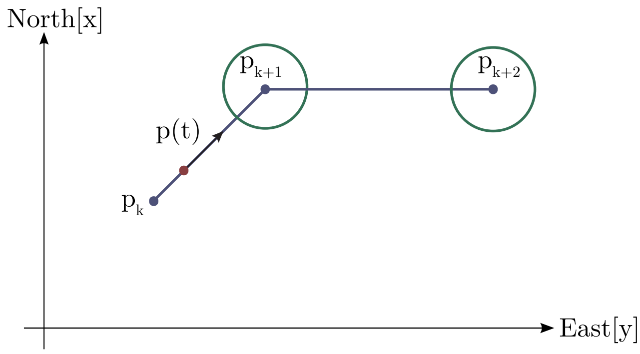

Figure 5.5: The figure shows the concept of the way-point switching algorithm. The circle of acceptance is the circle drawn around the way-points.

Way-point Tracking Control Implementation

The way-point tracking control is implemented in discrete time using MATLAB. The first trajectory to follow was a single straight line segment, there were some implementation issues because the rotation from the NED reference frame to the path-fixed reference frame was done incorrectly after this was sorted out the tracking control could follow a straight line. The vessel follows the path but it overshoots the path a bit because only the heading is controlled. To remove this overshoot a yaw velocity controller was implemented, together with the heading controller into a cascaded controller. By implementing the yaw velocity controller the vessel did not overshoot the path any more when it was on the path. The design parameter Δ was chosen to be a constant for the first tests. If Δ is large the vessel converges very slowly towards the path and might miss the way-points. If Δ is very small the vessel will converge to the path very fast and might end up overshooting the path. Therefore it is chosen to make Δ dependent on the the cross-track distance so it changes dependent on how close the vessel is to the path. The results of this is that the vessel converges to the path very fast but when it comes close to the path it converges slowly to prevent overshoot. This increased the performance of the way-point tracking control a lot but it needed to be improved further to accommodate the requirements mentioned in Chapter 3. To improve the performance of the control further, the circle of acceptance is changed. This means the vessel has some more time to turn and reach the new line segment without overshooting it. The results of this implementation can be seen in the next section.

5.2.1 Way-point Tracking Control Implementation and Verification

The control system has been implemented as a cascade controller containing heading controller and yaw rate controller. The first implementation only contained a heading controller which overshot the path, and never travelled along the path. Therefore it was determined to implement a yaw rate controller to take care of the excess velocity the vessel had when turning towards the path. After the implementation of the yaw rate controller the vessel travelled along the path when it was near the path, but still it overshoots when switching way-points. To accommodate this overshoot the radius of acceptance has to be changed as will be explained later in this section.

The way-point tracking control is verified using the same noise levels used in section 4.3, for the same reasons. The first requirement to be tested is regarding the maximum turn angle and the maximum cross-track error as determined in Chapter 3. The maximum cross-track error is verified by making a 180° turn following a straight line because it is expected to be the point where the cross-track error will become largest. The vessel is set to sail on a straight line and at the end of this line the way-point switches so it returns to its starting point, the path is illustrated in figure 5.6(a).

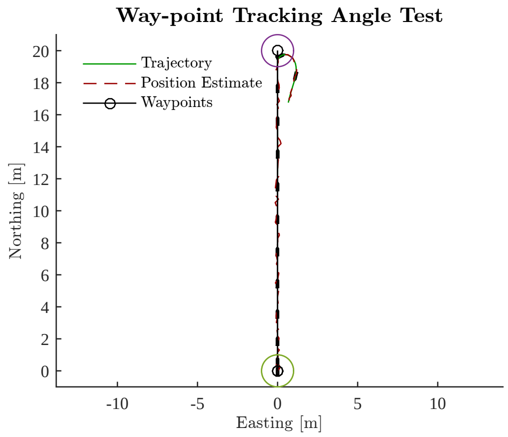

(a)

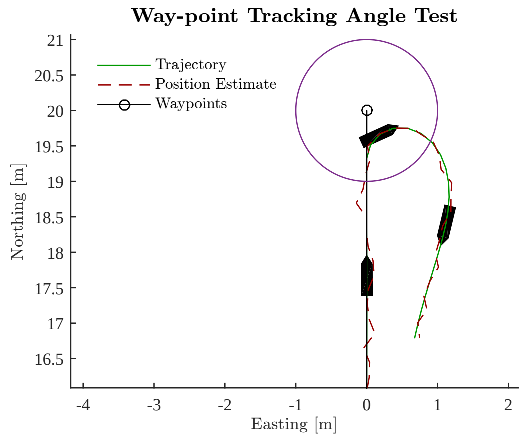

(b)

Figure 5.6: The first figure shows the trajectory of vessel during the 180° angle test. The second figure shows a close up of how the vessel turns during a 180°.

The result of this verification is that while taking a 180° turn, the vessel's maximum cross-track error becomes 1.1993m. This cross-track error means that the vessel can make a 180° turn without violating the maximum cross-track error requirement of 3m. The maximum cross track error can also be seen in figure 5.6(b). To test the maximum cross-track while AAUSHIP surveys the seabed, another path is generated. The generated path is based on the expected path which AAUSHIP is to follow when surveying, the path can be seen in figure 5.7(a).

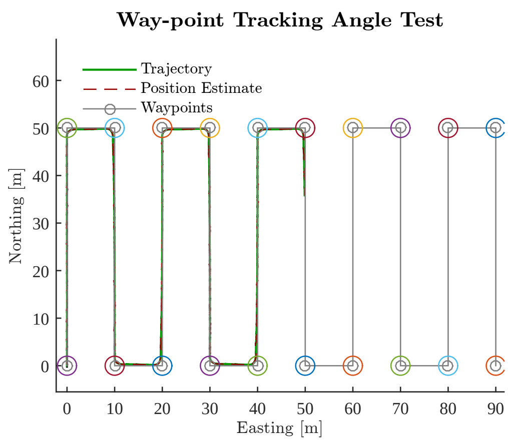

(a)

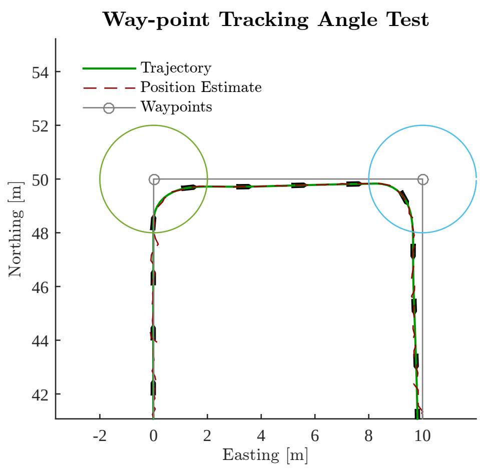

(b)

Figure 5.7: The first figure shows the travelling trajectory of the vessel during the surveying test. The second figure is a close up of how the vessel turns during a 90°

turn.

The maximum cross-track error obtained by following this path is 1.9721m , which is below the maximum requirement of 3m. The maximum cross-track error is larger than in the angle test, this is due to the tuning of the way-point switching. The radius of the acceptance circle radius described earlier can be reduced so the vessel switches way-point closer to the actual aimed for way-point. The problem by doing so is that the vessel will overshoot the path, which is not desired. It is wanted for the vessel to stay on the inside of the path because if it is assumed that the shore/quay is at the top and the bottom of the path, then collisions are avoid by staying inside or on the path, see figure 5.7(b). In this way the circle of acceptance can be used as a secondary tuning parameter besides the controller gain.

The last requirement for the way-point tracking control is to maintain a speed of 2m/s. It can be seen from figure 5.8(a) that the speed of the vessel is maintained around 2m/s while travelling along the path. It can also be seen from figure 5.8(b) that the vessel obtains the speed of 2m/s after 5s. This time can be increased with the implementation of a surge velocity controller which is not considered in the present thesis.

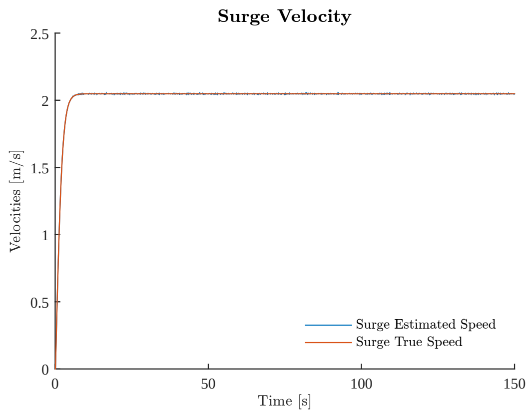

(a)

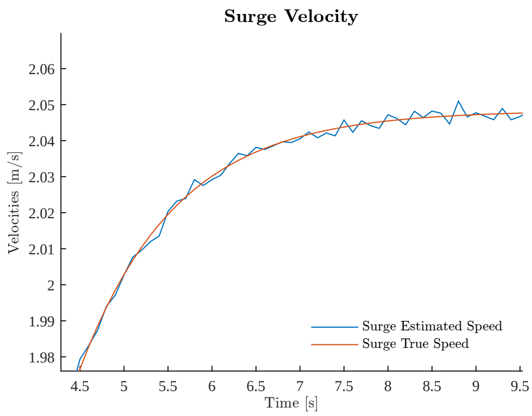

(b)

Figure 5.8: The figure shows the velocity evolution during the travelled path, it can be seen from the figure that the vessel maintains a velocity of 2m/s when the velocity is reached.

Subconclusion

The way-point tracking control has been designed and verified. The verification of the way-point tracking control has be done to determine if the system complies with the system requirements. The way-point tracking control system complies with the requirements specified in the system requirements, the results are compared in Table 5.1. The requirement of a maximum cross-track error of 3m is fulfilled with a margin of 1m to the requirement which is a rather larger margin, one third of the requirement. The vessel is able to handle a 180° turn without violating the maximum cross-track error requirement of 3m. The requirement to travel with a constant surge velocity of 2m/s is passed, because after 5s the vessel reaches a surge velocity of 2.045 m/s and maintains this velocity until simulation stop.

Based on the results obtained it can be determined that the vessel complies with one of the main requirement. The vessel should never deviate more than 3m form the path ccording to one of the main requirements. By calculating the mean cross track error it can be seen that the vessel has a averaged mean cross track error of 0.1753m. Based on this result it can be concluded with a certain amount of security that the vessel will never deviate more than 3m from the path. The only case where the vessel would achieve a cross track error larger than 3m is if the circle of acceptance is changed.

Identifier	Requirement	Requirement Value	Obtained Result
SS1.M4	Maximum Cross-track Error	3m	1.9721m
SS1.R2	Turning Radius	180° (with a error < SS1.R1)	1.1993m
SS1.R3	Constant Speed	2m/s	Passed

Table 5.1: The table shows the requirements for the path following controller along with the obtained results during the verification.

The controller has been designed and implemented. Based on the results obtained in simulation the controller passed all of its requirements and also complied with one of the main requirements. The next chapter will determine the faults to be detected by the fault diagnosis. This will be used in the design of an active fault diagnosis scheme.

Chapter 6

Fault Analysis

The purpose of this chapter is to identify the faults that can occur in the system together with how they propagate through the system. The end result will be a set of faults which shall be used for further work in the present thesis.

The fault analysis are divided into 4 parts, model partitioning, fault propagation analysis, fault assessment, fault specification. This approach is inspired by the work of [Izadi-Zamanabadi 99] and [Sloth 09], just reduced for the problem considered in the present thesis.

The model partitioning is done to divide the model into smaller and less complex systems, this gives a good overview of how the faults propagate through the system. The fault propagation analysis is done to determine how the faults propagate and what end-effects they lead to. The fault assessment is done to choose a set of faults which will be chosen for further work in the present thesis. The last part of the fault analysis is to make a fault specification, this will determine in which way the faults enters the system and the consequences of this fault. The next section will describe in what way the model partitioning is done.

6.1 Model Partitioning

The system model is divided into appropriate sub-models to simplify the fault propagation analysis. The sub-systems is then considered separately, which makes it possible to identify all possible component faults in each of the sub-models. The model of the vessel is divided into three sub-models based on their separate functionalities:, heading control system, speed control system and LOS guidance system. Each of the sub-models are shown in Figure 6.1. It is only needed to consider the components which is part of a closed loop system, because they are the only ones affecting the operation of the vessel.

In this project only a subset of possible faults are considered, faults concerning the hull of the vessel is excluded from the fault propagation analysis. This is done because they are faults which can not be accommodated, e.g there is a hole in the boat that makes it sink, this can not be accommodated. The next subsections will give an overview of the different components present in the three sub-models.

Heading Sub-model

The heading sub-model is based on the components utilised in the heading control system. The heading control system consists of a heading sensor, a heading controller, DC-motors, propellers, and propulsion. The heading sensor is fed back to the heading controller and together they form a closed loop. From the heading controller a reference signal is fed to the DC-motors and based

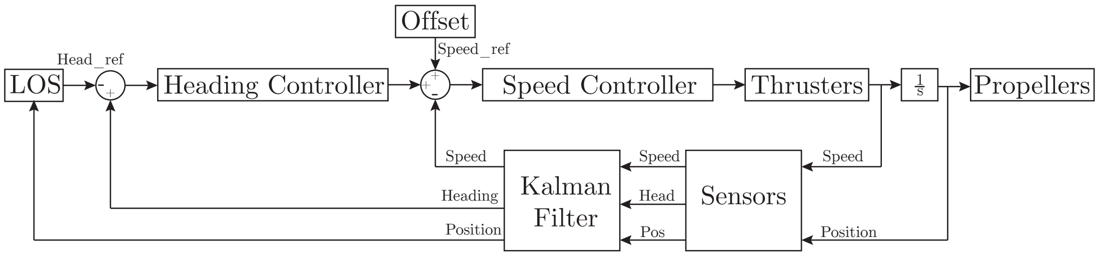

Figure 6.1: The figure illustrates a simplified overall structure of the system. The states between some of the blocks are neglected.

on this reference signal the DC-motors creates propulsion. The propulsion is made using the propellers which is connected to DC-motors via shafts.

Position Sub-model

The position sub-model is based on the components utilised in the LOS guidance system. The LOS guidance system is based on the following components, a position sensor, a LOS guidance system, a heading controller, DC-motors, and propellers. The position sensor is used to determine how far the vessel is from the way-point it is travelling towards. The distance is then used in the LOS guidance system to calculate the heading reference which is utilised in the heading control system. The propagation from the heading controller and on is identical to the propagation described in the above subsection.

Yaw Rate Sub-model

The velocity sub-model is based on the components utilised in the yaw rate control system. The yaw rate control system consists of the following components, a yaw rate sensor, a yaw rate velocity controller, DC-motors, and propellers. The yaw rate measurement is fed to the yaw rate controller. The yaw rate controller then calculates a reference signal which is fed to the DC-motors. The propagation steps is from this point on the same as described in the previous subsections.

The DC-motors and the propellers are represented in all three models because all the sub-models affects the propulsion of the vessel in some way. Based on the above described models a fault propagation analysis is done, which will be described in the next section. The fault propagation analysis will clarify which faults occur and in which way the propagate through the system.

6.2 Fault Propagation Analysis

The purpose of this section is to describe the propagation of faults through the system and to determine the effect of the possible faults on the different system components. The propagation analysis is done by performing a Failure Mode and Effect Analysis(FMEA) of the system. FMEA is a widely used method when considering reliability, [Carlson 12].

The propagation analysis starts at the lowest system component level and continues through all of the system components. For the case of AAUSHIP this is at the sensor level, so the FMEA diagrams seen in figure 6.2, 6.3, and 6.4 shall be interpreted as seen from a sensor level, i.e from the heading sensor to the heading controller and so forth. It shall be noted that the DC-motors and the propellers is present in all FMEA diagrams because all faults has a direct effect on the propulsion system.

The next sections will give a more thorough assessment of how the faults propagate through the system and which end-effects this leads to.

Yaw Rate Sensor

The yaw rate sensor which measures the angular velocity $\dot{\psi}$ are a candidate for a multiple of faults. As can be seen from figure 6.2 there are four faults represented for the current FMEA. Two of the least sever faults are the stuck low output and the no output. These two faults results in the vessel overshooting the path, this end-effect is not very sever if considered isolated but if shores/quays are close it might cause the vessel to collide with these. The bias of the sensor output will be handled by the controller so this fault is not very sever. The two other faults, random output and fixed high output, are faults affecting the yaw rate sensor leads to a more serious end-effect. The fixed high output will cause the vessel to become out of control because of the over-actuation this creates. The random output can possibly cause the vessel to become out of control dependent on the range of the random output, if it is a low variance random output it will only cause the vessel to overshoot the path as described earlier. If instead the random output is of high variance it will cause the vessel to become out of control because it over-actuates. The faults explained in the above and later sections will be assessed in a later section.

Heading Sensor

The heading sensor is used in the heading controller to steer the vessel in the direction of a given way-point. The heading sensor is affected by the same faults as for the yaw rate sensor but the end-effects for some of the faults are more sever than for the yaw rate sensor. The faults introduced from the heading sensor is very sever because they are used to determine the direction of travel for the vessel. This means that if the sensor gets stuck at high, low, random output, or no output the vessel will turn in circles. The result of this will be for the operator to fetch the vessel, because it has enter a uncontrollable state. While the vessel is in a uncontrollable state it might cause harm to itself or other vessels in the area of operation. The last fault is a biased sensor output, and this fault is not very sever because the vessel will still be operational, and the controller will handle the bias as an error.

Position Sensor

The position sensor is used in the Line of Sight guidance law, to determine the heading reference. The heading sensor faults affects the actual heading angle but the position influences the reference heading angle. The position sensor is subject to three faults; fixed output, random output and no output. These faults are all sever faults when using a heading controller that needs a heading reference. If a fault occurs on the position sensor the guidance law will calculate a reference heading based on a different position than the actual position of the vessel. It will cause the vessel to sail away from the path or make it think that it resides closer to the path than it really is. The consequence of these faults is that the vessel might cause harm to itself or others if not stopped.

DC-Motor

All of the faults from all three sensors propagate through to the thrusters, due to the two controllers designed. Even though that a lot of faults propagate to the motor, it is also a candidate which can lead to faults. The motor faults are present in all of the three FMEA diagrams because it is a part of all three closed loop systems. There are two obvious faults which the motor fosters itself, defect motor driver and wear of the motor. The defect motor driver fault will lead to improper commutation, which in the end will effect the actuation of the motor which will become slower. The second fault is inevitable when the motor is used for longer durations without being substituted and this will also lead to a slower actuation than expected from the motor. These types of faults is not as sever for the safety of the vessel and other vessels, compared to the sensor faults described previously.

Propeller

The propellers is a vital part of a marine vessel. Any faults subjected to the propeller will cause a degradation of the vessels thruster performance. When considering the propeller there are three faults caused by the propeller itself; a missing propeller wing, vegetation stuck to the propeller, and a broken propeller shaft. The most problematic of the three faults is the broken propeller shaft which will result in no propulsion of the vessel on the affected motor. This will cause the vessel to spin out of control because the second propeller will still be working. This will be a safety and health risk of the vessel and it will also be a possible health and safety risk for other vessels in the operational area of the vessel. The two other faults will lead to a degradation of the thrust performance, this degradation will be reduced if a surge speed controller is implemented on the vessel.

Propulsor		Changed E iciency	Changed Dynamics	Out of Control	No Propulsion	Over-shoot
DC Motor (1,2,3,4)	Speed O set					●
	No Speed				●	
	Full Speed			●		
	Random Speed			●		
	Slower Actuation		●			
Propeller	Lower E iciency	●				
	No Rotation				●	
	Lower Hydrodynamics		●			

Propeller	Lower E iciency	Lower Hydrodynamics	No Rotation
Missing Wing	●		
Vegetation		●	
Broken Shaft			●

DC Motor (1,2,3,4)		Speed O set	No Speed	Full Speed	Random Speed	Slower Actuation
Motor Wear						●
Defect Motor Driver						●
Speed Controller	Biased Output	●				
	Low Output		●			
	High Output			●		
	Random Output				●	

Yaw Rate Controller		Biased Output	High Output	Low Output	Random Output
Rate Sensor	Biased Output	●			
	Fixed Output		●	●	
	Random Output				●
	No Output		●	●	

Rate Sensor	Biased Output	Fixed Output	Random Output	No Output
Internal Faults	●	●	●	●

Figure 6.2: This propagation diagram shows the propagation of faults from the speed sensor

Propelment		Changed Efficiency	Changed Dynamics	Out of Control	No Propulsion	Over-shoot
DC Motor (1,2,3,4)	Angle Offset					●
	Zero Angle			●	●	
	Max Angle			●		
	Random Angle			●		
	Slower Actuation		●			
Propeller	Lower Efficiency	●				
	No Rotation				●	
	Lower Hydrodynamics		●			

Propeller	Lower Efficiency	Lower Hydrodynamics	No Rotation
Missing Wing	●		
Vegetation		●	
Broken Shaft			●

DC Motor (1,2,3,4)		Angle Offset	Zero Angle	Max Angle	Random Angle	Slower Actuation
Motor Wear						●
Defect Motor Driver						●
Heading Controller	Biased Output	●				
	Low Output		●			
	High Output			●		
	Random Output				●	

Heading Controller		Biased Output	High Output	Low Output	Random Output
Heading Sensor	Biased Output	●			
	Fixed Output		●	●	
	Random Output				●
	No Output		●	●	

Heading Sensor	Biased Output	Fixed Output	Random Output	No Output
Internal Faults	●	●	●	●

Figure 6.3: This figure shows the propagation of faults in the heading sensor

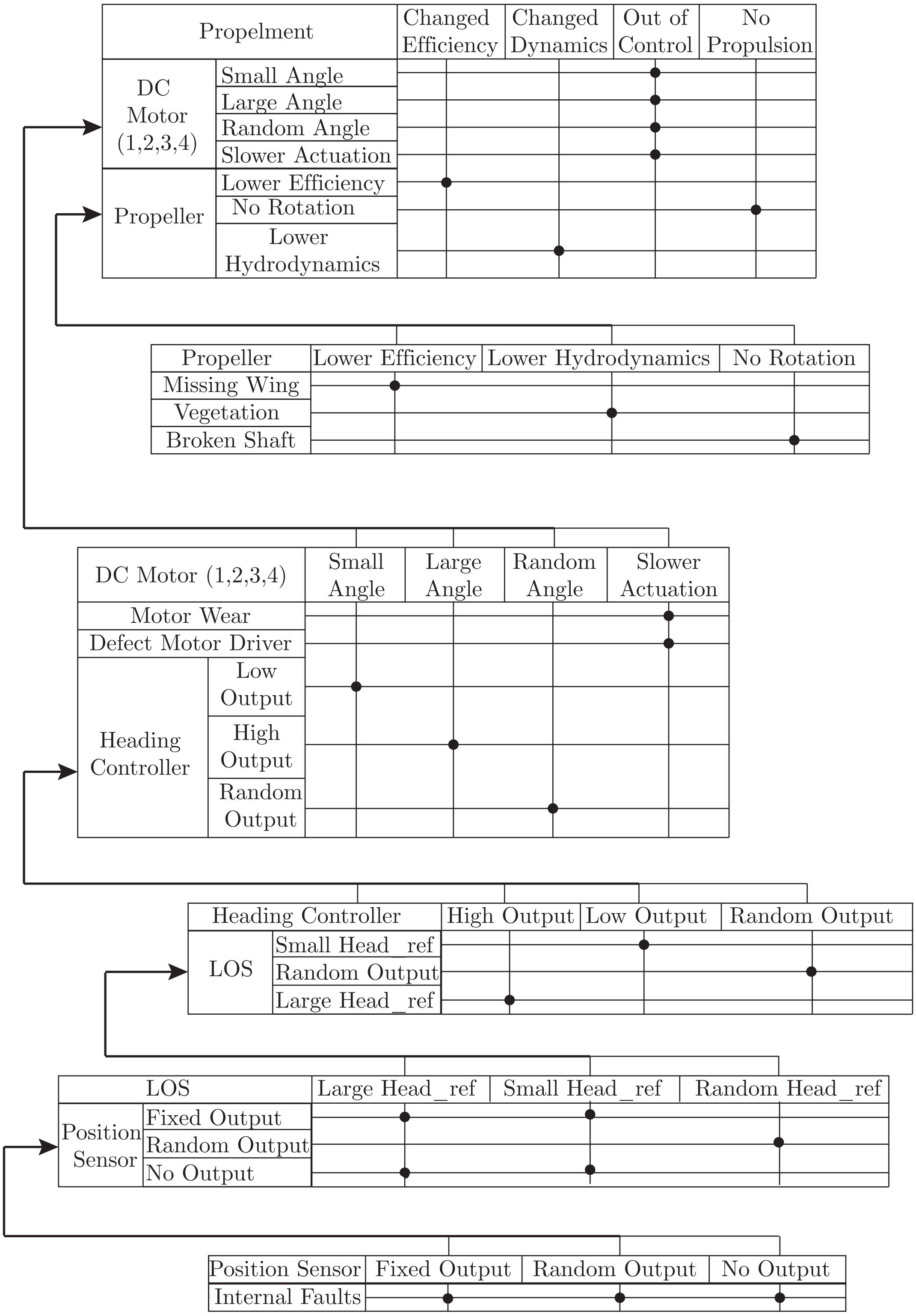

Figure 6.4: This figure shows the propagation of faults in the position sensor

6.3 Fault Assessment

The objective of this section is to evaluate the severity and occurrence of the end-effects of the faults determined in the propagation analysis, and to determine which of the faults are to be treated later in the present thesis. The fault assessment is based on two terms, severity and occurrence, these terms will be explained and used to determine the faults to assess.

Severity

Severity is a ranking number describing the seriousness of the end-effect of a certain failure mode, and it is based on a severity scale as is seen in table 6.1. It is a relative number from 1-10, determined by the user based on statistical data if available. The severity scale used in the present fault assessment, is based on the scale used for the automotive industry as described in [Carlson 12, pp. 34], this is done because no statistical data is available for AAUSHIP and this scale has been widely used. The severity index is used to determine if a fault shall be assessed or not, together with the occurrence index explained in the next section.

Effect	Customer Effect	Rank
Failure to Meet Safety Requirements	Potential failure mode affects safe vehicle operation without warning	10
	Potential failure mode affects safe vehicle operation with warning	9
Loss or Degradation of Primary Function	Loss of primary function (Vehicle inoperable, does not affect safe vehicle operation)	8
	Degradation of primary function (Vehicle operable but at a reduced performance level)	7
Loss or Degradation of Secondary Function	Loss of secondary function (Vehicle operable, but comfort/-convenience functions inoperable)	6
	Degradation of secondary function (Vehicle operable, but comfort/convenience functions at reduced level of performance)	5
Annoyance	Appearance or audible noise, vehicle operable, item does not conform and noticed by most customers (>75%)	4
	Appearance or audible noise, vehicle operable, item does not conform and noticed by many customers (50%)	3
	Appearance or audible noise, vehicle operable, item does not conform and noticed by discriminating customers (<25%)	2
No Effect	No discernible effect	1

Table 6.1: This table shows the Severity evaluation criteria used for the FMEA

Occurrence

The occurrence index is a ranking number describing the probability for a failure mode to occur. The occurrence probability can be determined by evaluating statistical data if these are become available. For the present there are no statistical data available so the occurrence index is determined based on the author's knowledge. The occurrence rankings are shown in table 6.2 and is based on [Carlson 12, pp. 39]. The occurrence number is a relative value used to determine the need for accommodation of a fault together with the severity index, this can be seen in figure 6.5 in the next section.

Likelihood of Failure	Probability	Rank
Very High	1 in 10 or more	10
High	1 in 20	9
	1 in 50	8
	1 in 100	7
Moderate	1 in 500	6
	1 in 2000	5
	1 in 10000	4
Low	1 in 100000	3
	1 in 1000000	2
Very Low	Failure eliminated by preventive control	1

Table 6.2: The table shows the Occurrence evaluation criteria used for the FMEA

Severity and Occurrence Analysis

Each fault determine in the fault propagation analysis has been evaluated according to the severity and occurrence tables described in the previous sections. Based on this evaluation the faults is prioritised to determine the most sever faults. It is wanted to take the most sever fault from each sensor and one affecting the propellers because these faults are abrupt, which should make them easier to detect and thereby verify the detection method described in the next chapter. The faults chosen for further processing is the faults which lie in the critical characteristics part of the square. The faults located in the orange part of the square is faults which is significantly critical but is not considered in the present thesis. The faults located in the yellow part of the square is annoyance faults, such as a stuck low output from the yaw rate sensor.

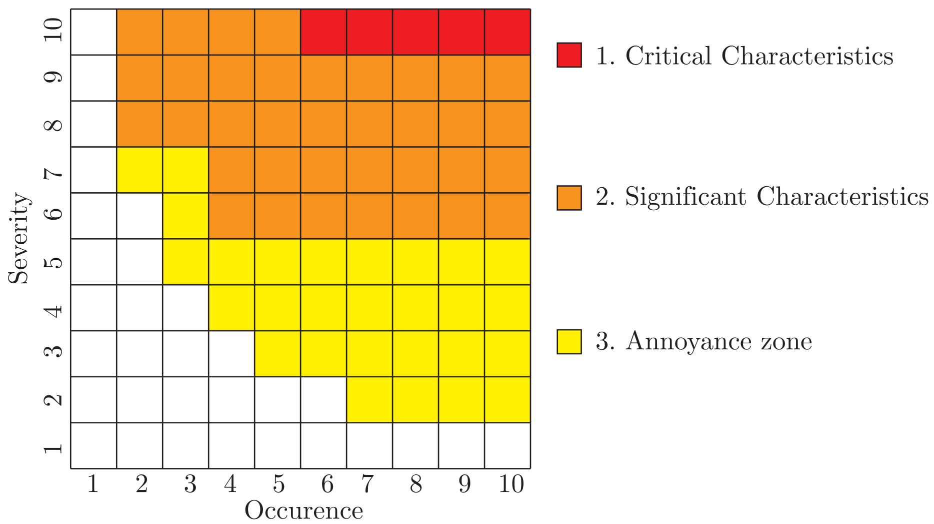

Figure 6.5: The figure shows a grid used to describe the criticality of a fault based on the severity and occurrence index.

The faults chosen for further work can be seen in Table 6.3. The faults concerns each of the sensors and the propellers. The table shows the faults together with their severity and occurrence indexes, the indexes can be compared to Figure 6.5.

A complete table containing all the faults and their severity and occurrence index can be seen in

Effect	Fault	O	S
	Position Sensor - No Output	9	10
Out of Control	Heading Sensor - No Output	6	10
	Yaw Rate Sensor - Fixed High Output	6	10
No Propulsion	Propeller - Broken Shaft	7	10

Table 6.3: This table shows the five most critical faults concerning the vessel and their respective severity and occurrence index.

Appendix D. In future work it might be desired to also accommodate many of the other faults to improve the security of the vessel and other vessels in its operational area. The next section will show how the faults chosen actually affects AAUSHIP during operations.

6.4 Fault Specification

This is section shall give an overview of the consequences when the faults determined in the previous section enters the system. The section shall be seen as a verification of the stated end-effects determined in the previous section.

The four faults specified in the previous section enters the system in different ways. The different ways leads to different consequences. When the heading sensor has no output it means that the heading sensor output is just noise. The heading controller will then calculate a error reference based on the noise and the desired heading, the result of this is a vessel out of control as can be seen in Figure 6.6.

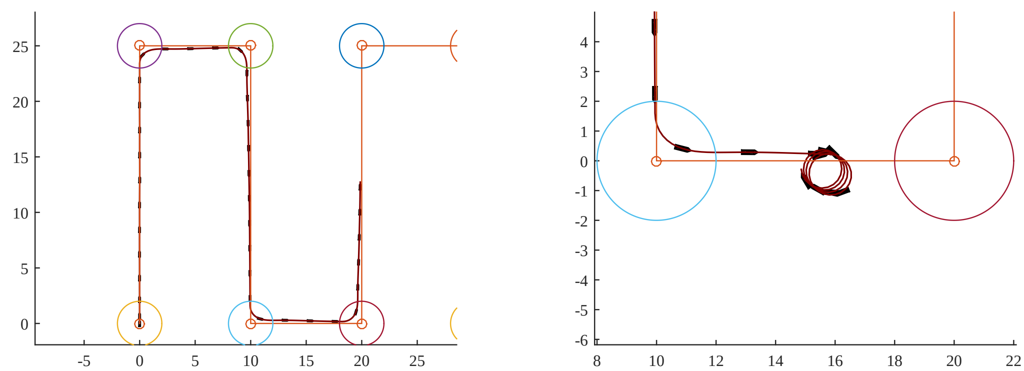

(a) (b)

Figure 6.6: The figure shows a comparison of the nominal trajectory and the trajectory when the heading sensor gives no output.

The fault on the position sensor enters the system in the same way as the heading fault, but the consequences are a bit different. The position measured by the position sensor is used to determine the distance away from the circle of acceptance and the cross-track distance. When then position sensor fails it cannot determine how close it is to a way-point or the path. The vessel will therefore continue in the travelling direction until it meets an obstacle, this can be seen in Figure 6.7.

The fault affecting the yaw rate sensor has a direct influence on the yaw rate controller. When the yaw rate controller receives a fixed high output from the sensor it will believe that the rotation

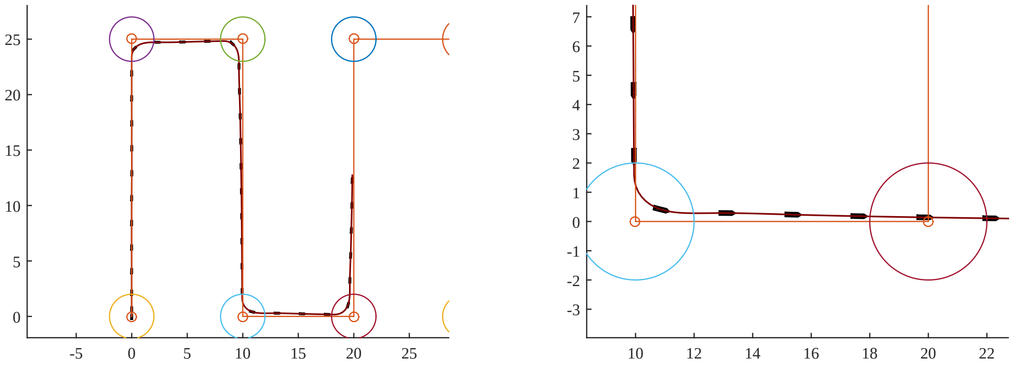

(a) (b)

Figure 6.7: The figure shows a comparison of the nominal trajectory and the trajectory when a position sensor gives no output.

velocity of the vessel is higher than it is in reality. The yaw rate controller will try to compensate for the increased velocity by actuating in the other direction. The consequence of this is seen in Figure 6.8, the vessel will deviate from the path to compensate for the fixed high output.

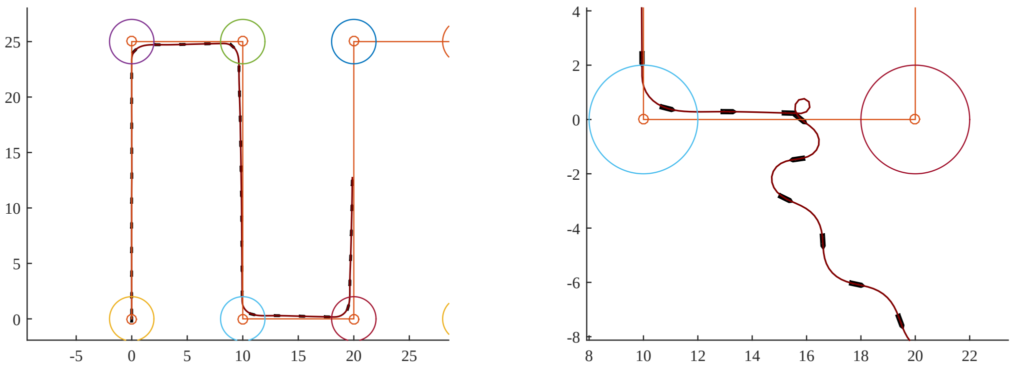

(a) (b)

Figure 6.8: The figure shows a comparison of the nominal trajectory and the trajectory when the yaw rate sensor is giving a fixed high output.

When a propeller shaft breaks the vessel becomes disabled because only one thruster is available. The vessel will attempt to travel towards the targeted way-point but only one thruster will create propulsion. This will make the vessel turn, and when the heading passes the desired heading the vessel will try to use the broken thruster, this will create a deadlock when waves and wind is not considered, this is shown in Figure 6.9.

This section has shown the end-effects of the faults determined in the fault assessment and explained the reason behind the end-effect. The chapter has analysed the vessel model to determine

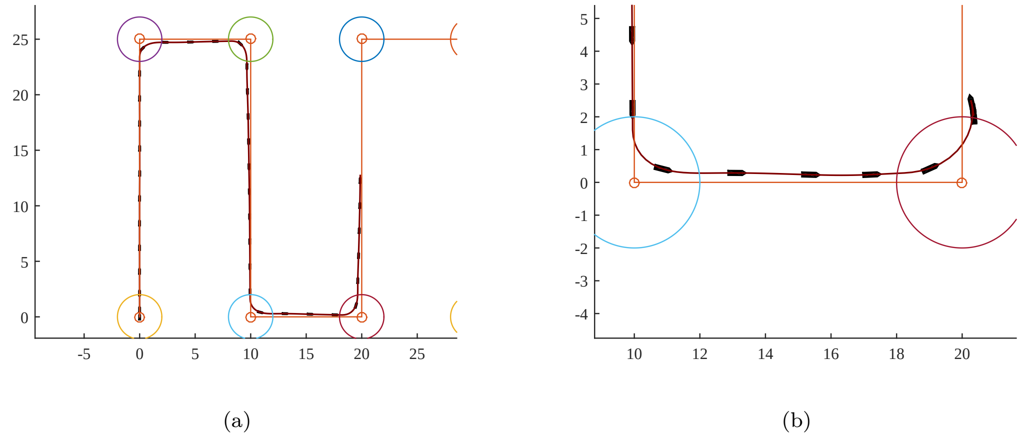

Figure 6.9: The figure shows a comparison of the nominal trajectory and the trajectory when a propeller shaft brakes.

which faults are the most critical. The most critical fault affecting each sensor is chosen for further work. Besides the sensor faults it is also chosen to detect a fault in the propulsion system. The faults specified shall be used in the next chapter to design a fault diagnosis scheme.

Chapter 7

Fault Diagnosis

The following chapter will explain the fault diagnosis method designed to detected the faults determined in Chapter 6. The start of the chapter will describe some of the terminology used when considering fault diagnosis. After the explanation of terminology, existing fault diagnosis methods will be introduced. The last part of the chapter concerns the design of an auxiliary signal for fault diagnosis.

7.1 Introduction to Fault Diagnosis

The first part of this section will give a short introduction to the terminology used within the field of fault detection. The following section will then give an overview of other existing fault detection methods just to show the other methods exists other than the one method used in the present thesis.

Terminology

A ***fault tolerant control system*** is a system which accommodates component failures to prevent them from becoming failures on system level. It is for some control systems allowable to have a degraded performance when exposed to a fault. A ***fault*** is a change in the characteristic behaviour of a system item while ***failure*** results in a complete dysfunctional system component, it is important to distinguish between these terms. There are in general two types of fault tolerant control, an active and a passive approach. An ***passive fault tolerant control system*** accommodates faults using only one controller which is utilised in case of nominal behaviour and faulty behaviour. A ***active fault tolerant control system*** utilises, opposed to the passive fault tolerant control system, different controllers for the nominal behaviour and the faulty behaviour. This implies a needed for fault diagnosis algorithms to determine the current state of the system, the information from the fault diagnosis algorithms are passed on to a ***supervisor*** which reconfigures the control system to accommodate faults. ***Fault diagnosis*** is used in active fault tolerant control systems and consists of multiple parts. The faults have to be detected, isolated and for some cases estimated. ***Fault detection*** shall be able to detect a fault and relies on either an active or passive approach. ***Passive fault detection*** detects faults by comparing the expected system behaviour with the observed system behaviour, the method does not affect the system and is considered an observing problem. The ***active fault detection*** acts upon the system by injection of auxiliary signals into the system, this is done to separate the nominal and faulty system. ***Fault isolation*** are used to determine which component is faulty. This information is important, especially when multiple faults can occur, to determine which control strategy the supervisor should choose. The way faults occur are dependent on the component exposed to the fault, some faults are not turned on or off but have some intermediate state. To determine the fault size ***fault estimation*** can be used in order to accommodate these faults. Faults can be classified into two categories; abrupt and incipient. An abrupt is generally easier to detect compared to incipient faults, but they are in most cases more destructive for the system because they happen immediately.

Existing Fault Diagnosis Methods

Several methods for designing fault diagnosis algorithms already exist and they will be outlined in this subsection.

There exists two major methods for fault detection either passive or active. The passive fault detection methods include the model-based residual generators as described in [Chen 99]. The methods for residual generation mentioned in [Chen 99] is based on a Luenberger observer but with some alterations. The alterations made to the Luenberger observer guarantees detection with model uncertainties, disturbances and noise also referred to as unknown inputs. The residual generator can be designed using either a unknown input observer design or by left eigenstructure assignment. The two approaches considers the uncertainty of the system to act upon the linear system as an unknown input. The unknown input vector is not known but the unknown input vector distribution matrix is known. The information gained from knowing the distribution matrix can be used to de-couple the unknown input from the residual. Thus robust fault detection and isolation is possible using the disturbance de-coupled residual. The unknown input observer decouples the residual by decoupling the state estimation error from the unknown input. The left eigenstructure assignment takes a different approach to the task of de-coupling the residual, it directly de-couples the unknown input from the residual and not from the state estimation error. Another way of performing passive fault detection by using the parity space approach. The parity space approach is based on analytical redundancy relations, the residuals can be very susceptible to noise if they are not filtered. The above mentioned methods are geometric approaches, it is also possible to perform passive fault detection using statistical approaches such as Kalman filtering. The active fault detection methods are based on the design of a auxiliary signal used to perturb the system. The multi-model formulation described in [Campbell 04] uses two models one for the faulty system and one for the nominal system. When the system is perturbed by the off-line calculated auxiliary signal it is possible to determine if the system is faulty, by the use of a hyperplane test. These are some of the methods which can be used to detect faults, the method presented in this thesis will be an active fault detection approach based on the work done bt [Campbell 04].

The previous section has explained some of the terminology used within the field of fault diagnosis. Some of the available fault diagnosis methods have been introduced to show that other methods exists which might also detect the faults determined. The next section will explain the active fault diagnosis method used in the present thesis to detect the faults determined in the Chapter 6.

7.2 Auxiliary Signal Design in Fault Detection

The following section is based on the work done by [Campbell 04] and [Sloth 09]. The problem to be solved is presented in the first section to give an overview of what shall be accomplished. The subsequent section will then explain how an auxiliary signal is constructed based on the previously stated problem. The last section concerns the calculation of an auxiliary signal and the characteristcs of the designed signal.

Problem Formulation for Auxiliary Signal Design

The active fault detection method considered in the present thesis, detects by acting upon the system on a periodical basis or at critical times. This is done by using an auxiliary signal, also called a "test signal". The auxiliary signal is used to determine whether a system exhibits possible abnormal behaviour, i.e the system have become faulty. The decision of whether the system is faulty or not is made at the end of the test period. When designing an auxiliary signal a multi-model approach can be used, one model for the normal behaviour and one for the faulty behaviour. The nominal model is represented by the set $\mathbf{A}_0$, which represent the set of $\{\mathbf{u}, \mathbf{y}\}$ associated with the behaviour of the nominal system. The set $\mathbf{A}_1$ includes the set of $\{\mathbf{u}, \mathbf{y}\}$ behaviours associated with the faulty behaviour. The challenge of auxiliary signal design is to create a reasonable sized auxiliary signal such that the two sets can be separated.

$$\mathbf{A}_0 \cap \mathbf{A}_1 = \emptyset \tag{7.1}$$

This means that the observed pair $\mathbf{u}, \mathbf{y}$ is only to come from one of the possible models, as is described in Equation 7.1. A reasonable auxiliary signal will not perturb the normal operation noticeable within the test period. In general this means that the energy of the auxiliary signal should be small. If the auxiliary signal is to small the sets A_0 and A_1 will have a union that is not an empty set, and therefore the nominal system is also perturbed by the set of u,y of the faulty model, this is illustrated in Figure 7.1.

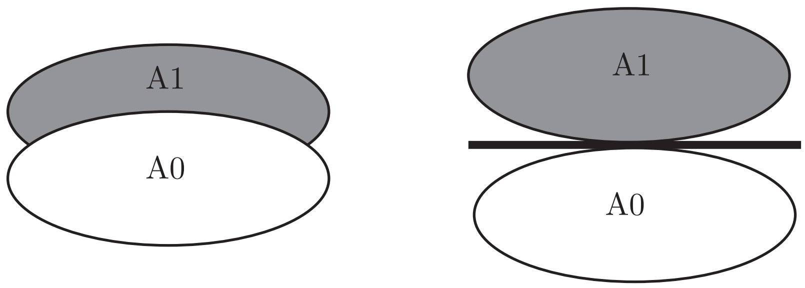

Figure 7.1: The first figure shows two sets of u,y that are not separable by a hyperplane, and therefore the auxiliary signal used is not a proper optimal auxiliary signal. The second figure shows two sets of u,y which are separable by a hyperplane, this means the the auxiliary signal used is optimal and proper.

By increasing the size of the auxiliary signal, it is possible to move the sets further apart. When the sets are moved so far apart that they can be separated by a hyperplane, a proper auxiliary signal is obtained which guarantees failure detection. It is wanted to perturb the system with the smallest possible signal, i.e an optimal proper auxiliary signal. The separation of two sets using a proper optimal auxiliary signal is illustrated in figure 7.1

7.2.1 Design of An Auxiliary Signal

The design of an auxiliary signal is based on a multi-model formulation, this denotes a model for the faulty behaviour and one for the non-faulty behaviour, see Equation 7.2. The non-faulty model used is the state space model described in Subsection 2.6.1. The faulty model is designed similarly to the non-faulty model but with some discrepancies, for instance the faulty model has to include some form of fault. The models considered are linearised models of a non-linear system and they are both perturbed by additive noise, which is given as a distribution matrix $\mathbf{N}$ and $\mathbf{M}$ multiplied by a stochastic noise process $\mathbf{w}$.

$$\dot{\mathbf{x}}_i(\mathrm{t}) = \mathbf{A}_i\mathbf{x}_i(t) + \mathbf{B}_i\mathbf{u}(t) + \overline{\mathbf{B}}_i\boldsymbol{\mu}(t) + \mathbf{M}_i\mathbf{w}_i(t) \tag{7.2a}$$

$$\mathbf{E}_i\mathbf{y}(\mathbf{t})_i = \mathbf{C}_i\mathbf{x}_i(t) + \mathbf{D}_i\mathbf{u}(t) + \overline{\mathbf{D}}_i\boldsymbol{\mu}(t) + \mathbf{N}_i\mathbf{w}_i(t) \tag{7.2b}$$

where

i	if the system is in nominal operation ($i = 0$) or if in faulty operation ($i = 1$)
$\mathbf{w}(\mathrm{t})$	is the additive uncertainty of the model i e.g noise
$\boldsymbol{\mu}(\mathrm{t})$	is the proper optimal auxiliary signal
$\overline{\mathbf{B}}_i$	is the auxiliary signal input matrix
$\overline{\mathbf{D}}_i$	is the auxiliary signal feedforward matrix
$\mathbf{N}_i$	is the sensor noise distribution matrix
$\mathbf{M}_i$	is the process noise distribution matrix
$\mathbf{E}_i$	is matrix used to eliminate output

The only conditions on the system matrices are on the matrix $\mathbf{N}$ which has to have full row rank, i.e all measurements are affected by some noise. The design of an auxiliary signal is based on knowledge of the uncertainties present in the system. There are two types of uncertainty which is additive and model uncertainty. The additive uncertainty covers either disturbances or noise added to either the input or the output. The model uncertainty covers uncertainties in the model itself, which might be caused by inaccuracy in the model parameters. It is deemed to be beyond the scope of the present thesis to consider model uncertainties, therefore only additive uncertainties are considered.

To separate the two models consideration about the allowable uncertainty has to be made, this is done by bounding the uncertainty. The uncertainty bound can according to [Campbell 04] be expressed as seen in Equation 7.4. As it can be seen from Equation 7.4 the noise, $\mathbf{w}$, is not the only uncertainty in the system, the initial condition is also an uncertainty in the system. It can also be seen from Equation **??** that the uncertainty bound constraints the uncertainty of the system to be below one. If this constraint is violated a fault has occurred due to a unlikely noise trajectory which means that $\mathbf{u}$ and $\mathbf{y}$ is not consistent with the non-faulty model. The uncertainty bound allows for both additive and model uncertainty, but one major difference is that when considering additive noise the matrix $\mathbf{J}_i = \mathbf{I}_{n\times n}$ and thus becomes $s = \mathrm{T}$ in Equation 7.4.

$$\mathrm{S}_i(\boldsymbol{\mu}(\mathrm{t}), s) = \mathbf{x}_i^{\mathrm{T}}(0)\mathbf{P}_{i,0}^{-1}\mathbf{x}_i(0) + \int_0^{\mathrm{s}} \mathbf{w}_i^{\mathrm{T}}\mathbf{J}_i\mathbf{w}_i dt \tag{7.3}$$

$$\mathrm{S}_i(\boldsymbol{\mu}(\mathrm{t}), s) < 1, \forall\, \mathrm{s} \in [0, \mathrm{T}] \tag{7.4}$$

where

$\mathbf{P}_{i,0}^{-1}$	is the initial condition weighing matrix
$\mathbf{J}_i$	is a signature matrix

The main idea behind active fault detection is to have access to a set $\mathbf{u}$ and $\mathbf{y}$, given a $\boldsymbol{\nu}$, which is consistent with one of the models. The problem is to design a optimal $\boldsymbol{\mu}$ which by observation of $\mathbf{u}$ and $\mathbf{y}$ gives enough information to decide from which model $\mathbf{u}$ and $\mathbf{y}$ are generated.

The design of an auxiliary signal is based on a optimisation problem, which seeks to find the signal with the smallest amount of energy, needed to separate the faulty and non-faulty system. The uncertainty bound can be rewritten into an optimization problem by considering the noise consistent with both models to always be to large. The noise required by one of the models to produce a $\mathbf{y}$ consistent with both the models is defined by the solution to Equation 7.2. If there are no solution to Equation 7.2 the noise required by one of the models to generate a $\mathbf{y}$ consistent with both models will always be too large. This is way of considering the problem are expressed mathematically in Equation 7.5b.

$$\sigma(\boldsymbol{\mu}(\mathrm{t}), \mathrm{s}) \geq 1 \quad \text{for some s} \tag{7.5a}$$

where

$$\sigma(\boldsymbol{\mu}(\mathrm{t}), \mathrm{s}) = \inf_{\substack{\mathbf{w}_0, \mathbf{w}_1, \mathrm{u}, \mathrm{y}, \\ \mathbf{x}_0, \mathbf{x}_1}} \max(\mathrm{S}_0(\boldsymbol{\mu}(\mathrm{t}), \mathrm{s}), \mathrm{S}_1(\boldsymbol{\mu}(\mathrm{t}, \mathrm{s}))) \tag{7.5b}$$

The maximum of two numbers can be rewritten into the expression seen in Equation 7.6, which is a maximisation of a linear combination of the two numbers over a interval ϵ.

$$\max(\mathrm{S}_0(\boldsymbol{\mu}(t), s), \mathrm{S}_1(\boldsymbol{\mu}(t, s))) = \max_{0\leq\epsilon\leq 1}(\epsilon \mathrm{S}_0(\boldsymbol{\mu}(t), s) + (1-\epsilon)\mathrm{S}_1(\boldsymbol{\mu}(t), s)) \tag{7.6}$$

To make the algorithms that follows valid it is needed to transform the inf max problem to a max inf problem. The reason that this operation is valid can be found in [Campbell 04, pp. 115].

$$\sigma(\boldsymbol{\mu}(t), s) = \max_{\epsilon\in[0,1]} \phi_\epsilon(\boldsymbol{\mu}(t), s) \tag{7.7a}$$

where

$$\phi_\epsilon(\boldsymbol{\mu}(t), s) = \inf_{\substack{\mathbf{w}_0, \mathbf{w}_1, u, y, \\ \mathbf{x}_0, \mathbf{x}_1}} (\epsilon \mathrm{S}_0(\boldsymbol{\mu}(t), s) + (1-\epsilon)\mathrm{S}_1(\boldsymbol{\mu}(t), s)) \tag{7.7b}$$

A indicator of how good the two models can be separated is the separability index:

$$\gamma^* = \left(\inf_{\boldsymbol{\mu}\in V} \int_0^T ||\boldsymbol{\mu}(t)||^2 \, dt \right)^{-\frac{1}{2}} \tag{7.8}$$

where
γ^* is the separability index for the two models.

From Equation 7.8 it can be seen that if there exist a small proper auxiliary signal the separability index will become large because the models are easily separated, and if the models are hard to separate the separability index will be very small. To find the smallest possible auxiliary signal that separates the two models, it is needed to rewrite the constraint seen in Equation 7.4 into an optimisation problem. This is done by combining the faulty and nominal models into a single model, this makes it possible to form a single optimisation problem.

$$\mathbf{F} = \begin{bmatrix} \mathbf{F}_0 & \mathbf{F}_1 \end{bmatrix} = \begin{bmatrix} \mathbf{E}_0 \\ \mathbf{E}_1 \end{bmatrix}^\perp \tag{7.9}$$

The combination of the two models is done in two separate steps, the first step calculates a matrix $\mathbf{F}$ which is used to eliminate the output and the second step combines the two models into one. The two models can then be combined into one model by using the state space matrices for each of the systems.

$$\begin{gathered}
\mathbf{x}(t) = \begin{bmatrix} \mathbf{x}_0(t) \\ \mathbf{x}_1(t) \end{bmatrix}, \mathbf{w}(t) = \begin{bmatrix} \mathbf{w}_0(t) \\ \mathbf{w}_1(t) \end{bmatrix}, \mathbf{A} = \begin{bmatrix} \mathbf{A}_0 & 0 \\ 0 & \mathbf{A}_1 \end{bmatrix}, \mathbf{B} = \begin{bmatrix} \mathbf{B}_0 \\ \mathbf{B}_1 \end{bmatrix}, \mathbf{M} = \begin{bmatrix} \mathbf{M}_0 & 0 \\ 0 & \mathbf{M}_1 \end{bmatrix}, \\
\mathbf{C} = \begin{bmatrix} \mathbf{F}_0\mathbf{C}_0 & \mathbf{F}_1\mathbf{C}_1 \end{bmatrix}, \quad \mathbf{D} = \mathbf{F}_0\mathbf{D}_0 + \mathbf{F}_1\mathbf{D}_1, \quad \mathbf{N} = \begin{bmatrix} \mathbf{F}_0\mathbf{N}_0 & \mathbf{F}_1\mathbf{N}_1 \end{bmatrix}, \\
\mathbf{P}_\epsilon^{-1} = \begin{bmatrix} \epsilon\mathbf{P}_{0,0}^{-1} & 0 \\ 0 & (1-\epsilon)\mathbf{P}_{1,0}^{-1} \end{bmatrix}, \mathbf{J}_\epsilon = \begin{bmatrix} \epsilon\mathbf{J}_0 & 0 \\ 0 & (1-\epsilon)\mathbf{J}_1 \end{bmatrix}
\end{gathered} \tag{7.10}$$

After the combining the two models into one model, the expression seen in Equation 7.7 can be rewritten into a single optimisation problem.

$$\phi_\epsilon(\boldsymbol{\mu}(t), s) = \inf_{\mathbf{w}(t), \mathbf{x}(t)} \mathbf{x}^T(0)\mathbf{P}_\epsilon^{-1}\mathbf{x}(0) + \int_0^s \mathbf{w}(t)^T \mathbf{J}_\epsilon \mathbf{w}(t) \tag{7.11}$$

subject to

$$\begin{aligned}\dot{\mathbf{x}}(\mathrm{t}) &= \mathbf{Ax}(\mathrm{t}) + \mathbf{B}\boldsymbol{\mu}(\mathrm{t}) + \mathbf{Mw}(\mathrm{t})\\ 0 &= \mathbf{Cx}(\mathrm{t}) + \mathbf{D}\boldsymbol{\mu}(\mathrm{t}) + \mathbf{Nw}(\mathrm{t})\end{aligned}$$

The objective of the optimisation problem is to find a minimal energy input signal that separates the systems. The optimisation problem can be rewritten as a consequence of this objective, the optimisation problem then becomes:

$$\min_{\boldsymbol{\mu}(\mathrm{t})} \int_0^T \boldsymbol{\mu}^T(\mathrm{t})\boldsymbol{\mu}(\mathrm{t})\mathrm{dt} \tag{7.13}$$

subject to

$$\phi_\epsilon(\boldsymbol{\mu}(\mathrm{t}), s) \geq 1$$

The optimisation problem to be solved to find a proper optimal auxiliary signal can be written as seen below:

$$\mathbf{J}(\mathrm{s}, \mathbf{w}(\mathrm{t}), \mathbf{x}(\mathrm{t})) = \max_{\boldsymbol{\mu}} \inf_{\mathbf{w}(\mathrm{t}),\mathbf{x}(\mathrm{t})} \mathbf{x}^{\mathrm{T}}(0)\mathbf{P}_\epsilon^{-1}\mathbf{x}(0) + \int_0^s (\mathbf{w}^{\mathrm{T}}(\mathrm{t})\mathbf{J}_\epsilon\mathbf{w}(\mathrm{t}) - \boldsymbol{\mu}^{\mathrm{T}}(\mathrm{t})\lambda\mathrm{I}\boldsymbol{\mu}(\mathrm{t}))dt \tag{7.14}$$

subject to

$$\begin{aligned}\dot{\mathbf{x}}(\mathrm{t}) &= \mathbf{Ax}(\mathrm{t}) + \mathbf{B}\boldsymbol{\mu}(\mathrm{t}) + \mathbf{Mw}(\mathrm{t})\\ 0 &= \mathbf{Cx}(\mathrm{t}) + \mathbf{D}\boldsymbol{\mu}(\mathrm{t}) + \mathbf{Nw}(\mathrm{t})\end{aligned}$$

Construction of a proper optimal auxiliary signal

To construct a proper optimal auxiliary signal it is needed to solve the optimisation problem derived in the previous section. A solution to the optimization problem is, according to [Campbell 04, page 80], to solve the derivative Riccati equation on the interval [0,T] shown in Equation 7.15. If there is a solution to the Riccati equation, there is a solution to the optimization problem shown in Equation 7.14.

$$\begin{aligned}\dot{\mathbf{P}} =&(\mathbf{A} - \mathbf{S}_{\lambda,\epsilon}\mathbf{R}_{\lambda,\epsilon}^{-1}\mathbf{C})\mathbf{P} + \mathbf{P}(\mathbf{A} - \mathbf{S}_{\lambda,\epsilon}\mathbf{R}_{\lambda,\epsilon}^{-1}\mathbf{C})^{\mathrm{T}} - \mathbf{PC}^T\mathbf{R}_{\lambda,\epsilon}^{-1}\mathbf{CP}\\ &+ \mathbf{Q}_{\lambda,\epsilon} - \mathbf{S}_{\lambda,\epsilon}\mathbf{R}_{\lambda,\epsilon}^{-1}\mathbf{S}_{\lambda,\epsilon}\end{aligned} \tag{7.15}$$

where

$$\begin{bmatrix}\mathbf{Q}_{\lambda,\epsilon} & \mathbf{S}_{\lambda,\epsilon}\\ \mathbf{S}_{\lambda,\epsilon}^{\mathrm{T}} & \mathbf{R}_{\lambda,\epsilon}\end{bmatrix} = \begin{bmatrix}\mathbf{M} & \mathbf{B}\\ \mathbf{N} & \mathbf{D}\end{bmatrix}\begin{bmatrix}\mathbf{J}_\epsilon & 0\\ 0 & -\lambda\mathbf{I}_{4\times4}\end{bmatrix}\begin{bmatrix}\mathbf{M} & \mathbf{B}\\ \mathbf{N} & \mathbf{D}\end{bmatrix}^{\mathrm{T}} \tag{7.16}$$

It is wanted to find the maximum separability index by solving the derivative Riccati equation. This is done by making a grid of values of ϵ ranging from zero to one, the number of grid values are dependent on the wanted precision. The matrices are indexed because they should be recalculated every time λ or ϵ is changed. At each value of ϵ the largest value of λ, for which there is a solution to the Riccati equation on the interval zero to T, is found by iteration. The iteration of the values of λ and ϵ is done by the use of a bisection method. It shall be noted that the values of λ can in some cases become large but this does not affect the generation of an auxiliary signal.

The maximum separability index is denoted as λ^* and it is calculated at ϵ^*, which is the value of ϵ where it has been computed. At this point where the separability index is at its maximum, it is expected that the auxiliary signal contains the least amount of energy to separate the two models. The solution of the Riccati equation at the found optimum ϵ^* is then used to calculate the optimum input. This is done by determining the solution to the two-point boundary value problem(TPBVP) expressed in Equation 7.17.

$$\begin{bmatrix} \dot{\mathbf{x}}(\mathrm{t}) \\ \boldsymbol{\zeta}(\mathrm{t}) \end{bmatrix} = \begin{bmatrix} \boldsymbol{\Omega}_{11} & \boldsymbol{\Omega}_{12} \\ \boldsymbol{\Omega}_{21} & \boldsymbol{\Omega}_{22} \end{bmatrix} \begin{bmatrix} \mathbf{x}(\mathrm{t}) \\ \boldsymbol{\zeta}(\mathrm{t}) \end{bmatrix} \tag{7.17}$$

where

$$\begin{aligned} \boldsymbol{\Omega}_{11} &= \mathbf{A} - \mathbf{S}_{\lambda^*,\epsilon^*}\mathbf{R}^{-1}_{\lambda^*,\epsilon^*}\mathbf{C} \\ \boldsymbol{\Omega}_{12} &= \mathbf{Q}_{\lambda^*,\epsilon^*} - \mathbf{S}_{\lambda^*,\epsilon^*}\mathbf{R}^{-1}_{\lambda^*,\epsilon^*}\mathbf{S}^{\mathrm{T}}_{\lambda^*,\epsilon^*} \\ \boldsymbol{\Omega}_{21} &= \mathbf{C}^{\mathrm{T}}\mathbf{R}^{-1}_{\lambda^*,\epsilon^*}\mathbf{C} \\ \boldsymbol{\Omega}_{22} &= -\boldsymbol{\Omega}^{\mathrm{T}}_{11} \end{aligned}$$

The boundaries for the two-point boundary value problem is seen in equation 7.18. It is seen that if the matrix P(t) from the TPBVP stays non-singular from zero to t, the TPBVP only have a zero solution. This means that at some time near the end of the interval to time T or at the end of the interval, the matrix $\mathbf{P}(t)$ has to become singular, to make $\mathbf{x}(\mathrm{T})$ different from zero.

$$\mathbf{x}(0) = \mathbf{P}(0)\boldsymbol{\zeta}(0) \tag{7.18a}$$

$$\boldsymbol{\zeta}(\mathrm{T}) = 0 \tag{7.18b}$$

From Equation 7.19 it is seen that $\mathbf{x}(T)$ must be in the null space of $\mathbf{P}^{-1}(T)$. This is only possible because $\mathbf{P}(t)$ becomes singular at time T when solving the Riccati equation.

$$\mathbf{x}(\mathrm{t}) = \mathbf{P}(\mathrm{t})\boldsymbol{\zeta}(\mathrm{t}) \tag{7.19}$$

When the TPBVP has been solved the calculated trajectories of $\mathbf{x}(t)$ and $\boldsymbol{\zeta}(t)$ can be used to calculate the auxiliary signal as is shown in Equation 7.20. The only way to get the optimal proper auxiliary is to choose α such that $||\mu^*(t)|| = 1/\gamma^*$.

$$\boldsymbol{\mu}^*(\mathrm{t}) = \alpha\left((\mathbf{S}_{\lambda^*,\epsilon^*}\mathbf{R}^{-1}_{\lambda^*,\epsilon^*}\mathbf{D} - \mathbf{B})^{\mathrm{T}}\boldsymbol{\zeta}(\mathrm{t}) + \mathbf{D}^{\mathrm{T}}\mathrm{R}^{-1}_{\lambda^*,\epsilon^*}\mathbf{C}\mathbf{x}(\mathrm{t})\right)/\lambda^* \tag{7.20}$$

The design of a optimal proper auxiliary signal is now done, and the next step is to design a on-line detection test which determines which hypothesis to accept.

Design of a Hyperplane Detection Test

The detection of faults is done by separating the two models, this can be done by a realisability test or a hyperplane test. The realisability test is the standard solution to the on-line detection problem. The realisability of a given output pair $\{\mathbf{u}, \mathbf{y}\}$ for a given model can be determined by a single inequality test. In a perfect world it would be sufficient to use a single realisability test for one of the two models, since by construction:

$$\mathcal{A}_0(\boldsymbol{\mu}^*) \cap \mathcal{A}_1(\boldsymbol{\mu}^*) = \emptyset \tag{7.21}$$

In the real world the models considered are not perfect, therefore both realisability tests has to be used for on-line detection. The second test used in on-line detection is the hyperplane test. It is only for some cases it is possible to construct a hyperplane, a separating hyperplane exists if the output sets of $\mathcal{A}_i(\boldsymbol{\mu})$ are convex.

There are different ways to determine which of the hypotheses are the most probable. When choosing a detection test some considerations of the use is needed. The computational complexity of the different methods decides which detection method to use. If the system has restricted computational power it might be preferable to choose a method which is not very computational complex but has some other weaknesses. If the computational power is unlimited it might be preferable to choose a method which is more computational complex to obtained a more precise detection. The test is meant to be run online, therefore it is chosen to use a method that relies on two offline calculated signals combined with the output of the system. The method used is based on the calculation of a hyperplane that is to separate the two models.

The separating hyperplane test can be described in continuous time as Equation 7.22.

$$\int_0^T \mathbf{h}(t)^{\mathrm{T}} \left(\mathbf{y}(t) - \mathbf{y}^*(t)\right) dt \lesseqgtr 0 \tag{7.22}$$

$$\mathbf{h} = \left(\mathbf{F}\begin{bmatrix}\mathbf{E}_0 \\ -\mathbf{E}_1\end{bmatrix}\right)^{\mathrm{T}} \mathbf{R}_{\lambda^*,\epsilon^*}^{-1} \left(\mathbf{C}\mathbf{x} + \mathbf{S}_{\lambda^*,\epsilon^*}^{\mathrm{T}}\boldsymbol{\zeta}\right) \tag{7.23}$$

$$\mathbf{y}^* = \alpha \begin{bmatrix}\mathbf{E}_0 \\ \mathbf{E}_1\end{bmatrix}^{\dagger} \left(\begin{bmatrix}\mathbf{C}_0 & \mathbf{0} \\ \mathbf{0} & \mathbf{C}_1\end{bmatrix}\mathbf{x} - \boldsymbol{\psi}_{\lambda^*,\epsilon^*}\begin{bmatrix} -\boldsymbol{\zeta} \\ \mathbf{F}^{\mathrm{T}}\mathbf{R}_{\lambda^*,\epsilon^*}^{-1}\left(\mathbf{C}\mathbf{x} + \mathbf{S}_{\lambda^*,\epsilon^*}^{\mathrm{T}}\boldsymbol{\zeta}\right)\end{bmatrix}\right) \tag{7.24}$$

where

$$\boldsymbol{\psi}_{\lambda^*,\epsilon^*} = \begin{bmatrix}\mathbf{J}_{\epsilon^*} & \mathbf{0} \\ \mathbf{0} & -\lambda\mathbf{I}_{4\times4}\end{bmatrix}^{-1} \begin{bmatrix}\mathbf{M} & \mathbf{B} \\ \mathcal{N} & \mathcal{D}\end{bmatrix}^{\mathrm{T}} \tag{7.25}$$

and

$$\mathcal{N} = \begin{bmatrix}\mathbf{N}_0 & \mathbf{0} \\ \mathbf{0} & \mathbf{N}_1\end{bmatrix}, \ \mathcal{D} = \begin{bmatrix}\mathbf{D}_0 & \mathbf{0} \\ \mathbf{0} & \mathbf{D}_1\end{bmatrix} \tag{7.26}$$

In the general case $\mathbf{y}^*(t)$ has a value between the two sets of outputs from the systems. The signal $\mathbf{h}(t)$ has some certain properties which ensures that Equation 7.22 gets the correct sign. This entails that $\mathbf{h}(t)$ must retain the following properties:

- Change sign when $\mathbf{y}(t) - \mathbf{y}^*(t)$ changes sign
- Have a large magnitude when the outputs of the two models are far apart.
- Have a small magnitude when the outputs of the two models intersect.

The general concept behind a hyperplane test can be seen in Figure 7.2. The auxiliary signal shown in the figure is designed for a wind turbine, but the concepts are the same. The auxiliary signal act upon the pitch actuator which yields a certain output. The output is used to determine if a fault has occurred, based on the hyperplane test performed. The hyperplane test results in a integral which changes sign dependent on if there is a fault present or not, this is illustrated in the last picture in Figure 7.2.

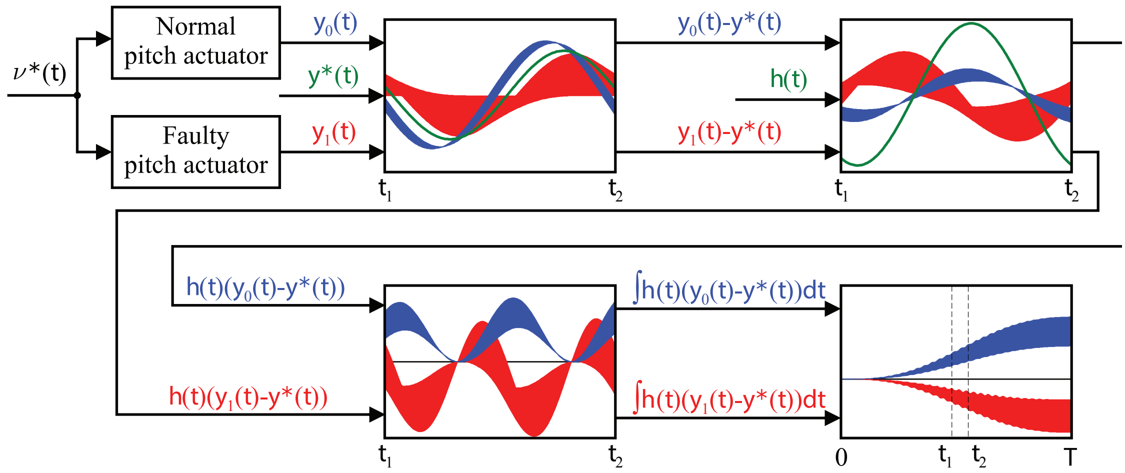

Figure 7.2: The figure shows the general concepts behind the design of an auxiliary signal used on a wind turbine [Sloth 09]. The auxiliary signal is denoted as ν in this figure. It can be see nhow the auxiliary signal enters the system, and the resulting output is checked using a hyperplane test.

The previous section has presented the design of an auxiliary signal together with the the design of a hyperplane detection test. The only thing which remains is the realization of the auxiliary siganl.

7.2.2 Auxiliary Signal Realization

When solving the optimization problem used to design an auxiliary signal there sometimes exist some numerical issues, because the matrix $\mathbf{P}$ ideally becomes singular at time T. To circumvent this issue Equation 7.15 is solved from zero to $\mathrm{T}-\delta$, where δ is a small fraction of T. From $\mathrm{T}-\delta$ until T a equivalent Riccati equation is utilised for $\mathbf{P}^{-1}$ which implies that $\mathbf{P}^{-1}$ is obtained at time T. $\mathbf{P}^{-1}$ is used to calculate $\mathbf{x}(\mathrm{T})$ based on the null space of $\mathbf{P}^{-1}$ as explained in the previous section. However it is not numerically reliable to solve the optimization problem from zero to T because the solver may break down before providing a singular $\mathbf{P}^{-1}$. Therefore the method described in the previous section is used together with the Riccati equation for $\mathbf{P}^{-1}$. The optimization problem is solved using Equation 7.15 from zero to $\mathrm{T}-\delta$ and for the rest of the interval Equation 7.27 is utilised. The solution to Equation 7.27 at time T is utilised to calculate $\mathbf{x}(\mathrm{T})$ in the two-point boundary value problem from the rest of the interval the trajectories calculated using Equation 7.15. It is not certain that it is needed to utilise this method to calculate the auxiliary signal but it can become necessary.

$$
\begin{aligned}
-\dot{\mathbf{P}}^{-1} &= \mathbf{P}^{-1}(\mathbf{A}-\mathbf{S}_{\lambda,\epsilon}\mathbf{R}_{\lambda,\epsilon}^{-1}\mathbf{C}) + (\mathbf{A}-\mathbf{S}_{\lambda,\epsilon}\mathbf{R}_{\lambda,\epsilon}^{-1}\mathbf{C})\mathbf{P}^{-1} \\
&\quad - \mathbf{C}^{\mathrm{T}}\mathbf{R}_{\lambda,\epsilon}^{-1}\mathbf{C} + \mathbf{P}^{-1}(\mathbf{Q}_{\lambda,\epsilon} - \mathbf{S}_{\lambda,\epsilon}\mathbf{R}_{\lambda,\epsilon}^{-1}\mathbf{S}_{\lambda,\epsilon}^{\mathrm{T}})\mathbf{P}^{-1}
\end{aligned} \tag{7.27}
$$

The fault to be detected with the designed auxiliary signal is a stuck heading sensor. The detection time is chosen to be 5s which is based on the mission objective and travelling speed of AAUSHIP.

The generation of an auxiliary signal is based on the relationship between the parameters ϵ and λ. The parameter ϵ is for implementation purposes a grid of values between zero and one. For the present thesis it is chosen to use 100 values between zero and one as this gives the best result. It is then wanted to determine the smallest value of λ where the Riccati equation, described earlier, has a solution. The Riccati equation will at some point in time diverge because of the quadratic term in the equation. The magnitude of this divergence is used to determine when the smallest value for λ is found. The Riccati equation is implemented using MATLAB's ordinary differential equation solver, `ode45`.

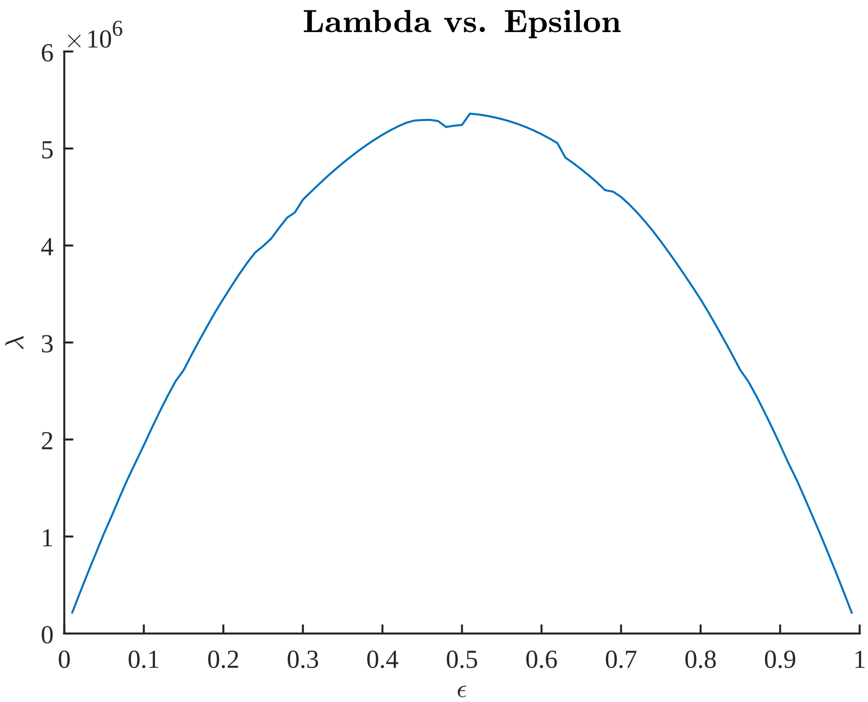

Figure 7.3: The plot shows the relation between the iterated λ and ϵ. There can be seen some in regularities in the plot which is caused by integration tolerances in MATLAB

The iteration of the parameters λ and ϵ is done using a bisection method because of its speed. When the iteration is done, the result, as can be seen in Figure 7.3, is used to determine the maximum λ value and the corresponding ϵ value. When these values are found the Riccati equation is solved at these values. The solution returned from the Riccati equation is then used to determine $\mathbf{x}(\mathrm{T})$ which shall be used to solve the two-point boundary value problem. When the two-point boundary value problem is solved it is possible to determine a auxiliary signal.

The auxiliary signal designed consists of four signal of 3 different amplitudes. It can be seen from the signals that their amplitudes are determine by the thrust allocation determined in a Section 2.7. This is very natural when the bottom row in the allocation matrix influences the heading of the vessel, by weighing the thrust inputs.

The designed auxiliary signal seems plausible because of the magnitude of the signal and the duration of the signal matches the 5s chosen. It is difficult to verify the auxiliary signal by it self, therefore it is chosen to verify the fault diagnosis during the acceptance test. The next section will describe the acceptance test performed to verify the overall system and the fault diagnosis.

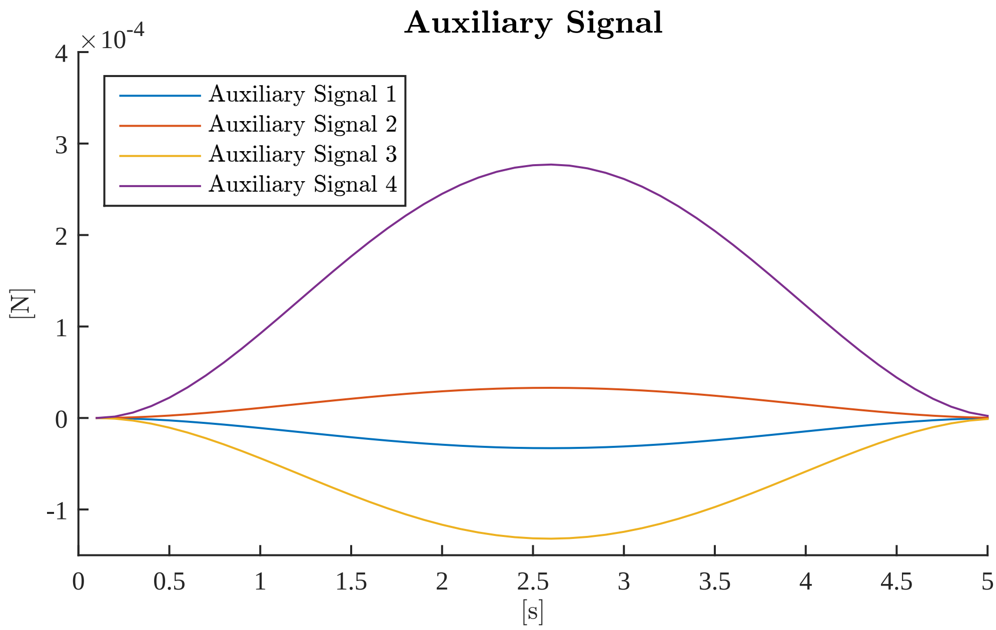

Figure 7.4: The figure shows the designed auxiliary signal. There presented four signals one for each of the thrusters. The signal shown in the figure is the signal to be implemented during the acceptance test

Chapter 8

Acceptance Test

The acceptance test of the overall system design is based on the requirements presented in Chapter 3. The acceptance test scenario is set up to be a surveying mission where the vessel shall follow a lawnmower pattern as shown in Chapter 5. During the mission the vessel will experience a fault in the heading sensor after 40 seconds. The implemented fault detection is designed to detect faults whenever the vessel is a certain distance away from the aimed for way-point. The concept behind active fault detection is to perturb the system with a signal of appropriate size to separate two models. When the signal is acting on the system the vessel might deviate from the path, this can during turns become very critical. The implementation of it is done by using a modified version of the inequality used in the way-point switching, see Equation 8.1.

$$(x_{\mathrm{k}+1} - \hat{x}(\mathrm{t}))^2 + (y_{\mathrm{k}+1} - \hat{y}(\mathrm{t}))^2 \leq \hat{u}\mathrm{T} \tag{8.1}$$

During the fault detection test it is seen that the system does not perform as expected. The expected behaviour of the fault detection is to indicate the occurrence of a fault by changing the sign of a integral. The results obtained during the test, indicates that there is something wrong with either the design of the auxiliary signal or the implementation of the fault detection.

Acceptance Test Results

The first test performed was a test of the integral characteristics when no faults have entered the system. The integral should be positive when the system is operating nominally, but this is is not what the results indicate. The integral starts out by altering between positive and negative with a magnitude of 10^5, this is shown in Figure 8.1(b). When the simulation time reaches 25s the integral increases its value to a magnitude of 10^8, as can be seen in figure 8.1(a). It is expected that this is when the vessel reaches the first way-point on its path, which is confirmed by looking at the heading angle change, see Figure 8.1(c).

The results obtained during the first test was unsatisfying and it is expected that further tests also would fail when performed but the tests were still performed to investigate what the cause of this problem might be. The next test performed was identical to the previous test, but with one change the fault has entered the system at the beginning of operations.

This test showed a negative integral with a different characteristic than expected. The magnitude of the integral is also lower than the magnitude for the previous test. The integral reaches zero at a simulation time of 25s because the inequality in Equation 8.1 is not obeyed, This can also be seen Figure 8.3. The heading shown in Figure 8.3 is seen in the NED reference frame, and implies a vessel which turns in circles.

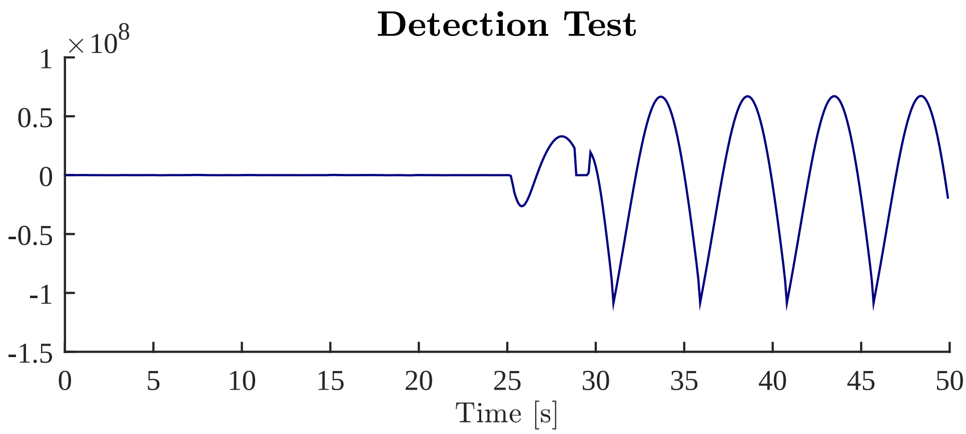

(a)

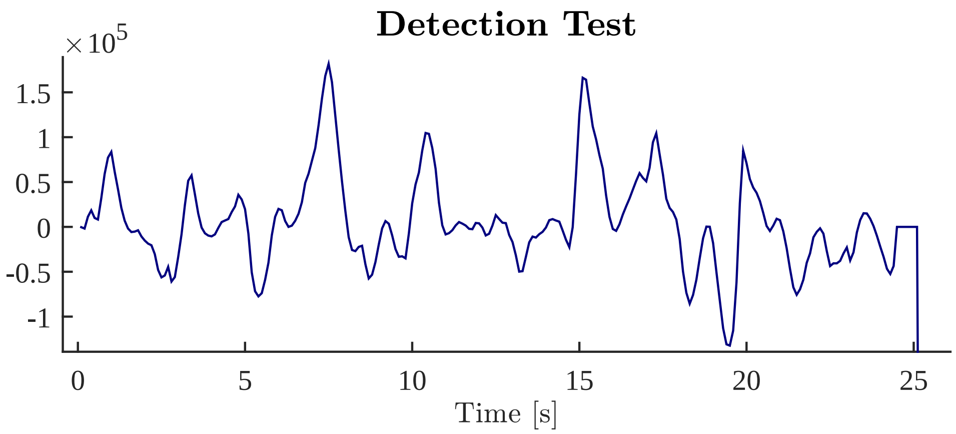

(b)

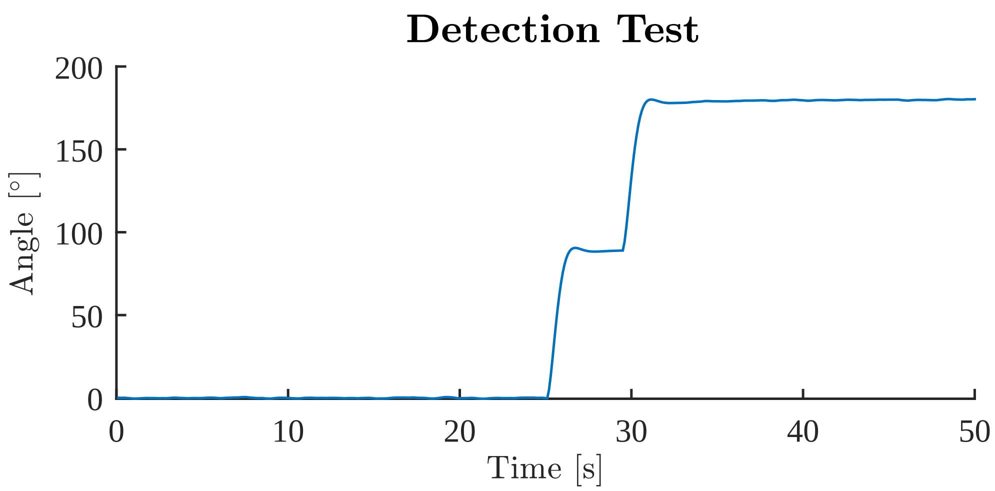

(c)

Figure 8.1: The first figure shows the evolution of the detection integral. The second figure shows the first 25s of the detection integral. The third figure shows the heading evolution during the detection test.

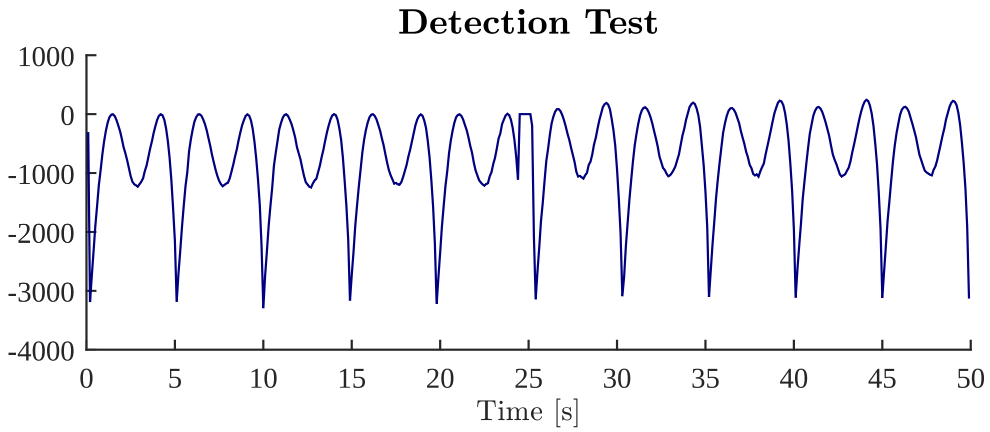

Figure 8.2: The figure shows the detection integral when a fault is present in the system from the simulation start. It can be seen from the integral that it is negative at almost all times, but the integral do not exhibit the desired behaviour.

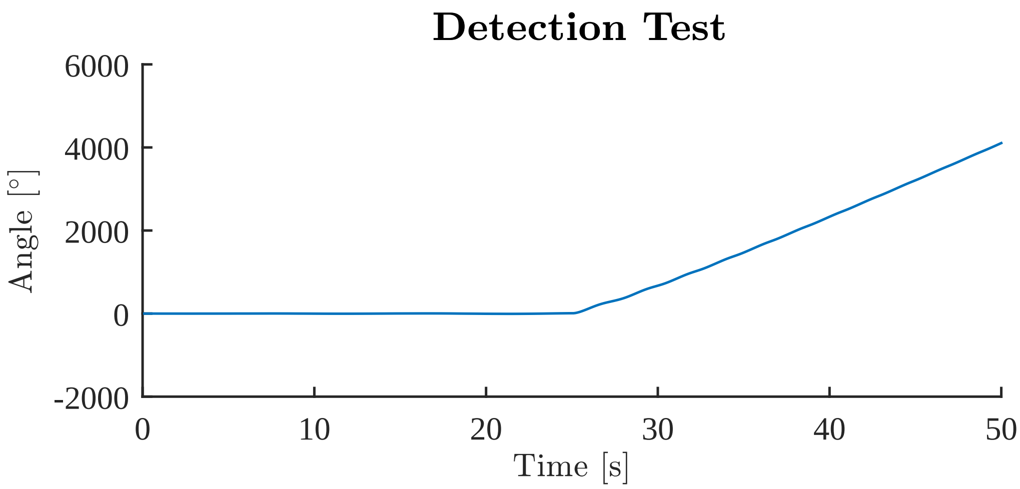

Figure 8.3: The figure shows the heading evolution during the detection test with a fault present at the start of simulation. The vessel gets out of control after the first way-point is reached, this is why the magnitude of the y-axis is so large, the vessel turn in circles.

It is decided to perform a last test of the system although the previous tests have failed. The last test is based on the overall system verification explained in Chapter 3. The vessel will survey along the path, during the survey a fault which should be detected, will enter the system.

The integral during this test shows the same characteristics as observed in the previous tests see Figure 8.4(a). The first 25s the integral's magnitude is 10^5 as seen in Figure 8.1(b). After a simulation time of 25s the integral increases to a magnitude of 10^8 as seen in the previous tests. The fault enters the system after 40s which also can be seen in the integral, see Figure 8.4(b). This implies that it is possible to distinguish between the two systems but the integral exhibits some unwanted characteristics.

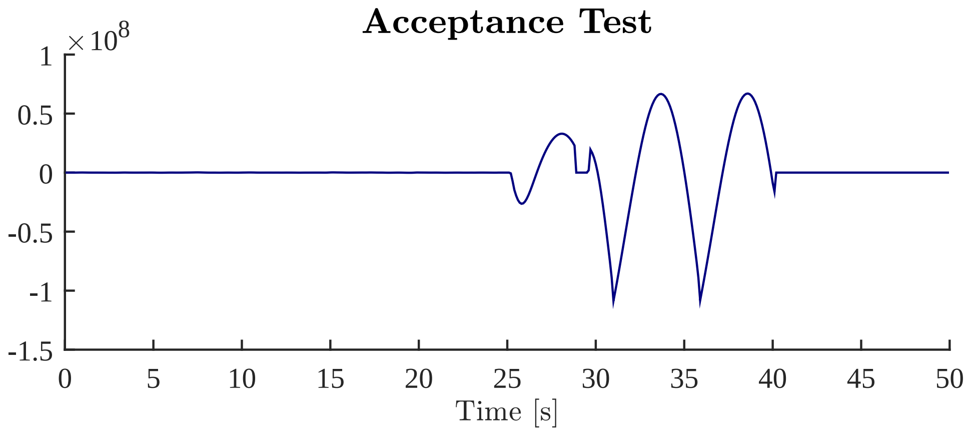

(a)

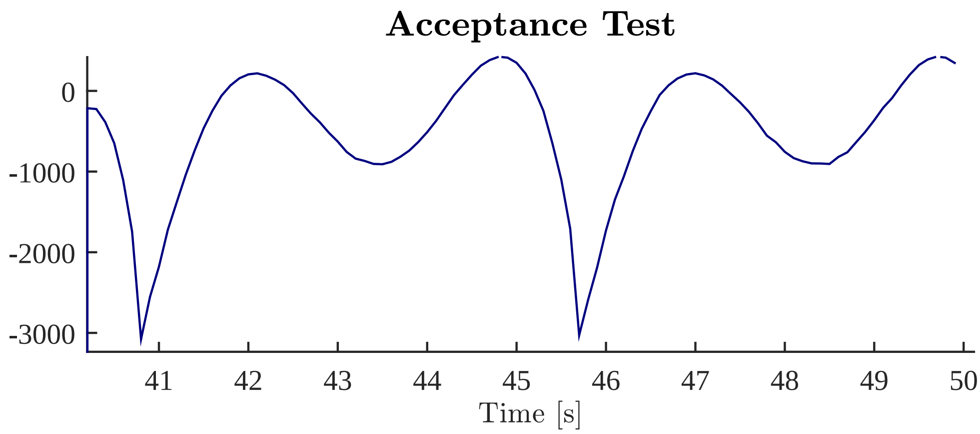

(b)

Figure 8.4: The figure shows the detection integral during the acceptance test. It can be seen from the figure that the integral changes when a fault occurs, but when there is not fault present the integral has some unwanted behaviour.

The next section will discuss the results obtained and try to determine some of the possible causes for this unwanted behaviour.

Acceptance Test Result Discussion

The results obtained in the acceptance test was not satisfying. Therefore it is wanted to investigate some of the possible causes of this undesirable performance. Four different causes are considered in this section

- Use of linear theory on a non-linear model
- Existence of separating hyperplane
- The Auxiliary Signal is not designed correctly
- Implementation error.

The fact that the theory used to design an auxiliary signal is based on linear theory and the model is a non-linear model might cause some problems when implementing the auxiliary signal. This is because the input-output relationship is different in the linear model than in the non-linear model.

The second possible cause of the exhibited behaviour is the existence of a separating hyperplane. According to [Campbell 04, pp. 87] a separating hyperplane does not always exist. This means that there may exist a hyperplane, but it is not able to separate the two models. To make sure that a separating hyperplane exists a convexity analysis of the output set shall be performed. If the output set is convex there exist a separating hyperplane. The convexity analysis is not performed during the present project.

Another cause might be a wrongly designed auxiliary signal. When designing a auxiliary signal many parameters can be tuned to alter the characteristics of the signal. The auxiliary signal designed has been made by using Equation 7.15 for the whole interval zero to T. This gives a solution to the optimization problem but it is not necessarily the right one. This is because it might not be numerically reliable to compute $x(\mathrm{T})$ this way, as stated in [Campbell 04, pp. 89], there it might be necessary to used the alternative method mentioned in 7.2.2 where a different Riccati equation is used to determine $x(\mathrm{T})$. The bisection method used to determine the relationship between λ and ϵ, iterates the value of λ based on a limit on the maximum magnitude of $\mathbf{P}$. This limit if set differently changes the auxiliary signal characteristic, this is also a plausible cause for the exhibited behaviour during the acceptance test. It is also possible to change the ODE solvers tolerances, this will also change the characteristics of the signal. There are other parameters which can be changed to change the characteristics of the signal.

The last source of error is a MATLAB implementation error. The simulation environment used to test the auxiliary signal contains many other system and between the implementation and testing of each system, it is possible that the hyperplane test has been implemented incorrectly.

It can be concluded, based on this section, that there are many plausible sources for the behaviour seen, so it is hard to determine which is one is the right cause. In future work some of the mentioned cause should e investigated to determine which error causes the behaviour seen in the acceptance test.

The next chapter will concluded on all the presented results in the present thesis.

Chapter 9

Closure

The present thesis presents a complete navigation system in preparation for autonomous hydrographic surveying together with an active fault diagnosis scheme to improve the reliability. The following chapter will summarise the results and conclusions stated in the different chapter and provide some recommendation for future work.

9.1 Conclusion

Based on the accomplishments of this project a set of conclusions are made:

- The extended Kalman filter and the unscented Kalman filter has been described. The focus have been on analysing the sensors variances and noise types, to be able to produce results which also will work when implemented on AAUSHIP. The two filters have been compared to see which one of them captures the non-linear characteristic of the model, the best. The results showed that both filters complied with the requirements of 0.5m position deviation, 0.1m/s velocity deviation and 3.6° angle deviation. The extended Kalman filter is chosen for future implementation because it out performed the unscented Kalman filter in two out of three requirements.
- A Line of Sight guidance law has been presented to navigate the vessel autonomously. The focus have been on implementing a controller which could follow a operator specified path. To steer the vessel a control system has been designed using a cascade control approach. The Line of Sight Guidance law is used to provide a desired heading reference for the designed heading controller. The implementation of the heading controller by itself was deemed insufficient because it overshot the path. A yaw rate controller was then designed to prevent the vessel from overshooting. The results showed that it was possible to navigate a surface vessel autonomously without violating the requirements of, maximum path deviation of 2.5m, a minimum turn radius of 180° and a constant speed of at least 2m/s. The controller and way-point switching algorithm was tuned to avoid the vessel from overshooting the path and instead keep itself on the inside of the path.
- A fault analysis was presented to determine the most critical faults and to chose which should be detected. To simplify the system a model partition was done. The model partition divided the system into 3 simpler systems. A fault propagation analysis was then made using the 3 simple systems to determine in what way the faults propagate through the system. The faults determined is the assessed using a severity and occurrence analysis. Based on the severity and occurrence analysis four faults have been chosen for further work. The faults chosen are the most sever fault on all the sensors and one fault on the propeller.

- An active fault diagnosis scheme has been designed based on an auxiliary signal design approach. The approach used to design an auxiliary signal is called a multi-model formulation. There have been designed two models, one describing the nominal model and one which describes the faulty model. The auxiliary signal has been designed and implemented on the system. With the work done within fault diagnosis, it can not be definitively determined whether an active fault detection scheme can improve the reliability of AAUSHIP. The results obtained in the acceptance test does not exhibit the expected behaviour. Different sources of error has been presented in the previous chapter and they shall be considered as future work. It is expected that a functioning fault diagnosis scheme would help improve the reliability of AAUSHIP.

The next section will explain some of the recommendations for future work.

9.2 Recommendations

- A better model will ensure better results when implementing systems on AAUSHIP. There are some parameters in the damping and restoring forces matrices which have not been determined. If an opportunity arises to get the vessel tested in a commercial testing facility it should be considered to achieve are more truthful model.
- The present thesis did not consider any environmental disturbances. To make sure that the vessel performance as expected, it would be desired to have the environmental disturbances modelled. With the environmental disturbances modelled there will also be a possibility to perform wave estimation.
- To make a more accurate sensor model it is needed to model the sensors. The noise affecting the sensors are not a white Gaussian process as is assumed in the present thesis. Almost all the sensors are filtered which changes the sensor noise to coloured noise. Additionally the GPS measurement shows that it is affected by drift noise caused by clock drift.
- If a fault diagnosis scheme is implemented, there would be a possibility to investigate the use of fault tolerant control on the vessel. This can be done either by designing a controller bank or an active fault tolerant control scheme.
- To determine the performance of the fault diagnosis it would be desired to implement other fault diagnosis schemes to determine the one bes suited for the task.

There are many other things to be designed and modelled before the vessel is ready for the first test implementation.

Appendix

Appendix A

Calculations within the Extended Kalman Filter

This appendix will present the equations used to implement the extended Kalman filter and unscented Kalman filter algorithm.

Firstly initial values are chosen appropriately according to the system dynamics, so the error is realistic and so the initial state is close to the true state. The prediction of the system is calculated using the non-linear system model, together with the previous state estimate and the previous input.

$$\hat{\mathbf{x}}^{-}_{\mathrm{k+1}} = f(\hat{\mathbf{x}}_{\mathrm{k}}, \mathbf{u}_{\mathrm{k}}) \quad , f \text{ is smooth} \tag{A.1}$$

$$\hat{\mathbf{z}}_{k} = g(\hat{\mathbf{x}}^{-}_{\mathrm{k+1}}) \tag{A.2}$$

This prediction of the state estimate is used to give a hint of where the system is to the present time step, based upon the previous state estimate. The next part of the prediction step is to determine the a priori error covariance, which indicates how far off the state estimate is. The a priori error covariance is calculated by using the linearised system dynamics, the Jacobian of the system dynamics.

$$\mathbf{P}^{-}_{\mathrm{k+1}} = \mathbf{\Phi}_{\mathrm{k}} \mathbf{P}^{+}_{\mathrm{k}} \mathbf{\Phi}^{\mathrm{T}}_{\mathrm{k}} + \mathbf{Q} \tag{A.3}$$

where

$\mathbf{P}^{-}_{\mathrm{k+1}}$ is the predicted error covariance
$\mathbf{P}_{\mathrm{k}}$ is the error covariance matrix of the previous time step
$\mathbf{Q}_{\mathrm{k}}$ is the state noise covariance
$\mathbf{\Phi}_{\mathrm{k}}$ is the Jacobian of the function $f(\hat{\mathbf{x}}_{\mathrm{k}}, \mathbf{u}_{\mathrm{k}})$

The model of the vessel is model in state space form as previously mentioned, the A matrix represented in the state space model is in fact the model Jacobian. Included in model Jacobian is the non-linearities owing to the vessel's dampening force. The model Jacobian is calculated to every time step, due to the change in the state estimate, which is the operating point for the linearisation.

$$\mathbf{\Phi}_{\boldsymbol{k}} = \frac{\partial f(\hat{\mathbf{x}}_{\mathrm{k}}, \mathbf{u}_{\mathrm{k}})}{\partial \mathbf{x}} \tag{A.4}$$

It is not certain that it is only in the system dynamics there is non-linearities. The non-linearities can also be presented in the sensor model, in this case there are no non-linearities in the sensor model. For the sake of keeping to the correct procedures, the sensor model will be handle as it was non-linear. To accommodate the non-linearities, the sensor model Jacobian is calculated. The sensor model Jacobian is calculated at every time step, because it is wanted to make a linearisation around the previous estimate to approximate the sensor dynamics at the next time step.

$$\mathbf{H}_{\mathrm{k}} = \frac{\partial\, g(\hat{\mathbf{x}}^{-}_{\mathrm{k+1}})}{\partial \mathbf{x}} \tag{A.5}$$

The update step contains the Kalman gain together with the posteriori estimate and the posteriori error covariance. The Kalman gain is used as an observer gain, it is used to pull the estimate towards the true state. The larger K the faster convergence, the smaller K the slower convergence.

$$\mathbf{K}_{\mathrm{k}} = \mathbf{P}^{-}_{\mathrm{k+1}}\mathbf{H}_{\mathrm{k}}(\mathbf{H}_{k}\mathbf{P}^{-}_{\mathrm{k+1}}\mathbf{H}^{\mathrm{T}}_{\mathrm{k}} + \mathbf{R}) \tag{A.6}$$

The Kalman gain is used as measure of how much the output error is trusted relative to the a priori state estimate. The output error are defined as $\mathbf{Z} - \hat{\mathbf{z}}$, where $\mathbf{Z}$ defines the output measurement and z is the estimated output. The posteriori estimate is calculated using the a priori state estimate together with the Kalman gain, and the measurement error. If the measurement and the estimated measurement are equivalent the posteriori state estimate is equal to the a priori state estimate. If this is not the case, the posteriori state estimate is also influenced by the weighted measurement error.

$$\hat{\mathbf{x}}_{\mathrm{k}} = \mathbf{x}^{-}_{\mathrm{k+1}} + \mathbf{K}_{\mathrm{k}}(\mathbf{Z}_{k} - \hat{\mathbf{z}}_{\mathrm{k}}) \tag{A.7}$$

The posteriori error covariance is calculated to show how far off the estimate is. The posteriori error covariance are calculated using the sensor model, Kalman gain and the posteriori error covariance.

$$\mathbf{P}^{+}_{\mathrm{k}} = (\mathrm{I} - \mathbf{K}_{\mathrm{k}}\mathbf{H}_{\mathrm{k}})\mathbf{P}^{-}_{\mathrm{k+1}} \tag{A.8}$$

After the calculation of the posteriori error covariance, the filter return to calculate the prediction step for the next time step, due to its recursive structure.

A.1 Unscented Kalman Filter

The extended Kalman filter can only accurately estimate non-linear dynamic systems with a behaviour which can be approximated to a first order Taylor series expansion. For dynamic systems with non-linearities higher than what can be approximated accurately with a first order Taylor series expansion. For dynamic systems with large non-linearities, it is needed to find another estimator to determine the attitude.

The unscented Kalman filter is based on the unscented transform, which is a family of transforms. The state distribution is a Gaussian random variable, which is represented as set of carefully chosen sample points within this distribution. These sample points captures the true mean and covariance of the random variable. The sample points are then propagated through the non-linear dynamic system which captures the posteriori mean and covariance. The unscented transform can capture non-linearities up to a third order Taylor expansion. Basically the unscented transform is a method for calculating the statistics of a random variable which undergoes a non-linear transformation in the sense of propagating the sigma points through the non-linear dynamic model

The first step is to choose a set of sigma points(sample points) and the true mean. The posterior estimate to k-1 is used as a mean for time k.

$$\boldsymbol{\chi}_0 = \bar{\mathbf{x}} \tag{A.9}$$

Around this mean there will be chosen sigma points, which are estimates spread around the mean according to the statistical distribution of the states. The number of sigma points are 2L + 1, where L is the number of states.

$$\boldsymbol{\chi}_{\mathrm{i,k}} = \bar{\mathbf{x}}_{\mathrm{k}} + \left(\sqrt{(\mathrm{L}+\lambda)\mathbf{P}_{\mathrm{k}}}\right)_{\mathrm{i}} \quad , \quad \mathrm{i} = 1, ..., \mathrm{L} \tag{A.10}$$

$$\boldsymbol{\chi}_{\mathrm{i,k}} = \bar{\mathbf{x}}_{\mathrm{k}} - \left(\sqrt{(\mathrm{L}+\lambda)\mathbf{P}_{\mathrm{k}}}\right)_{\mathrm{i}} \quad , \quad \mathrm{i} = \mathrm{L}+1, ..., 2\mathrm{L} \tag{A.11}$$

Where lambda is a scaling parameter, described in equation A.12, where α describes the the spread of the sigma points around the mean, $\bar{\mathrm{x}}$. κ is a secondary scaling parameter which is usually set to 0 or 1. β is used to incorporate prior knowledge of the distribution of x and is usually set to 2 for a Gaussian distribution, if the state distribution is different from Gaussian another value of β has to be chosen.

$$\lambda = \alpha^2(\mathrm{L}+\kappa) - \mathrm{L} \tag{A.12}$$

A weighing are calculated for both the predicted state estimate and for the error covariance. The first sigma point related to the mean are weighted different from the additional sigma points, this is because it is more likely that the next estimate should be close to the next estimate. The same is the case for the calculation of the predicted error covariance

$$\mathrm{W}_0^{(m)} = \lambda/(\mathrm{L}+\lambda) \tag{A.13}$$

$$\mathrm{W}_0^{(c)} = \lambda/(\mathrm{L}+\lambda) + (1-\alpha^2+\beta) \tag{A.14}$$

$$\mathrm{W}_i^{(m)} = 1/(2\mathrm{L}+2\lambda) \tag{A.15}$$

$$\mathrm{W}_i^{(m)} = \mathrm{W}_i^{(c)} \tag{A.16}$$

The sigma points are then propagated through the non-linear model, which marks the end of the unscented transform. Every sigma point propagated through the dynamic system represents are model of the system at that sigma value.

$$\boldsymbol{\chi}_{\mathrm{k}} = f(\boldsymbol{\chi}_{\mathrm{k}-1}, \mathbf{u}_{\mathrm{k}-1}) \tag{A.17}$$

The state estimate can only be a Lx1 vector, and therefore the different sigma model has to be joint to one predicted state estimate. The way the predicted state estimated is calculated is by weighing all the sigma point and then summing them from i equal zero to 2L. This creates a joint predicted state estimate based on the distribution of the state estimate and the true mean.

$$\hat{\mathbf{x}}_k^- = \sum_{i=0}^{2\mathrm{L}} \mathrm{W}_i^{(m)} \boldsymbol{\chi}_i \tag{A.18}$$

The a priori error covariance is calculated by weighing the covariance for every sigma value and them summing them together to calculated the predicted error covariance. As for the predicted state estimate, the covariance related to the mean is the covariance which is weighted most, because it will be expected to be in the vicinity of the posteriori error covariance for time step k-1.

$$\mathbf{P}_{\mathrm{k}}^{-} = \sum_{i=0}^{2\mathrm{L}} \mathrm{W}_i^{(c)} \left[\boldsymbol{\chi}_{i,k} - \hat{\mathbf{x}}_k^{-}\right] \left[\boldsymbol{\chi}_{i,k} - \hat{\mathbf{x}}_k^{-}\right]^{\mathrm{T}} \tag{A.19}$$

To take care of any possible non-linearities in the sensor model, there is also made an unscented transform of the sensor model. This is done by propagating the sigma points through the non-linear model of the sensor model. This results in a matrix containing the different sensor sigma models.

$$\boldsymbol{\mathcal{Y}}_{\mathrm{i,k}} = h(\boldsymbol{\chi}_{i,k-1}, \mathbf{u}_{k-1}) \tag{A.20}$$

The sigma point sensor models are then joint together to one output estimate. This is done by weighing the sigma values according to their index, this means that as for the state estimate the mean value is weighted most. The weighted sigma sensor models are then summed to one output estimate.

$$\hat{\mathbf{y}}_{\mathrm{k}} = \sum_{i=0}^{2\mathrm{L}} W_i^{(m)} \boldsymbol{\mathcal{Y}}_{\mathrm{i,k}} \tag{A.21}$$

The covariance of the measurements are calculated as weighted covariance of the different sigma sensor models. These weighted covariances are then summed to one output covariance, describing the predicted output error covariance.

$$\mathbf{P}_{\mathrm{yy,k}} = \sum_{i=0}^{2\mathrm{L}} W_i^{(c)} \left[\boldsymbol{\mathcal{Y}}_{\mathrm{i,k}} - \hat{\mathbf{y}}_{\mathrm{k}}\right] \left[\boldsymbol{\mathcal{Y}}_{\mathrm{i,k}} - \hat{\boldsymbol{y}}_k\right]^{\mathrm{T}} \tag{A.22}$$

The cross-correlation covariance between the states and the measurements are calculated as the covariance of the states multiplied by the covariance of the output. These covariances are then summed to a joint covariance, describing the variance between them.

$$\mathbf{P}_{\mathrm{xy,k}} = \sum_{i=0}^{2\mathrm{L}} W_i^{(c)} \left[\boldsymbol{\chi}_{i,k} - \hat{\mathbf{x}_k}^{-}\right] \left[\boldsymbol{\mathcal{Y}}_{\mathrm{i,k}} - \hat{\mathbf{y}}_k\right]^{\mathrm{T}} \tag{A.23}$$

The Kalman gain is approximated by the cross-correlation and measurements covariance. The Kalman gain has the same objective as in the extended Kalman filter, to determine how much the measurements should be trusted. The Kalman gain is like an observer gain and determine how fast the filter converges.

$$\mathbf{K} = \mathbf{P}_{\mathrm{xy,k}} \mathbf{P}_{\mathrm{yy,k}}^{-1} \tag{A.24}$$

To determine the posteriori estimate, it is needed to know the predicted estimate, measurements and the Kalman gain. The posteriori estimate is determine as the Kalman gain weighing output measurement and estimate added to the predicted estimate. Depending on this weighting the measurements will have more or less influence on the posteriori estimate.

$$\hat{\mathbf{x}} = \hat{\mathbf{x}}_{\mathrm{k}}^{-} + \mathbf{K}_k(\mathbf{y}_{\mathrm{k}} - \hat{\mathbf{y}}_{\mathrm{k}}) \tag{A.25}$$

The same for the posteriori error covariance, it is calculated based upon the predicted error covariance and the measurement covariance weighed by the Kalman gain, to determine in which degree the sensors should be trusted.

$$\mathbf{P}_{\mathrm{k}} = \mathbf{P}_{\mathrm{k}}^{-} - \mathbf{K}_{\mathrm{k}} \mathbf{P}_{\mathrm{yy,k}} \mathbf{K}_{\mathrm{k}}^{T} \tag{A.26}$$

The filter will then return to the start and find new sigma points to transform and then proceed through the filter again.

Appendix B

Sensor Noise Analysis

The sensors equipped on AAUSHIP is analysed to determine the noise characteristics. In general there exist three types of noise behaviour, Gaussian noise, drift noise, and shot noise. The Gaussian noise is a statistical noise with a distribution equal to the normal distribution. The drift noise is a time correlated random movement noise, this means that it is correlated with the previous sample, k, but the next sample, k+1, can move randomly from the previous sample, k. The shot noise is a sporadic noise with a similar amplitude among the bursts of noise, which occur at random times.

The behaviour of the noise is just a part of the characterisation of the noise, the noise can also be frequency-based which means it changes dependent on the frequency. In general there are 5 types of noise, white, pink, brown, blue, purple. Plotting the PSD of a white noise process will reveal a spectrum which is flat, this implies that the power of the noise is distributed equally across all frequencies. The PSD of pink noise will show a white noise process with the characteristics of a first order low-pass filter, this implies that the signal contains more power at low frequencies than higher frequencies. The brown noise is characterised as pink noise but its characteristics are similar to a second order filter instead, so the higher frequencies are dampened stronger. Blue and purple noise are as high pass filters, respectively first and second order.

These characteristics are determined for the sensor equipped to AAUSHIP, by the forthcoming sections. For the design of a Kalman filter and an auxiliary signal, it is needed to determine the variance of the sensors. For the auxiliary signal it is necessary to determine the needed signal power to overcome the noise. For the Kalman filter it is needed to determine the measurement covariance matrix, $\mathbf{R}$. The noise magnitudes has been determined utilising the available post-processed data, the magnitudes can be seen in table B.1

Sensor	σ^2	Unit
Magnetometer	10^{-6}	[G]
Accelerometer	10^{-4}	[g]
Gyroscope	10^{-1}	[°/s]
GPS Longitude	10^{-6}	[m]
GPS Latitude	10^{-5}	[m]

Table B.1: The table shows the magnitude of the noise expected on the output from each sensors based on the forthcoming analysis

The data is collected by performing a static sensor test, this means the vessel is kept stationary. AAUSHIP has been placed inside a building yard on campus, see figure B.1. The sensor data has then been measured and logged during a window of 3 hours. The test have been performed by group 14gr1034 in the fall semester 2014.

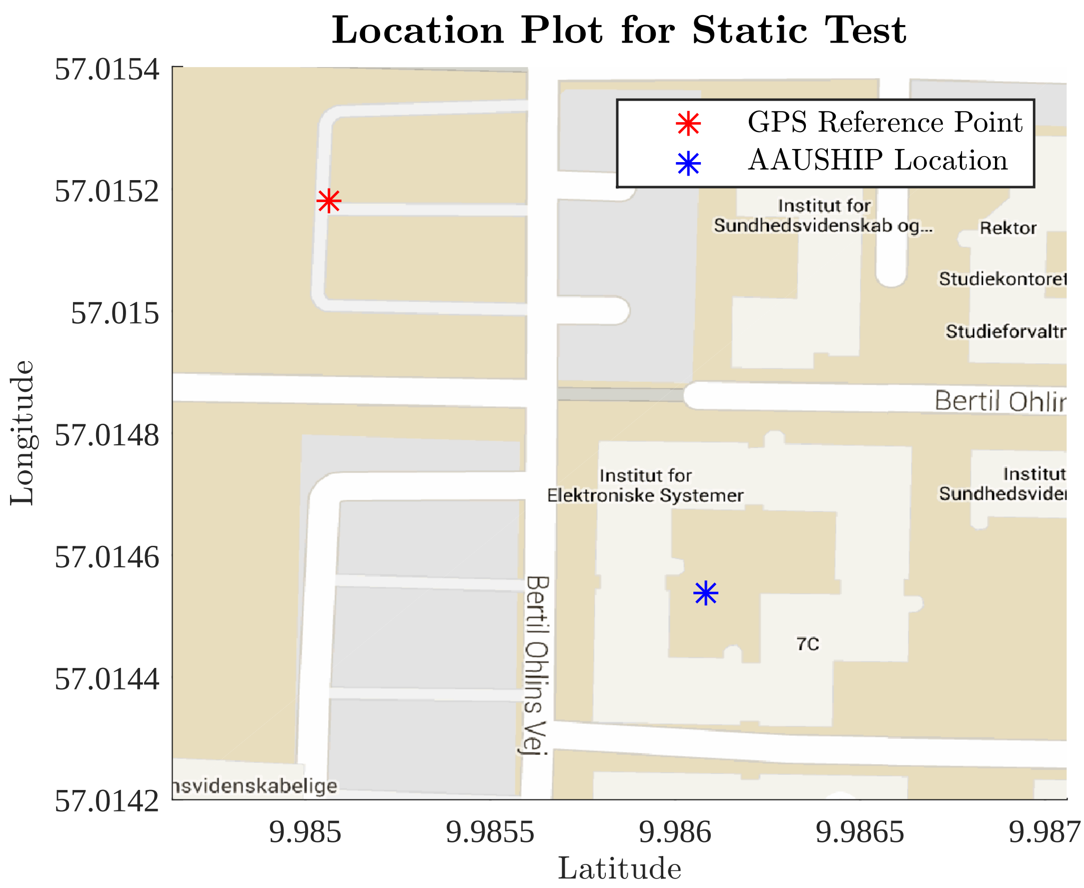

Figure B.1: The plot shows the placement of AAUSHIP together with the origin of the NED reference frame. The distances shown in plot B.2 and B.3 shall be compared to this origin in the NED reference frame.

The analysed will shortly be explained in the next section.

It can be seen from the GPS plots that the GPS is affected by drift noise. It is expected that the reason this is clock either at the satellite end or the receiver end. Because the GPS drifts it has to modelled differently. This will not be investigated further in the present thesis but is shall be noted when implementation is considered.

The IMU sensors are all affected by coloured noise which means that they as well should be model differently than the have been in the present thesis. The measurement model for the IMU should contain filtered white noise is it should depicted reality.

These are just some considerations made, in preparation for future work. Sensor noise modelling will not be considered in the present thesis.

The measurements collected has been analysed by calculating their PSD and ACF.

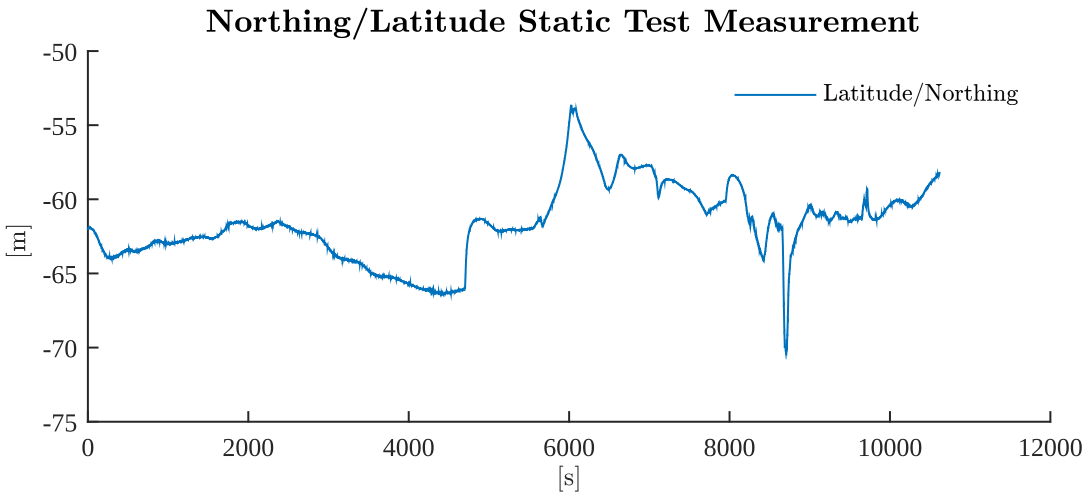

Figure B.2: The plot shows the static latitude measurement represented in the NED reference frame. Compared to the origin of the NED reference frame shown in B.1 the measurements are approximately 58-62 m away from the origin.

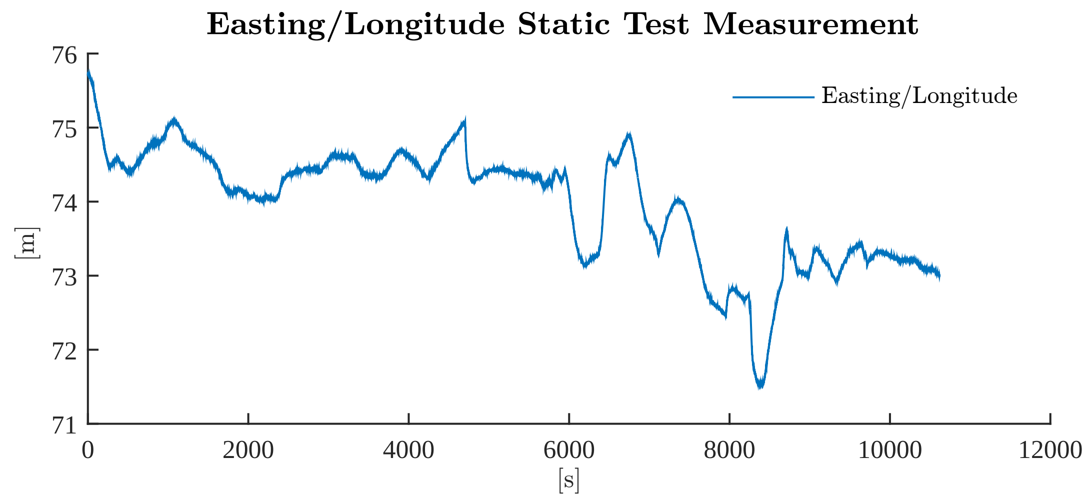

Figure B.3: The plot shows the static longitude measurement represented in the NED reference frame. The origin of the NED reference frame is placed approximately 73-75 meters away, see figure B.1

B.1 GPS

As for the GPS measurements it is straight forward to see that the samples are very correlated when looking at the autocorrelation function for both the latitude and longitude.

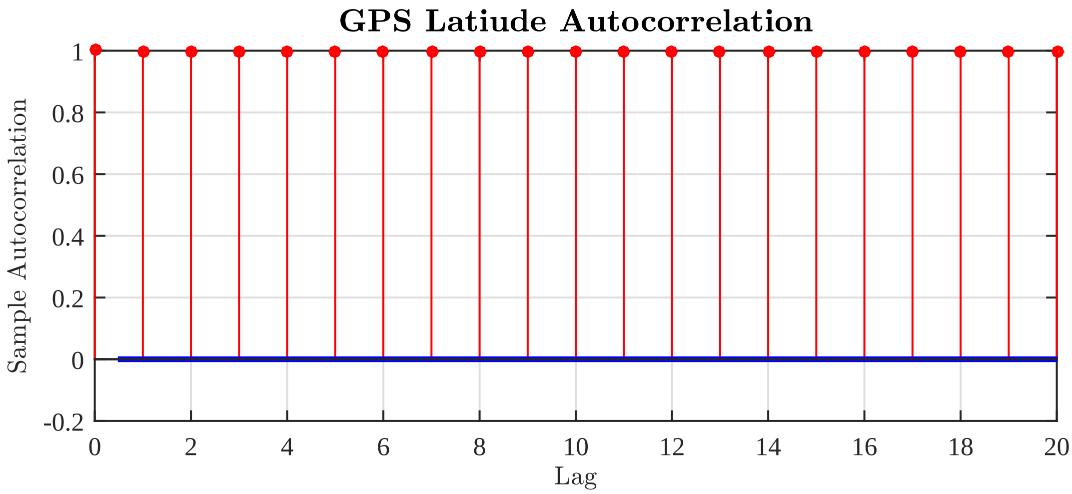

Figure B.4: The figure shows the autocorrelation function calculated for the GPS latitude measurement. It can be seen from the ACF that the samples are very correlated.

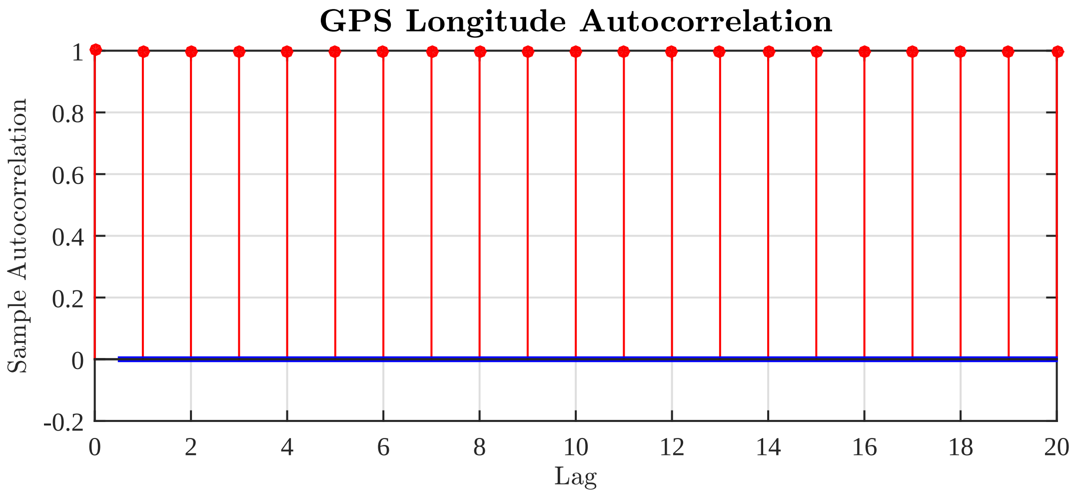

Figure B.5: The figure shows the autocorrelation function calculated for the GPS latitude measurement. It can be seen from the ACF that the samples are very correlated.

When looking at the PSD it can be seen that the noise does not have a flat spectrum and therefore it is not white noise.

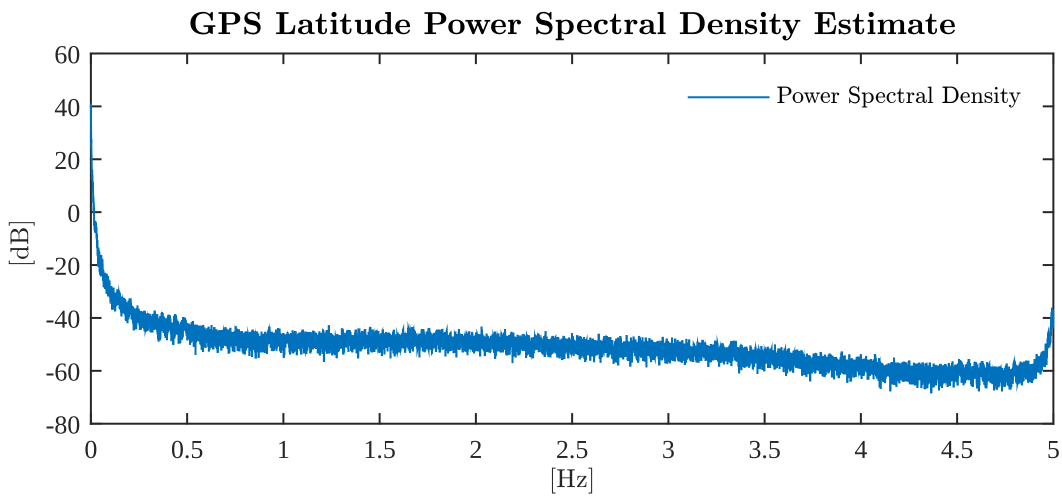

Figure B.6: The figure shows the PSD for the GPS latitude measurement. It can be seen from the slope of the graph that the noise is not white.

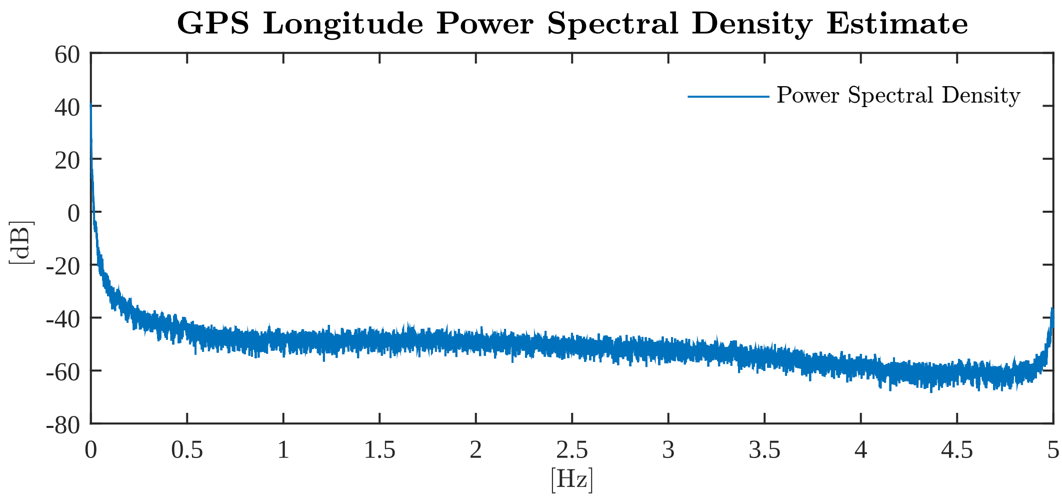

Figure B.7: The figure shows the PSD for the GPS longitude measurement. It can be seen from the slope of the graph that the noise is not white.

B.2 Magnetometer

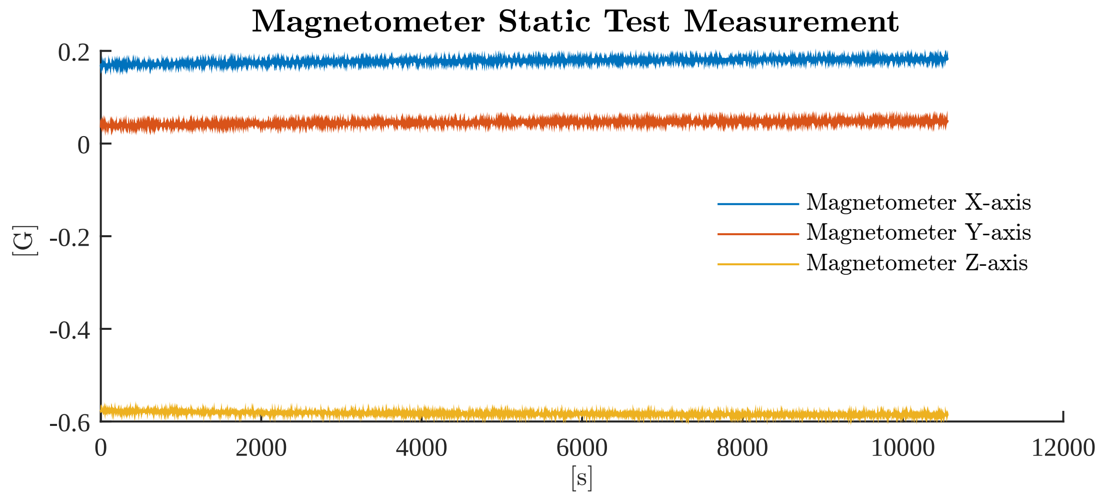

Figure B.8: The figure shows the magnetometer measurement from the static test

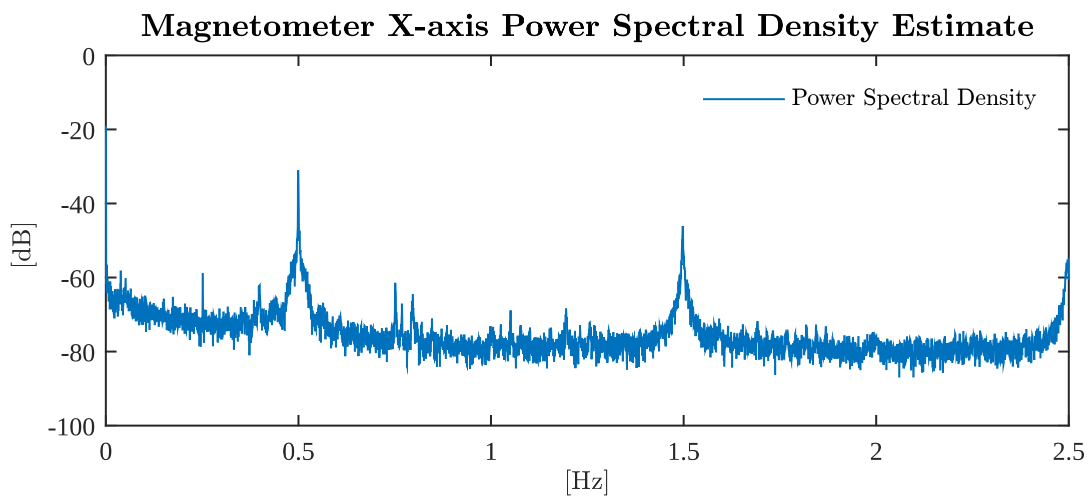

Figure B.9: The figure shows the PSD for the magnetometer x-axis. It can be seen from the figure that the noise is not white.

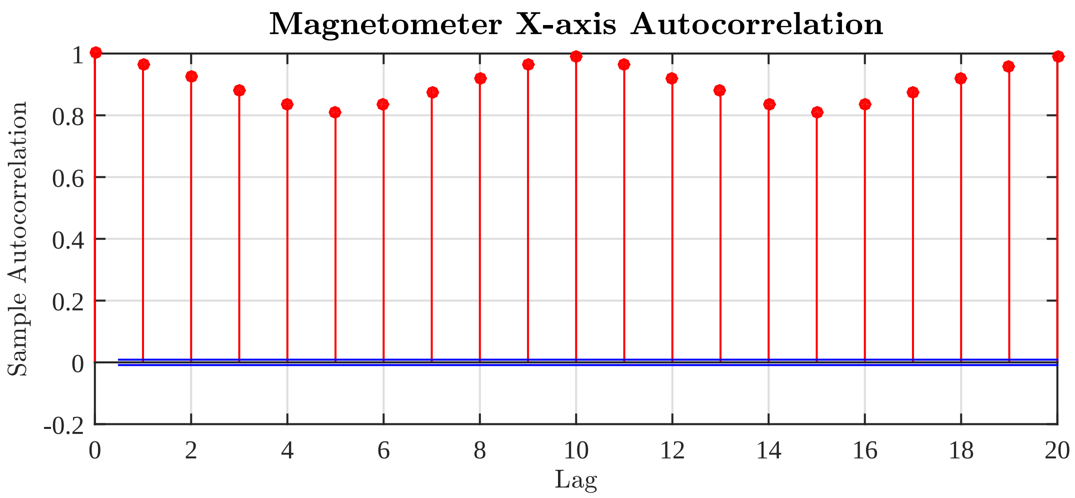

Figure B.10: The figure shows the ACF for the magnetometer x-axis which shows that the samples are very correlated.

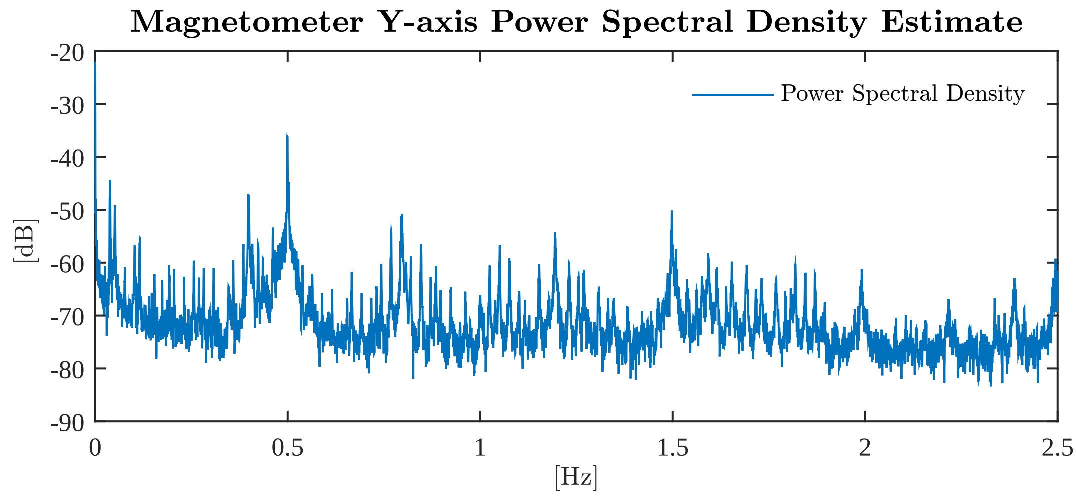

Figure B.11: The figure shows the PSD for the magnetometer y-axis. It can be seen from the figure that the noise is not white.

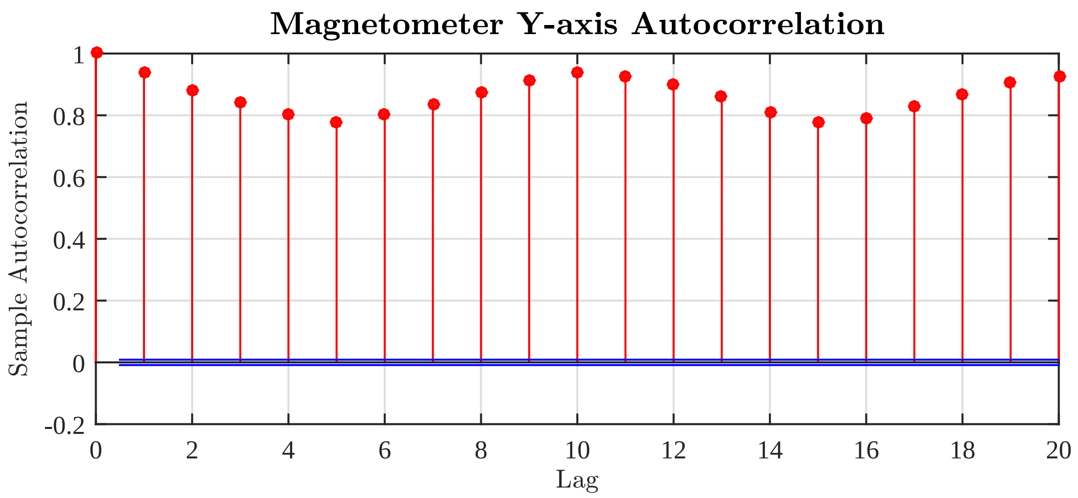

Figure B.12: The figure shows the ACF for the magnetometer y-axis which shows that the samples are very correlated.

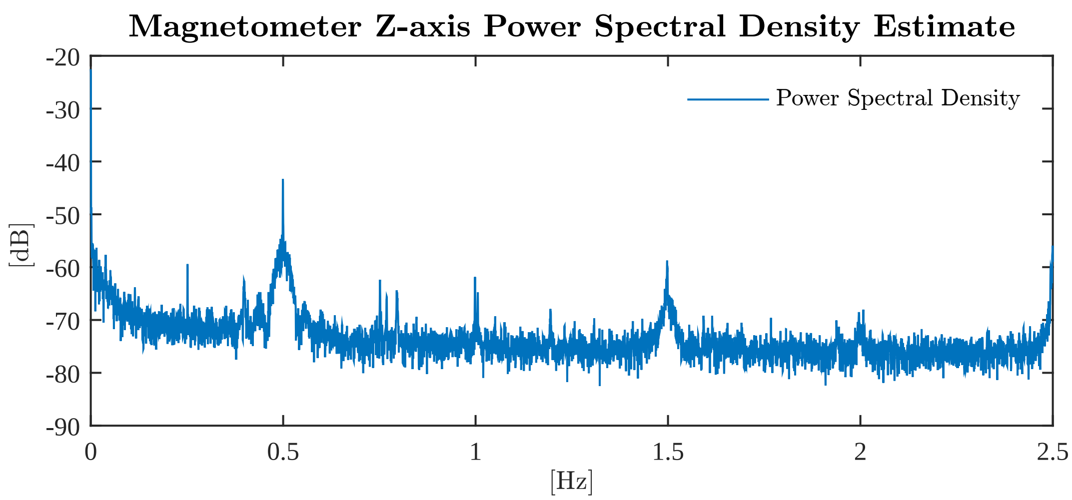

Figure B.13: The figure shows the PSD for the magnetometer z-axis. It can be seen from the figure that the noise is not white.

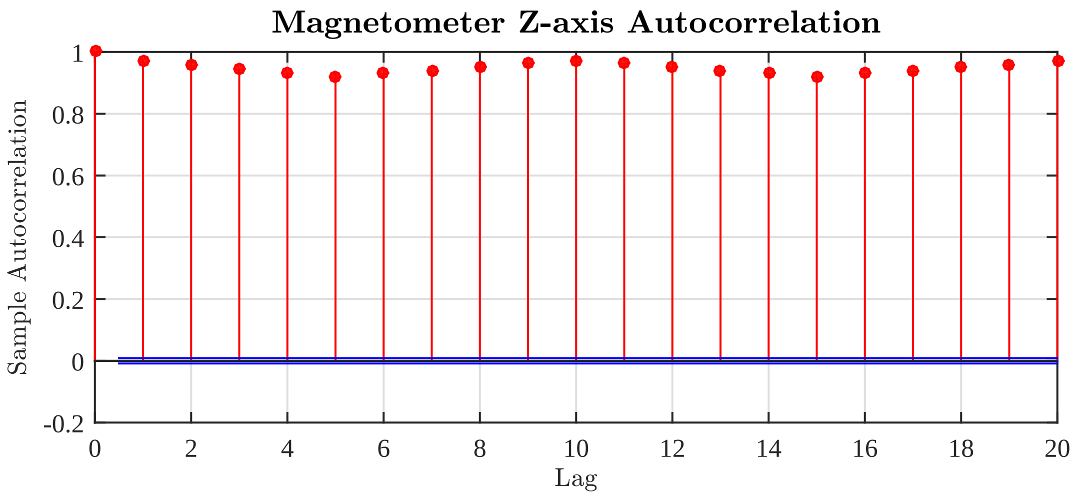

Figure B.14: The figure shows the ACF for the magnetometer z-axis which shows that the samples are very correlated.

B.3 Accelerometer

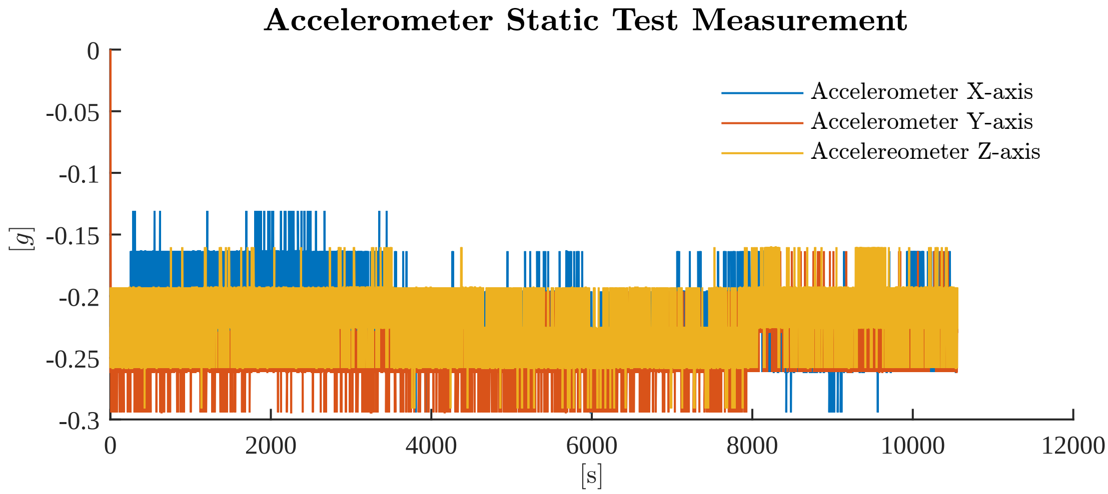

Figure B.15: The figure shows the accelerometer measurement during the static sensor test.

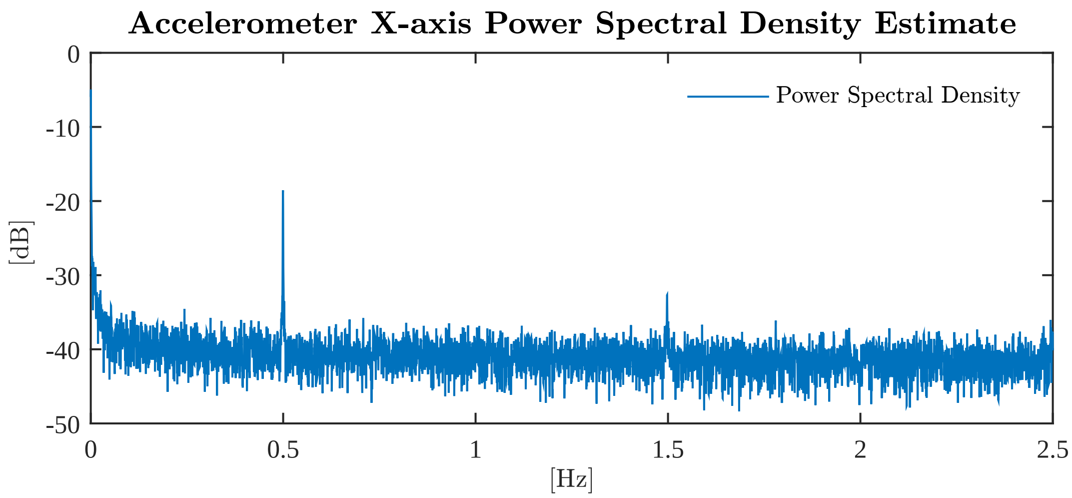

Figure B.16: The figure shows the PSD for the accelerometer x-axis. From the slope of the graph it can be seen that the noise is not white

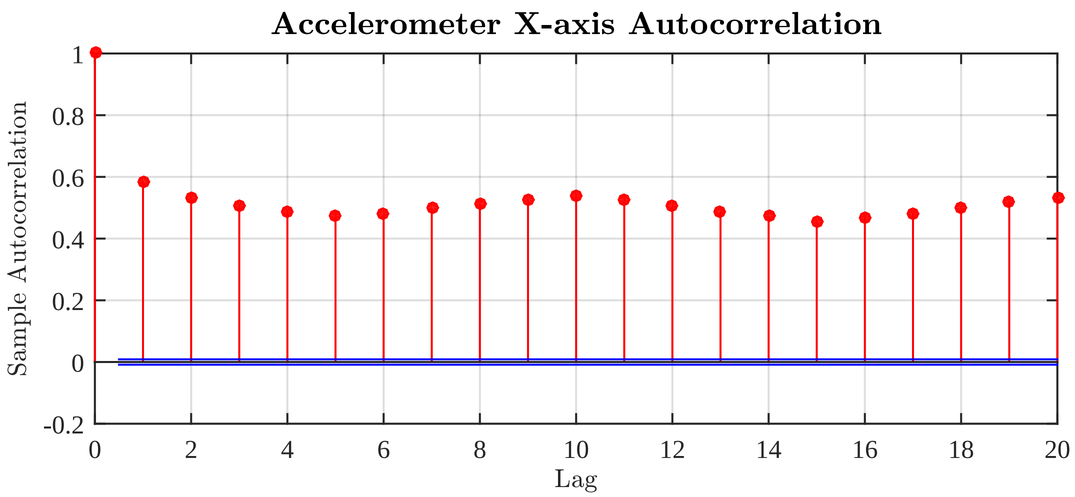

Figure B.17: The figure shows the ACF of the acelerometer x-axis. It can be seen from the figure that the samples are very correlated.

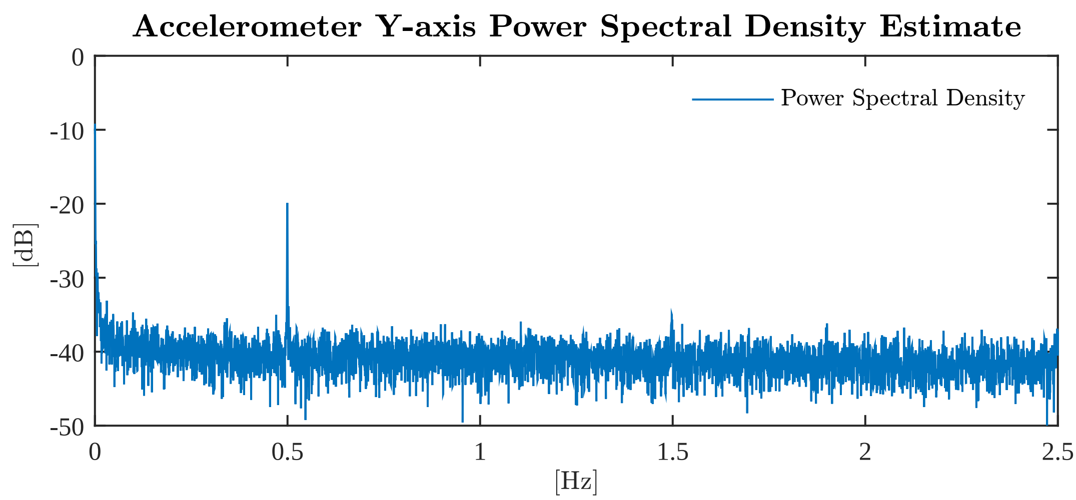

Figure B.18: The figure shows the PSD for the accelerometer y-axis. From the slope of the graph it can be seen that the noise is not white

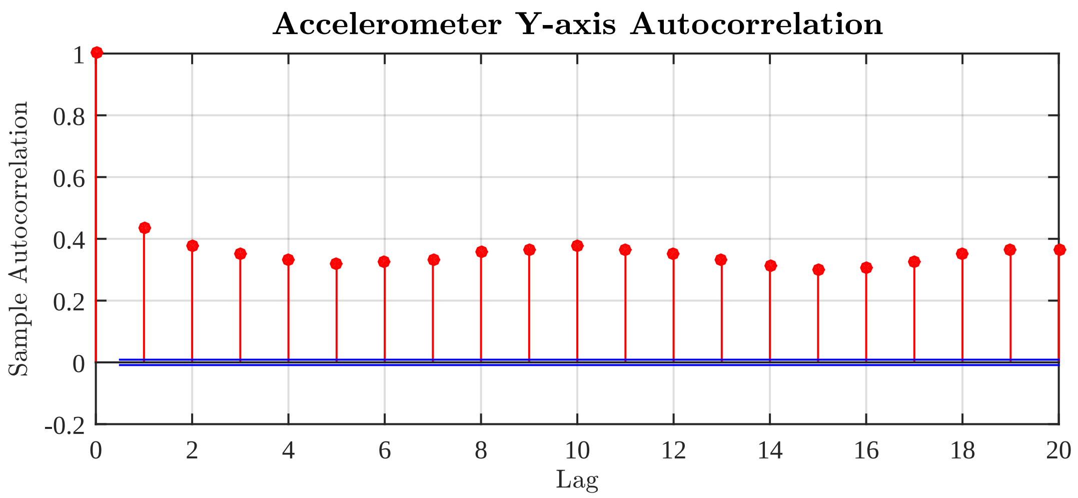

Figure B.19: The figure shows the ACF of the accelerometer y-axis. It can be seen from the figure that the samples are very correlated.

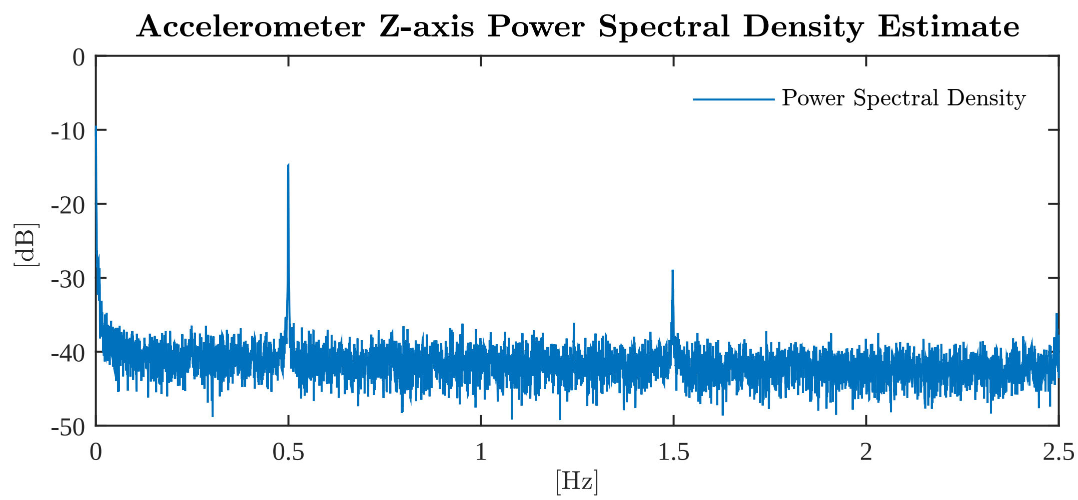

Figure B.20: The figure shows the PSD for the accelerometer z-axis. From the slope of the graph it can be seen that the noise is not white

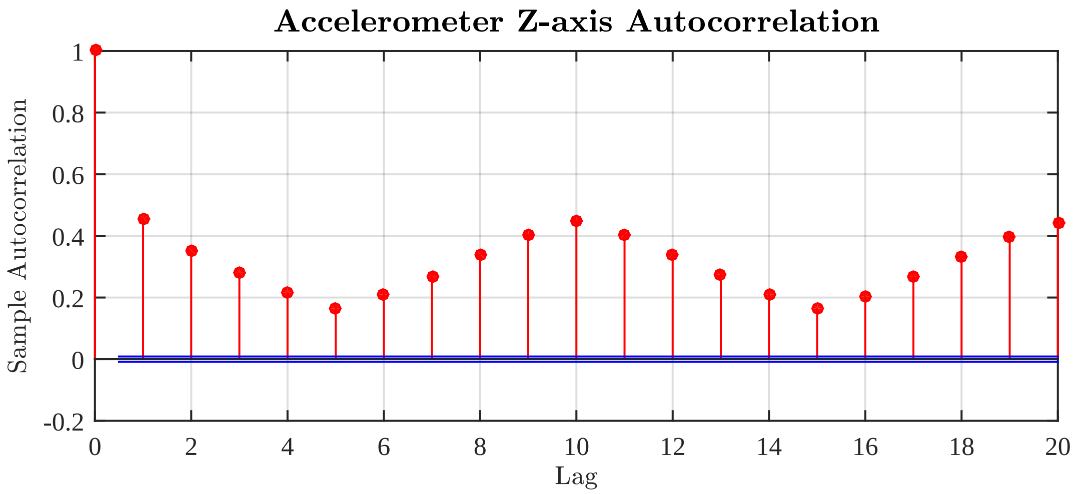

Figure B.21: The figure shows the ACF of the acelerometer z-axis. It can be seen from the figure that the samples are very correlated.

B.4 Gyroscope

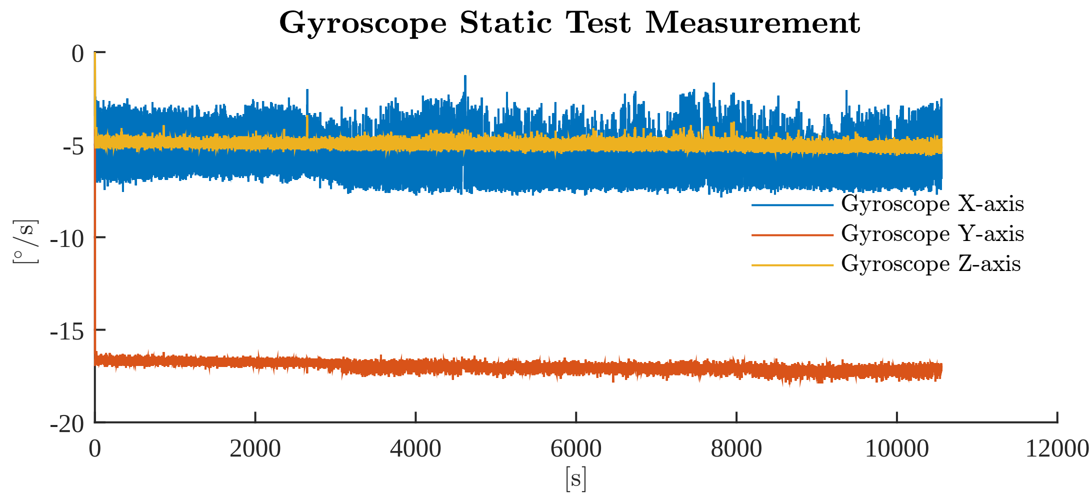

Figure B.22: The figure shows the measurement of the gyroscope during the static test.

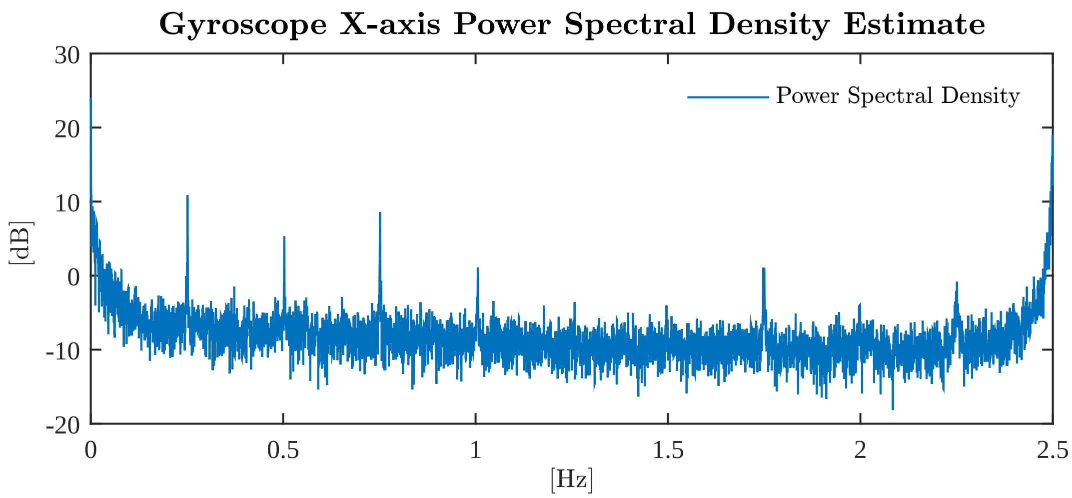

Figure B.23: The figure shows the PSD of the gyroscope x-axis. It can be seen from the slope of the graph that the noise is not white.

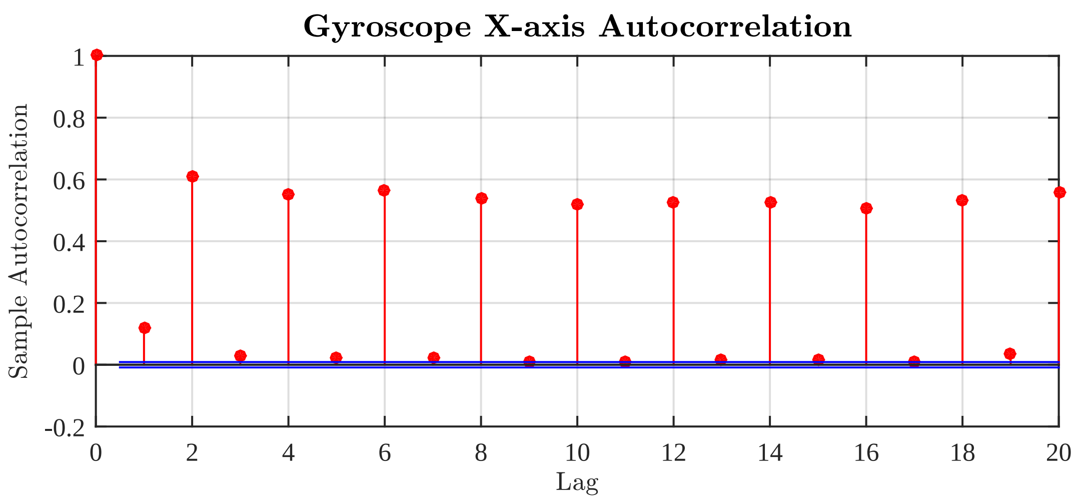

Figure B.24: The figure shows the ACF for the gyroscope x-axis. It can be seen from the graph that the samples are very correlated.

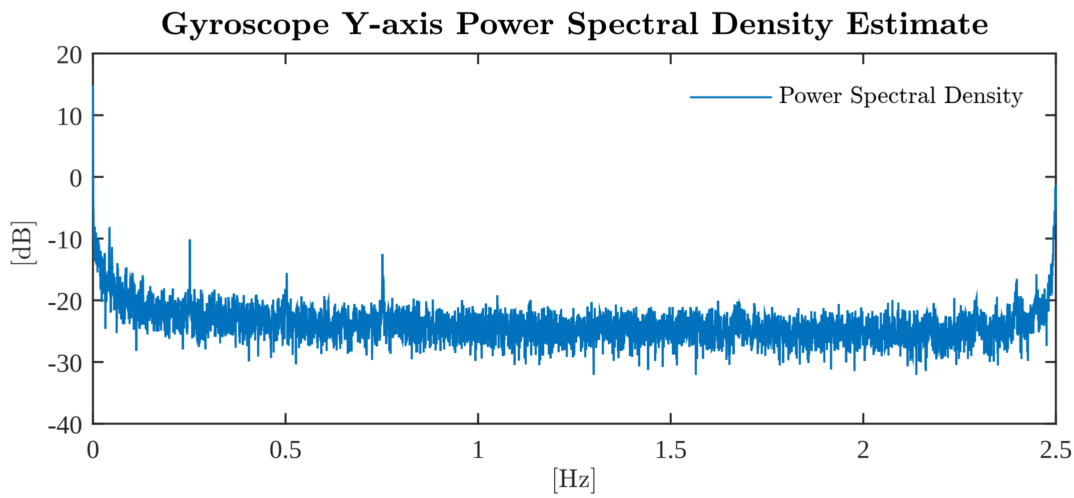

Figure B.25: The figure shows the PSD of the gyroscope y-axis. It can be seen from the slope of the graph that the noise is not white.

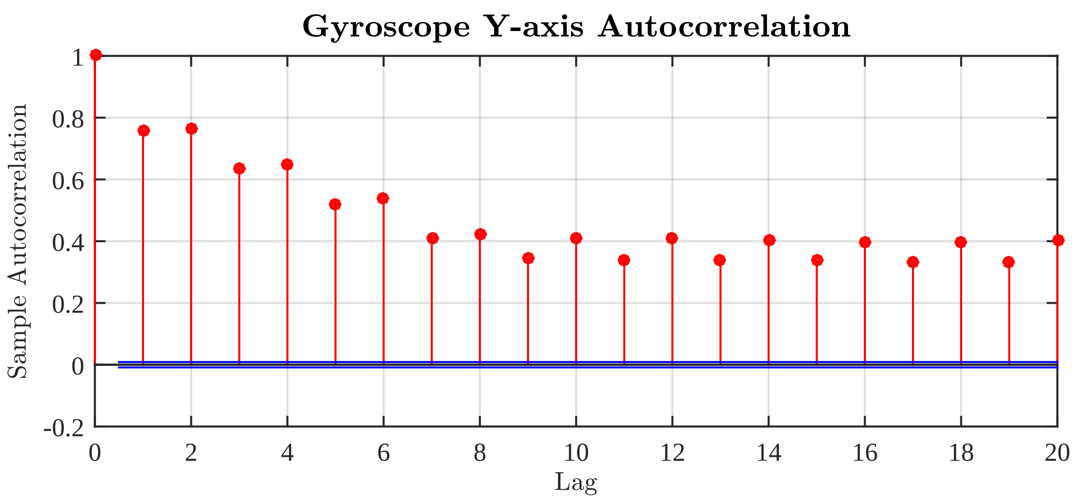

Figure B.26: The figure shows the ACF for the gyroscope y-axis. It can be seen from the graph that the samples are very correlated.

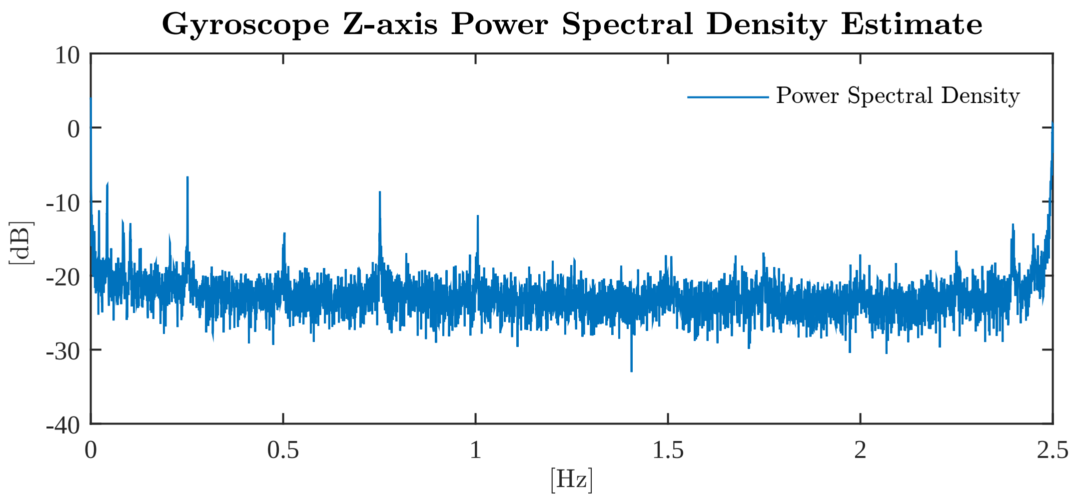

Figure B.27: The figure shows the PSD of the gyroscope z-axis. It can be seen from the slope of the graph that the noise is not white.

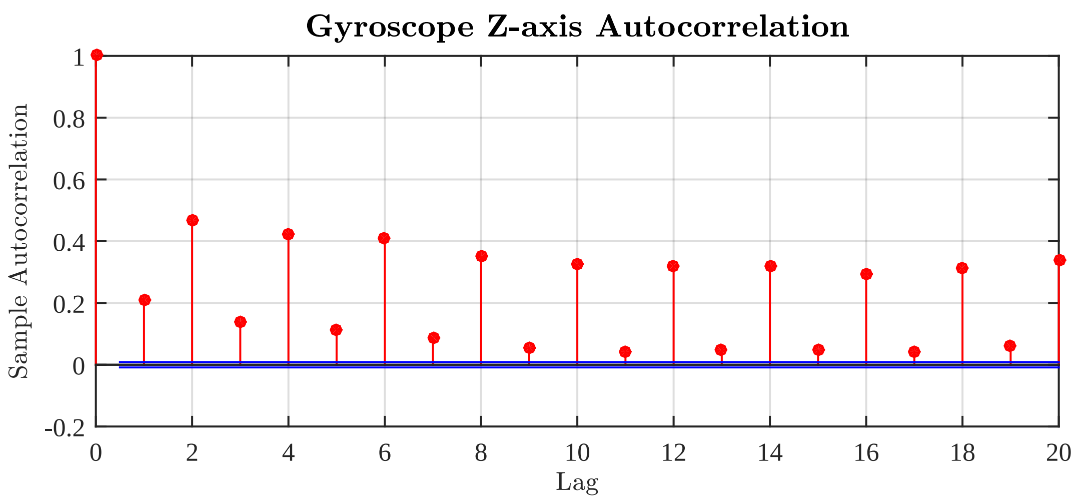

Figure B.28: The figure shows the ACF for the gyroscope z-axis. It can be seen from the graph that the samples are very correlated.

Appendix C

Model Derivations and Inertia Determination

C.1 Model Derivations

C.1.1 Rigid Body Kinetics

The Newton-Euler formulation are based upon Newton's Second Law, which relates forces to mass and acceleration. Based on Newton's Second Law Euler derived axioms which describes the conservation of momentum. The axioms are called Euler's first and second axioms. The first axiom describes the conservation of linear momentum, as is expressed in equation C.1. The conservation of linear momentum is expressed as a relation between the derivative of the linear momentum and force

$$ {}^{\mathrm{n}}\mathbf{f}(t) = \mathrm{m}\,{}^{\mathrm{n}}\dot{\mathbf{v}}(t) \quad , \tag{C.1} $$

where

${}^{\mathrm{n}}\mathbf{f}(t)$	is the force expressed in the inertial NED frame
m	is the mass
${}^{\mathrm{n}}\dot{\mathbf{v}}(t)$	is the acceleration expressed in the inertial NED reference frame.

The second axiom describes the conservation of angular momentum, as can be seen in equation C.2. The conservation of angular momentum is expressed as a relation between the derivative of the angular momentum and the torque

$$ {}^{\mathrm{n}}\mathbf{l}(t) = \mathrm{I}\,{}^{\mathrm{n}}\boldsymbol{\omega}(t) \quad , \tag{C.2} $$

where

${}^{\mathrm{n}}\mathbf{l}(t)$	is the angular momentum expressed in the inertial NED frame
I	is the inertia tensor
${}^{\mathrm{n}}\boldsymbol{\omega}(t)$	is the angular velocity expressed in the inertial NED frame.

The two axioms collectively describes the motion of a rigid body in $\mathbb{R}^3$. The axioms will in the forthcoming section be used to describe the motion of a marine craft. When deriving the equation of motion two assumptions is made: (1) the craft is rigid and (2) the NED frame is inertial, as is described in 2. The first assumption is made to eliminate considerations of forces acting between individual elements of the mass of the body. The second assumption eliminates considerations of forces due to the rotation of the Earth.

C.1.2 Translational Motion of a Rigid Body

The equations of motion for a marine craft can be divided into two parts, the equations describing the translational motion of the craft and the equations which describes the rotational motion of the craft. This section will derive the equations of translational motion whilst the next section will derive the equations of rotational motion.

The equations of translational motion is based upon Euler's first axiom as described in the previous section. It shall be noted that the axiom is represented in the NED frame, this is denoted by the left superscript as seen in equation C.3

$$ {}^{\mathrm{n}}\mathbf{f}(t) = {}^{\mathrm{n}}\dot{\mathbf{p}}(t) \quad , \tag{C.3}$$

where
${}^{\mathrm{n}}\dot{\mathbf{p}}(t)$ is the linear momentum expressed in the inertial NED frame.

By rotation the linear momentum can be expressed in a rotating reference frame instead of an inertial as can be seen in equationC.4. The rotation can be done by the use of rotation matrices or quaternions. The rotation matrices can be subject to gimbal-lock which means that there are some movements it cannot reach. The quaternion is free from these movement singularities, but is is only relevant to consider the use of quaternions if the body which is modelled is to make full rotations. Throughout the remainder of this report rotation matrices will be used to represent rotations because it is assumed that a surface vessel will never make a full rotation around all axes. The only axis it makes a full rotation around is the z-axis, i.e yawing motion

$$ {}^{\mathrm{b}}\mathbf{p}(t) = {}^{\mathrm{b}}_{\mathrm{n}}\mathbf{R}(t){}^{\mathrm{n}}\mathbf{p}(t) \quad , \tag{C.4}$$

where
${}^{\mathrm{b}}_{\mathrm{n}}\mathbf{R}(t)$ is the rotation matrix from the inertial NED frame to the BODY frame.

By taking the derivative of the linear momentum represented in the BODY frame, the translational force in the BODY frame can be determined. By the use of the product rule of differentiation, the linear momentum can be expressed as seen in equation C.5.

$$ {}^{\mathrm{b}}\dot{\mathbf{p}}(t) = {}^{\mathrm{b}}_{\mathrm{n}}\dot{\mathbf{R}}(t){}^{\mathrm{n}}\mathbf{p}(t) + {}^{\mathrm{b}}_{\mathrm{n}}\mathbf{R}(t){}^{\mathrm{n}}\dot{\mathbf{p}}(t) \quad , \tag{C.5}$$

The time derivative of a rotation matrix can be expressed as: ${}^{\mathrm{b}}_{\mathrm{n}}\dot{\mathbf{R}}(t) = -\left[{}^{\mathrm{b}}\boldsymbol{\omega}(t)\right] \times {}^{\mathrm{b}}_{\mathrm{n}}\mathbf{R}(t)$, the expression for the force can then be expanded into equation C.6

$$ {}^{\mathrm{b}}\dot{\mathbf{p}}(t) = -{}^{\mathrm{b}}\boldsymbol{\omega}(t) \times {}^{\mathrm{b}}_{\mathrm{n}}\mathbf{R}(t){}^{\mathrm{n}}\mathbf{p}(t) + {}^{\mathrm{b}}_{\mathrm{n}}\mathbf{R}(t){}^{\mathrm{n}}\dot{\mathbf{p}}(t) \quad , \tag{C.6}$$

where
${}^{\mathrm{b}}\boldsymbol{\omega}(t)$ is the angular velocity expressed in the body frame.

By changing the coordinates from the NED frame to the BODY frame, the expression can be reduced to equation C.7

$$ {}^{\mathrm{b}}\dot{\mathbf{p}}(t) = -{}^{\mathrm{b}}\boldsymbol{\omega}(t) \times {}^{\mathrm{b}}\mathbf{p}(t) + {}^{\mathrm{b}}\dot{\mathbf{p}}(t) \quad , \tag{C.7}$$

By substituting ${}^{\mathrm{b}}\mathbf{p}(t)$ with the expression for linear momentum as: ${}^{\mathrm{b}}\mathbf{p}(t) = m\mathbf{v}$, the expression is expanded in to equation C.8

$$ {}^{\mathrm{b}}\mathbf{f}(t) = -{}^{\mathrm{b}}\boldsymbol{\omega}(t) \times \mathrm{m}{}^{\mathrm{b}}\mathbf{v}(t) + {}^{\mathrm{b}}\mathbf{f}(t) \quad , \tag{C.8}$$

where
${}^{\mathrm{b}}\mathbf{f}(t)$ is the force expressed in the BODY frame.
This expression is the translational force represented in a rotating reference frame, this expression will be used in the forthcoming sections.

C.1.3 Rotational Motion of a Rigid Body

In this next section the rotational equations of motion are derived by using Euler's second axiom. The external torque of a rigid body is described as the derivative of the angular momentum as seen in equation C.9

$$^{\mathrm{n}}\dot{\mathbf{l}}(t) = {}^{\mathrm{n}}\boldsymbol{\tau}_{ext}(t) \quad , \tag{C.9}$$

where
$^{\mathrm{n}}\dot{\mathbf{l}}(t)$ is the angular momentum expressed in a inertial reference frame
$^{\mathrm{n}}\boldsymbol{\tau}_{ext}(t)$ is the external torque expressed in a inertial reference frame.

It shall be noted, as for the translational motion, that Euler's axioms is described in a inertial frame. To represent the rotational motion in a rotating reference frame, it is needed to rotate the angular momentum. By rotating the angular momentum the rotational motion can now be expressed in a moving reference frame as seen in equation C.10

$$^{\mathrm{b}}\mathbf{l}(t) = {}^{\mathrm{b}}_{\mathrm{n}}\mathbf{R}(t)^{\mathrm{n}}\mathbf{l}(t) \quad , \tag{C.10}$$

where
$^{\mathrm{b}}_{\mathrm{n}}\mathbf{R}(t)$ is the rotation matrix from a inertial reference frame to the body frame.

By taking the time derivative of the angular momentum the torque can obtained. The expression can then by use of the product rule of differentiation be expanded to equation C.11

$$^{\mathrm{b}}\dot{\mathbf{l}}(t) = {}^{\mathrm{b}}_{\mathrm{n}}\dot{\mathbf{R}}(t)^{\mathrm{n}}\mathbf{l}(t) + {}^{\mathrm{b}}_{\mathrm{n}}\mathbf{R}(t)^{\mathrm{n}}\dot{\mathbf{l}}(t) \quad , \tag{C.11}$$

As for the translational motion the time derivative of a rotation matrix can be described as: $^{\mathrm{b}}_{\mathrm{n}}\dot{\mathbf{R}}(t) = -\left[^{\mathrm{b}}\boldsymbol{\omega}(t)\right] \times {}^{\mathrm{b}}_{\mathrm{n}}\mathbf{R}(t)$, by substituting this into equation C.11 the expression seen in equation C.12 can be obtained.

$$^{\mathrm{b}}\dot{\mathbf{l}}(t) = -{}^{\mathrm{b}}\boldsymbol{\omega}(t) \times {}^{\mathrm{b}}_{\mathrm{n}}\mathbf{R}(t)^{\mathrm{n}}\mathbf{l}(t) + {}^{\mathrm{b}}_{\mathrm{n}}\mathbf{R}^{\mathrm{n}}\dot{\mathbf{l}}(t) \quad , \tag{C.12}$$

By a change of coordinate the expression is then rotated into the BODY frame. se equation C.13. The expression has now been rotated from a inertial frame to a rotating frame

$$^{\mathrm{b}}\dot{\mathbf{l}}(t) = -{}^{\mathrm{b}}\boldsymbol{\omega}(t) \times {}^{\mathrm{b}}\mathbf{l}(t) + {}^{\mathrm{b}}\boldsymbol{\tau}_{ext}(t) \quad , \tag{C.13}$$

The angular momentum of a rigid body is described as: $^{\mathrm{b}}\mathbf{l}(t) = \mathrm{I}_{\mathrm{body}}{}^{\mathrm{b}}\boldsymbol{\omega}(t)$, by substituting this expression into equation C.13 an expression for the torque can be obtained, see C.14

$$\begin{aligned} \mathrm{I}_{\mathrm{body}}{}^{\mathrm{b}}\dot{\boldsymbol{\omega}}(t) &= -{}^{\mathrm{b}}\boldsymbol{\omega}(t) \times \left(\mathrm{I}_{\mathrm{body}}{}^{\mathrm{b}}\boldsymbol{\omega}(t)\right) + {}^{\mathrm{b}}\boldsymbol{\tau}_{ext}(t) \\ {}^{\mathrm{b}}\boldsymbol{\tau}_{ext}(t) &= \mathrm{I}_{\mathrm{body}}{}^{\mathrm{b}}\dot{\boldsymbol{\omega}}(t) + {}^{\mathrm{b}}\boldsymbol{\omega}(t) \times \left(\mathrm{I}_{\mathrm{body}}{}^{\mathrm{b}}\boldsymbol{\omega}(t)\right) \quad , \end{aligned} \tag{C.14}$$

The expression for both translational motion and rotational motion for a rigid body in a moving reference frame has been derived. The next section will join these expressions into a matrix representation and include the hydrodynamic forces.

C.2 Inertia Determination

The inertia of the body have been determined, by group 14gr1034 per 20141008, to be:

$$\mathrm{I} = \begin{bmatrix} 0.06541 & -0.01260 & -0.05359 \\ -0.01260 & 1.08921 & -0.00108 \\ -0.05359 & -0.00108 & 1.10675 \end{bmatrix} \tag{C.15}$$

This shows the the inertia of the body is not exactly distributed along the principal axes. To determine if the inertia is approximately distributed along the principal axes, the matrix eigenvalues and eigenvectors are calculated.

$$\mathrm{V} = \begin{bmatrix} 0.9986 & 0.0134 & -0.0510 \\ 0.0123 & -0.9997 & -0.0215 \\ 0.0513 & -0.0208 & 0.9985 \end{bmatrix} \tag{C.16}$$

$$diag(\mathrm{D}) = \begin{bmatrix} 0.0625 \\ 1.0894 \\ 1.1095 \end{bmatrix} \tag{C.17}$$

If we subtract the diagonal of D with the diagonal of I, we will get an error describing how big a difference there are, this describes how close the inertia in the body frame is to the principal axes.

$$e = diag(\mathrm{I}) - diag(\mathrm{D}) = \begin{bmatrix} 0.0029 \\ -0.0001 \\ -0.0028 \end{bmatrix} \tag{C.18}$$

If we analyse the error and the matrix V it is seen that the inertia of the body frame lies very close to the principal axes. The error is very small (close to zero) and the eigenvectors of the inertia matrix is also close to unit size. This means that the inertia tensor can be assumed diagonal.

The mass of the body is, according to group 14gr1034 per 20141008, 13 kg, with this said the mass of 13 kg is multiplied with a identity matrix which gives:

$$\mathrm{mI}_{3\times3} = \begin{bmatrix} 13 & & 0 \\ & 13 & \\ 0 & & 13 \end{bmatrix} \tag{C.19}$$

Appendix D

Additions to the Fault Analysis

Based on the fault analysis performed the following severity and occurrence indexes has been determined. The indexes are determine based on the authors knowledge, this implies that the indexes is chosen subjectively.

Effect	Fault	O	S	RPN
Changed Efficiency	Propeller - Missing Wing	3	7	21
Changed Dynamics	Propeller - Vegetation	7	5	43
	DC-Motor - Motor Wear	2	4	8
	DC-Motor - Defect Motor Driver	4	7	28
Out of Control	Heading Sensor - Random Output	2	10	20
	Heading Sensor - No Output	6	10	60
	Yaw rate Sensor - Random Output	3	2	6
	Yaw rate Sensor - Fixed Output	6	10	60
	Position Sensor - Fixed Output	7	10	70
	Position Sensor - Random Output	6	10	60
	Position Sensor - No Output	9	10	90
No Propulsion	Propeller - Broken Shaft	7	10	70
	Yaw rate Sensor - No Output	2	3	6
	Heading Sensor - Fixed Output	3	8	24
Overshoot	Heading Sensor - Biased Output	2	3	6
	Speed Sensor - Biased Output	2	2	4

Appendix E

System Description

The vessel AAUSHIP can be divided into two parts, actuators and sensors. The forthcoming session will describe the different parts to give an overview of the existing system.

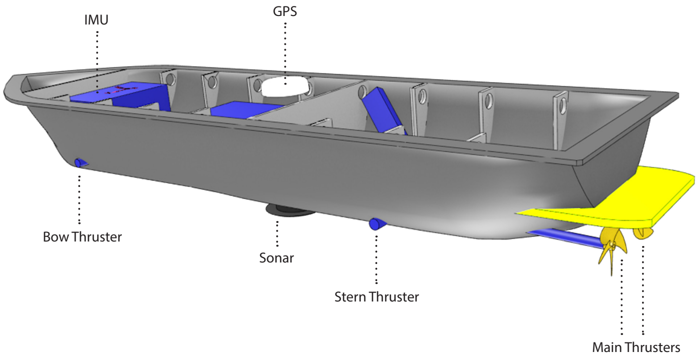

Figure E.1: A rendered image of the boat describing where the different parts are located

The IMU of AASHIP contains the magnetometer, accelerometer and gyroscope. The datasheet rating associated with each of the sensors can be seen in Table E.

By looking at the output noise for the sensors it can be seen that the noise levels stated here is much higher than the levels determined by the sensor noise analysis. The GPS equipped to AASHIP is a RTK GPS from the company Ashtech. The datasheet is very limited regarding technical information, such as noise characteristics. But some of the most significant specifications can be seen in Table E.

ADIS16405

Sensor	Property	
Gyroscope	Type	Triaxial Digital Gyroscope
	Range	$\pm 350\,^{\circ}/\mathrm{s}$
	Sensitivity	0.05 $^{\circ}$/s
	Output Noise	0.9 $^{\circ}$/s rms
	Linear Acceleration Effect on Bias	0.05 $^{\circ}/\mathrm{s}/g$
	Operational Temperature	-40 to +85 $^{\circ}$
Accelerometer	Type	Triaxial Digital Accelerometer
	Range	$\pm 18\,g$
	Sensitivity	3.33 mg
	Output Noise	9 mg rms
	Operational Temperature	-40 to +85 $^{\circ}$
Magnetometer	Type	Tri-axial Digital Magnetometer
	Range	$\pm 3.5\,\mathrm{G}$
	Sensitivity	0.5 mG
	Output Noise	1.25 mG rms
	Operational Temperature	-40 to +85 $^{\circ}$

Ashtech MB100

Sensor	Property	
GNSS Receiver	Type	Real Time Kinematic GNSS Receiver
	Sensitivity Horizontal	1 cm
	Sensitivity Vertical	2 cm
	Sampling Frequency	10 Hz
	Operational Temperature	-40 to +85 $^{\circ}$
	GNSS	GPS, GLONASS, Galileo

E.1 Actuator

AASHIP is equipped with four thrusters, the specifications for the thruster can be seen in the table listed below.

Graupner 750 In-Line

Actuator	Property	
Electric Motor	Type	Brushless DC-Motor
	Nominal Voltage	14.8 V
	No load speed	15318 RPM
	Output	1200 W
	Horse Power	1.6 Hk
	Poles	2
	ESC	Graupner 7237

Roxxy Inrunner 3656/09

Actuator	Property	
Electric Motor	Type	Brushless DC-Motor
	Nominal Voltage	28 V
	No load speed	34440 RPM
	Output	764 W
	Horse Power	1 Hk
	Poles	2
	ESC	Roxxy BL Control 940-6

Litterature

Bibliography

[Bencke 15] Karl Bencke. *Hals Barre*. 2015. http://www.denstoredanske.dk/Danmarks_geografi_og_historie/Danmarks_geografi/Indre_danske_farvande/Hals_Barre.

[Blanke 04] Mogens Blanke, Michel Kinnaert, Jan Lunze & Marcel Staroswiecki. Diagnosis and fault-tolerant control. Springer, 2004.

[Campbell 04] Stephen L. Campbell & Ramine Nikoukhah. Auxiliary signal design for failure detection. Princeton University Press, 2004.

[Carlson 12] Carl S. Carlson. Effective fmeas - achieving safe, reliable, and economical products and processes using failure mode and effects analysis. John Wiley and Sons, 2012.

[Chen 99] Jie Chen & R. J. Patton. Robust model-based fault diagnosis for dynamic systems. Kluwer Academic Publishers, 1999.

[Christensen 13] Rasmus L. Christensen, Frederik Juul, Nick Østergaard & Jesper A. Larsen. *Centralized State Estimation of Distributed Maritime Surface Oceanographers*. 2013. http://vbn.aau.dk/files/76957716/1st_robotics_workshop.pdf.

[Christensen 14] Rasmus L. Christensen. *Dynamic Positioning using Integrator-Backstepping - a non-linear Lyapunov stable observer-based approach*. 2014. http://kom.aau.dk/group/14gr1036/main.pdf.

[Crassidis 03] John L. Crassidis & F. Landis Markley. *Unscented Filtering for Spacecraft Attitude Estimation*. 2003. 26:4, pp. 536-542.

[Dam 14] Jeppe Dam & Nick Oestergaard. *Formation Control of an Autonomous Surface Vessel for Surveying Purposes*. 2014.

[Fossen 11] Thor I. Fossen. Handbook of marine craft hydrodynamics and motion control. Wiley, 2011.

[Google] Google. *Google Maps*. -. maps.google.com.

[Grewal 08] Mohinder S. Grewal & Angus P. Andrews. Diagnosis and fault-tolerant control. Wiley & Sons, 2008.

[Havn 15] Aalborg Havn. *Søopmåling og Oprensning*. 2015. http://www.aalborghavn.dk/S%C3%B8opm%C3%A5ling-og-oprensning.182.aspx.

[Izadi-Zamanabadi 99] Roozbeh Izadi-Zamanabadi. Fault-tolerant supervisory control- system analysis and logic design. University of Aalborg, 1999.

[Kim 11] Phil Kim. Kalman filter for beginners - with matlab examples. A-JIN Publishing Company, 2011.

[Maritime 15] Kongsberg Maritime. *M3 Bathy Application Note*. 2015. http://www.km.kongsberg.com/ks/web/nokbg0397.nsf/AllWeb/F27221215D7C3862C1257D9A002A19AD/$file/M3-Bathy-Application-Note.pdf?OpenElement.

[Moe 13] Signe Moe. *Path Following of Underactuated Marine Vessels in the Presence of Ocean Currents*. 2013. http://www.diva-portal.org/smash/get/diva2:649659/FULLTEXT01.pdf.

[Monster 15] Feed The Data Monster. *How can we see the seafloor beneath the ocean waves?* 2015. http://feedthedatamonster.com/home/2014/7/7/how-can-we-see-the-seafloor-beneath-the-ocean-waves.

[Oceanic 15] National Oceanic & Atmospheric Administration. *What is Hydrographic surveying*. 2015. http://www.nauticalcharts.noaa.gov/hsd/learn_survey.html.

[Skaldyrscenter 15] Dansk Skaldyrscenter. *Hydrodynamik*. 2015. http://e-learning.skaldyrcenter.dk/vandmiljoe/limfjordens-hydrodynamik/.

[Sloth 09] Christoffer Ege Sloth & Thomas Esbensen. *Fault Diagnosis and Fault-Tolerant Control of Wind Turbines*. 2009.

[Traffic 15] Marine Traffic. *Alba Tug Vessel Information*. 2015. http://www.marinetraffic.com/en/ais/details/ships/shipid:153610/mmsi:219001083/imo:0/vessel:ALBA.

[University 15] Aalborg University. *AAUSHIP*. 2015. http://www.auv.aau.dk/index.php?n=Main.AAUSHIP.

[Vinther 10] Kasper Vinther & Kasper Fuglsang Jensen. *Attitude Determination and Control System for AAUSAT3*. 2010.

[Wan] Eric A. Wan & Rudolph de Merwe. *The Unscented Kalman Filter for Nonlinear Estimation*. -. https://www.seas.harvard.edu/courses/cs281/papers/unscented.pdf.

[Wondergem 05] Michiel Wondergem. *Output Feedback Tracking of a Fully Actuated Ship*. 2005. http://www.diva-portal.org/smash/get/diva2:649659/FULLTEXT01.pdf.